

UNIVERSITY OF COPENHAGEN  
FACULTY OF SCIENCE



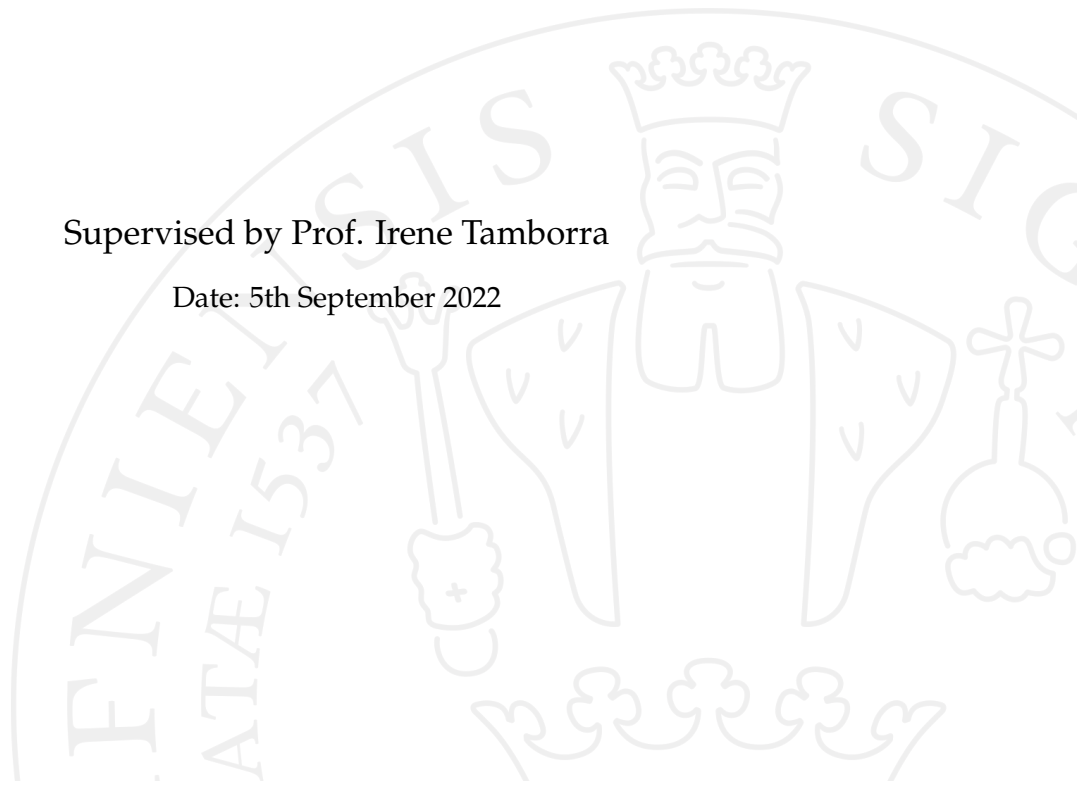
**MSc. Thesis**

**Matter-Neutrino Resonance  
in  
Binary Neutron Star Mergers**

Arun Krishna Ganesan

Supervised by Prof. Irene Tamborra

Date: 5th September 2022





*Dedicated to,  
My parents.*

# Acknowledgements

I am extremely grateful to my supervisor Prof. Irene Tamborra, for her patience, guidance and support even when things were not going as planned. I would like to extend my heartfelt gratitude to Dr. Shashank Shalgar for his valuable inputs throughout the duration of my work.

I'm also thankful to all my fellow members of the AstroNu group for maintaining a good social and research environment, it was opportunity for me to get a great learning experience. I'm really happy to have been a part of this group.

I would also like to thank Mr. Harish Meeran Mohammed, for allowing me to stay at his place at a crucial time and for teaching me some very essential cooking recipes to survive.

Last but not the least, I would like to thank my parents and my family for their constant moral support. Their love and support nurtured my passion to do pursue research in Physics, for which I would forever be grateful.



# Abstract

Matter-Neutrino Resonance (MNR) has been proposed to heavily influence the flavor evolution of neutrinos and anti-neutrinos emitted from binary merger remnants with consequences to heavy element production in these environments. This resonant phenomenon is quite unexplored as it can be influenced by multi-angle effects in the neutrino-neutrino interactions occurring close to the source of emission as shown in the literature.

In this work we explore the robustness of this phenomenon near the decoupling region which is close to the neutrino-emitting object, by approaching it in two ways. We begin by studying the multi-angle dependence of MNR by assuming a forward peaked angular distribution, individually, and on both neutrino and anti-neutrino beams. We study how the resonance is affected by increasing the angular contribution in steps, to the beams. We find that the Matter-Neutrino resonant flavor transformations are most suppressed when there is more angular dependence on neutrinos, though all the cases studied show a reduction in flavor transformation in accordance with what is reported in the literature. A difference in the flavor evolution of neutrinos and anti-neutrinos between normal and inverted mass hierarchies is observed which, in the context of MNR, is a new result. We then include the advective term to the flavor equations of motion and it is applied to model potentials to study its effects on MNR along two angular beams. It is found that the contributions from advection drastically suppresses the resonant flavor transformations.

We apply our understanding of this resonance to a realistic scenario by looking at the hydrodynamical simulation datasets of a Binary Neutron Star merger remnant. The parameters from the dataset are directly used to calculate the potentials occurring around the merger remnant. The system was explored for locations where Matter-Neutrino Resonance could happen using the potentials calculated and these resonance points were approached along multiple kinds of trajectories, which showed potential profiles quite different from what is studied in the literature thus far, and we find that none of them could produce the Matter-Neutrino Resonance.

# Table of contents

<b>1</b>	<b>Neutrinos</b>	<b>1</b>
1.1	Neutrinos & the Standard Model interactions . . . . .	1
1.2	Overview of the thesis. . . . .	3
<b>2</b>	<b>Flavor Transformations</b>	<b>5</b>
2.1	Formalism and EOMs . . . . .	6
2.2	Potentials . . . . .	8
2.2.1	Vacuum . . . . .	9
2.2.2	Matter interactions . . . . .	9
2.2.3	Self Interactions . . . . .	10
2.3	Equations of Motion . . . . .	12
2.4	Collective Oscillations . . . . .	14
<b>3</b>	<b>Matter-Neutrino Resonance</b>	<b>18</b>
3.1	Matter-Neutrino Resonance in Astrophysical scenarios . . . . .	18
3.1.1	Theory behind Matter-Neutrino Resonance . . . . .	19
3.1.2	Standard and Symmetric MNR . . . . .	22
3.2	Description of the Models studied . . . . .	23
<b>4</b>	<b>Study of Angle Dependence of MNR</b>	<b>26</b>
4.1	Angle Independent results . . . . .	27
4.1.1	Single Angle Scenario . . . . .	27
4.1.2	Multi-angle Scenario . . . . .	29
4.2	Angle dependence only on $\vec{P}$ . . . . .	30
4.3	Angle Dependence only on $\vec{P}$ . . . . .	33
4.4	Non-uniform angle dependence on both $\vec{P}$ & $\vec{P}$ . . . . .	35
4.5	Comparing Normal and Inverted Mass Hierarchies . . . . .	39
4.6	Advective effects . . . . .	43
4.6.1	Motivation . . . . .	43
4.6.2	Advection for two beams . . . . .	43
4.7	Summary . . . . .	50

<b>5</b>	<b>Binary Neutron Star Merger Data</b>	<b>52</b>
5.1	Calculation of Potentials . . . . .	54
5.2	Spatial distribution of potentials . . . . .	55
5.3	Radial Trajectories . . . . .	58
5.3.1	Angle Dependence on radial trajectories . . . . .	60
5.4	Generic trajectories . . . . .	61
5.4.1	Vertical Trajectories . . . . .	62
5.4.2	Horizontal trajectories . . . . .	63
5.4.3	Reversed vertical trajectories . . . . .	64
5.5	Inclusion of advective term . . . . .	66
5.6	Summary . . . . .	68
<b>6</b>	<b>Discussion &amp; Summary</b>	<b>70</b>
<b>7</b>	<b>Appendix</b>	<b>74</b>
7.1	Derivation of Bloch equation for Polarization vector . . . . .	74
7.2	Method of designing solver code . . . . .	75
7.2.1	Numerical scheme . . . . .	75
7.2.2	Implementation of the integrals . . . . .	76
7.2.3	General Multiangle-Single Energy case . . . . .	77
7.2.4	Advection Code . . . . .	78

# Chapter 1

## Neutrinos

Neutrinos are the neutral fermionic partners of the other charged leptons in the Standard Model, such as electrons, muons and taus. They participate only in the weak interactions & the gravitational interactions. They are identified with their ‘flavor’, which refers to the partner charged lepton they were produced or absorbed in an interaction with, thus neutrinos have three flavors.

They were initially proposed to be electrically neutral particles with zero mass, to explain the electron energy spectrum in the beta decay of neutrons by W. Pauli in 1930 and they were discovered experimentally in 1956 by Fred Reines & George Cowan.

Neutrinos are unique for many reasons, one of which is that they are the only neutral leptons to have been observed. They got the spotlight of modern physics with the discovery in 1998, which showed that they possess mass and they ‘mix’ their flavors, i.e, their mass and flavor states are not equal, which leads to flavor transformations while propagating, even when passing through vacuum. Neutrinos are important pointers in multi-messenger astronomy as the interaction scales governing neutrino interactions are minute and hence they can be used to infer the exact direction of the source. Neutrinos are the only evidence so far, for physics beyond the Standard model with a high degree of confidence.

### 1.1 Neutrinos & the Standard Model interactions

The Standard Model (SM) of Particle Physics is the best theoretical model we have to describe the behavior of fundamental particles. It is a gauge theory with the gauge group  $SU(3)_C \times SU(2)_L \times U(1)_Y$  and all the fundamental particles can be treated to be the irreducible representations of this gauge group.

In the Standard Model, the fundamental particles are categorized into fermions and bosons. There are three generations of fermions with two particles in each generation, further divided into quarks and leptons, hence adding up to 12 particles. The bosons act as force mediators,  $W^\pm, Z^0$ -bosons mediate the weak interactions, the photon  $\gamma$ , mediates the electromagnetic force and there are 8 gluons  $g$ , that

mediates the strong nuclear force. The Higgs boson is also included in the SM which gives mass to the bosons through the Higgs mechanism and to fermions through the Yukawa coupling.

The neutrinos in the SM, participates in only two kinds of weak interactions namely the charged current (CC) interaction and the neutral current (NC) interaction. The Lagrangians for the corresponding processes are,

$$\mathcal{L}_{CC} = \frac{-g'}{\sqrt{2}} \sum_l \bar{\nu}_{Ll} \gamma^\mu l_L^- W_\mu^+ + h.c, \quad (1.1)$$

$$\mathcal{L}_{NC} = \frac{-g'}{2 \cos \theta_W} \sum_l \bar{\nu}_{Ll} \gamma^\mu \nu_{Ll} Z_\mu^0, \quad (1.2)$$

where  $g'$  is the coupling constant,  $\theta_W$  is the electroweak Weinberg angle,  $\nu_{Ll}$  is the left-handed neutrino spinor of flavor  $l$  and  $\gamma^\mu$  are the Dirac gamma matrices. The above Lagrangians characterize the interaction of neutrinos of a particular flavor with their corresponding charged lepton through a  $W$ -boson and the scattering of neutrinos with other neutrinos through  $Z$ -boson.

Yukawa coupling is possible only if the fermions have both left-chiral and right-chiral components, where chirality is the way the Dirac spinors transform under the chiral projection operators, defined to be  $P_R \equiv (\mathbb{1} + \gamma^5)/2$  and  $P_L \equiv (\mathbb{1} - \gamma^5)/2$ , where  $\gamma^5 = i\gamma^0\gamma^1\gamma^2\gamma^3$  and  $P_R, P_L$  refer to the right and left chiral projections respectively [1]. This is also called as the particle's 'handedness'. This quantity is purely quantum mechanical and cannot change between frames of references. Since only left-handed neutrinos and right-handed anti-neutrinos are observed in nature, the SM describes neutrinos to be massless. Neutrinos appear as a part of the  $SU(2)$  doublets, one for each charged lepton as mentioned above and they do not participate in the interactions of the  $SU(3)_C$  &  $U(1)_Y$  group.

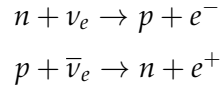
The discovery of neutrino masses and flavor mixing can be attributed to two problems and their resolution, namely, the solar neutrino problem and the atmospheric neutrino problem. Neutrinos are abundantly produced through nuclear fusion in the Sun and in hadronic shower reactions of cosmic rays in the atmosphere.

We can estimate the neutrino flux and the energies of the emitted neutrinos from the Sun and in the atmosphere using our understanding of the underlying processes. The Homestake experiment in 1968 detected the neutrinos from the Sun and reported a 2/3 deficit. Neutrino flavor deficits were also detected in the observations of atmospheric neutrinos produced by the interaction of cosmic rays with the Earth's atmosphere. The resolution to these problems came with the discovery of flavor transformations inside the Earth and resonant flavor transformations in the Sun by the Super-Kamiokande experiment and Sudbury National Observatory collaboration respectively in 1998 [2][3][4][5].

The flavor transformations are possible because neutrinos have small but non-zero masses and the different flavor eigenstates of the neutrino field are in coherent mixtures of the different mass eigenstates. Thus the propagation eigenstates develop different phases leading to flavor oscillations while travelling through vacuum or a medium. The Standard Model can be extended to include neutrino masses, but we need more experiments to confirm the right theory to explain the low value for the neutrino mass. We have some good experimental estimates about the various mixing angles between

the three different flavors, but the CP-violating phase associated with the flavor mixing is yet to be measured. [6].

Astrophysically, neutrinos are also produced copiously in Supernovae [7][8][9] and Binary Neutron Star (BNS/NS) mergers [10][11][12]. These processes emit a massive fraction of their energy in the form of neutrinos. The study of the flavor evolution of neutrinos is important in these sites because they can influence the dynamics, in the case of supernova and the rate of nucleosynthesis in the case of NS mergers. NS mergers are sites of r-process nucleosynthesis, referring to the rapid neutron capture process, which accounts for some of the production of heavier elements in the universe which requires an abundance of neutrons. The weak processes that converts a proton into a neutron or vice-versa, cannot happen without neutrinos, as seen below where typical reactions happening in these environments are presented,



Hence it is important to understand the role of neutrinos and their flavor evolution mechanisms in these systems. The flavor evolves through various potentials experienced by the neutrinos through their interactions with matter particles and other neutrinos in the media, all of which will be briefly described in the following sections.

## 1.2 Overview of the thesis.

This thesis studies the flavor transformation properties of neutrinos in neutrino-dense media where they are subjected to what is called ‘Collective oscillations’. In particular, we focus on the BNS merger systems where more anti-neutrinos are produced than neutrinos. This can create a cancellation between the matter potential and the neutrino-neutrino potential leading to a resonant flavor transformation called the ‘Matter-Neutrino Resonance’ (MNR). We aim to study the angular dependence of this novel phenomenon, which can occur in dense regions surrounding the NS mergers and the effects of advection on MNR occurring in such systems. We then apply our understanding to a hydrodynamical simulation of a BNS merger and we check the various kinds of potentials that occur in such a merger to produce flavor transformations through MNR to compare them with the kinds of profiles studied in the literature so far.

The thesis is organized in the following way, in chapter 2 we cover the basic theoretical phenomenology associated to the neutrino flavor transformations, where the equations of motion and the corresponding potentials are described in detail. In chapter 3, the theory behind the MNR phenomenon is described. The results obtained during the thesis are discussed and presented in chapter 4 and 5. Chapter 4 presents the work undertaken to study the angle dependence of MNR and discussion of the results. Chapter 5 covers the work done to study the possibilities of this resonance occurring in an actual astrophysical scenario and the various effects associated with it. Finally in chapter 6, the overall findings and results obtained through the project are discussed and summarized.



## Chapter 2

# Flavor Transformations

Neutrino flavor transformation is a rich phenomenological subject with a lot of interesting effects and resonances with significant implications on many astrophysical and cosmological processes.

For neutrinos there is no one-to-one correspondence between the mass states and the flavor states and so the flavor states are a coherent mixture of the mass states and vice-versa. Analytically, it means [6],

$$|\nu_\alpha\rangle = U_{\alpha i} |\nu_i\rangle \quad (2.1)$$

where  $\alpha$  refers to the flavor states ( $e, \mu, \tau$ ), the index  $i$  refers to the mass states and  $U_{\alpha i}$  is the unitary mixing matrix relating the two kinds of states.

For two flavors, this matrix is just the simple rotation matrix of the form,

$$U = \begin{pmatrix} \cos \theta & \sin \theta \\ -\sin \theta & \cos \theta \end{pmatrix} \quad (2.2)$$

For three flavors, this becomes the Pontecorvo-Maki-Nakagawa-Sakata (PMNS) matrix, which is the equivalent of CKM-mixing matrix for quarks. That is of the form,

$$U_{PMNS} = \begin{bmatrix} c_{12}c_{13} & s_{12}s_{13} & s_{13}e^{-i\delta_{CP}} \\ -s_{12}c_{23} - s_{23}c_{12}s_{13}e^{i\delta_{CP}} & c_{12}c_{23} - s_{12}s_{23}s_{13}e^{i\delta_{CP}} & s_{23}c_{13} \\ s_{12}s_{23} - c_{12}c_{23}s_{13}e^{i\delta_{CP}} & -c_{12}s_{23} - s_{12}c_{23}s_{13}e^{i\delta_{CP}} & c_{23}c_{13} \end{bmatrix} \quad (2.3)$$

where  $c_{ij} = \cos \theta_{ij}$  and  $s_{ij} = \sin \theta_{ij}$ .

For any generic  $n \times n$  unitary matrix, there are  $n^2$  parameters,  $n(n-1)/2$  angles and  $n(n+1)/2$  phases. But for the case of the leptons, not all the phases are physical. For  $n$  generation of leptons, we need to have  $2n$  fields corresponding to the matter and anti-matter fields, and including the conserved lepton number we can absorb  $2n-1$  phases from the total. Hence for our 3 neutrino case we have  $n=3$  and so  $n(n-1)/2 = 3$  angles and  $n(n+1)/2 - (2n-1) = 1$  CP-phase. It should be noted that this is true only if neutrinos are Dirac particles. If neutrinos are Majorana particles there

would be two more additional phases.

With the mixing matrices defined for two and three neutrino cases, we can switch from flavor basis to mass basis through unitary transformations.

## 2.1 Formalism and EOMs

Neutrinos can exist in mixed mass or flavor states and they are generally described through two formalisms, namely the density matrix formalism and the polarization vector formalism [13]. Both the formalisms are completely equivalent to each other as we shall see in this section.

In the density matrix formalism, the density matrix operator, defined as  $\hat{\rho}_{ij} = \sum_{i,j} |\psi_i\rangle \langle \psi_j|$ , where  $|\psi\rangle$  is the state vector of the neutrinos, has an expectation value matrix for the neutrino system, which we call as the density matrix. The diagonal elements of this matrix account for the occupation numbers of the individual neutrino flavors and the off-diagonal components describe the states that are existing as coherent superpositions of the individual flavor states in the diagonal. For two flavors, this density matrix takes the form,

$$\rho = \begin{pmatrix} \rho_{ee} & \rho_{ex} \\ \rho_{xe}^* & \rho_{xx} \end{pmatrix}; \quad x = \mu \text{ (or) } \tau, \quad (2.4)$$

where,  $\rho_{ee}, \rho_{xx}$  denotes the individual flavor occupation numbers and  $\rho_{ex}$  and its complex conjugate denotes the flavor mixing. A similar density matrix is assumed for the anti-neutrinos as well, denoted by  $\bar{\rho}$ .

The time evolution of such a density matrix will be equal to  $\rho(t) = e^{-iHt}\rho(0)e^{iHt}$ . If we differentiate this time-evolved density matrix with respect to time, we immediately obtain the von-Neumann equation, which governs the time evolution of the density matrices for neutrinos and anti-neutrinos. In natural units ( $c = \hbar = 1$ ) it takes the form,

$$i \frac{\partial \rho}{\partial t} = [H, \rho], \quad (2.5)$$

$$i \frac{\partial \bar{\rho}}{\partial t} = [\bar{H}, \bar{\rho}], \quad (2.6)$$

where, the right hand side is a commutation between the density matrix and the Hamiltonian matrix for neutrinos  $H$  and anti-neutrinos  $\bar{H}$ .

We can map this  $2 \times 2$  matrix into a 3-dimensional space, which we call the flavor space, as a vector. This is done by decomposing  $\rho$  in the following way,

$$\rho = \frac{\text{Tr}(\rho)}{2} (\mathbb{1} + \vec{P} \cdot \vec{\sigma})$$

$\vec{P}$  is called as the polarization vector for the system, and  $\vec{\sigma}$  are the Pauli matrices. Similarly for anti-

neutrinos, we get  $\vec{P}$ . The polarization vector encodes all the physical information of the neutrino system, being completely equivalent to the density matrix.

Since the density matrix can be a function of energy, momentum and (space)time, the corresponding polarization vector also inherits the same dependencies. The components of the polarization vector are given by,

$$\vec{P} = \begin{pmatrix} \text{Re}(\rho_{ex}) \\ \text{Im}(\rho_{ex}) \\ \rho_{ee} - \rho_{xx} \end{pmatrix} \quad (2.7)$$

The Hamiltonian matrix is also decomposed into a vector in the following way,

$$H = \frac{1}{2}(\mathbb{1} + \vec{H} \cdot \vec{\sigma})$$

The decomposition is normalized by the trace of the density matrix which signifies the neutrino population density, i.e  $\text{Tr}(\rho) = n = \rho_{ee} + \rho_{xx}$ , hence the polarization vectors have unit magnitude. By performing the decomposition, the von-Neumann equation becomes a classical Bloch equation [14] of the form (see 7.1 for the derivation),

$$\frac{d\vec{P}}{dt} = \vec{H} \times \vec{P}; \quad (2.8)$$

and for anti-neutrinos,

$$\frac{d\vec{P}}{dt} = \vec{H} \times \vec{P}, \quad (2.9)$$

which is just the equation describing the vector precession around the Hamiltonian, similar to the spin precession around an external magnetic field. Hence the polarization vector formalism helps in giving us a geometric picture of neutrino flavor transformation phenomena. This picture can then be used to understand many underlying mechanisms for neutrino flavor evolution [15]. In this thesis, we work with the polarization vector formalism.

From the definition of the polarization vector, Eq. (2.7), we can immediately see that if the system begins in a purely electron flavor state, the vector points in the  $+z$  direction in flavor space, and  $-z$  direction if it starts in purely  $x$  flavor state. This means that if the system undergoes complete flavor transformation from electron flavor, then the polarization vector flips its direction. In doing so, it would obey the classical Bloch equation of motion. The survival probabilities for neutrinos and anti-neutrinos after a time  $t$  in this formalism, is given by,

$$P_{ee} = P(\nu_e^i \rightarrow \nu_e^f) = \frac{1}{2} \left( 1 + \frac{P_z^f}{P_z^i} \right) \quad (2.10)$$

$$\bar{P}_{ee} = P(\bar{\nu}_e^i \rightarrow \bar{\nu}_e^f) = \frac{1}{2} \left( 1 + \frac{\bar{P}_z^f}{\bar{P}_z^i} \right) \quad (2.11)$$

where  $P_z^i$  and  $\bar{P}_z^i$  are the initial values of the z components of the polarization vectors. The Hamiltonian contains all the relevant interactions that can influence the flavor transformation.

In this thesis we consider contributions from three factors, namely, vacuum, matter and self interactions. Hence our Hamiltonian essentially is made up of three terms corresponding to each of the fore-mentioned potentials.

$$\vec{H} = \vec{H}_v + \vec{H}_m + \vec{H}_{\nu\nu}$$

The polarization vector, is then influenced by the cross-product with the total Hamiltonian vector as the system evolves in flavor space, thus resulting in flavor transformations if possible, as shown in the figure below. For flavor transformation to occur, the directions of the vector must change. In the potential profiles we study in this thesis, the Hamiltonian vectors change with the evolution of the system and since the polarization vectors precess around the corresponding Hamiltonians, they are responsible for guiding the polarization vectors to flavor transform. For such a transformation to occur, the change in the Hamiltonian must be very close to being adiabatic, i.e very slow compared to the precessional frequency of the polarization vector. This process is depicted in the figure below.

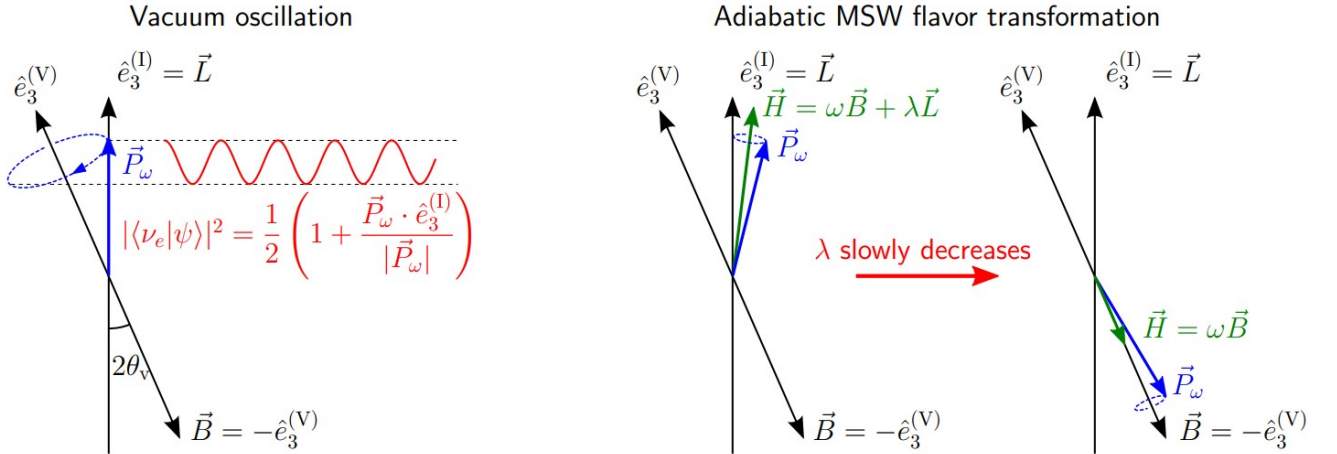


Figure 2.1: Graphical representation of flavor transformation occurring through adiabatic MSW resonance. (from [16])

## 2.2 Potentials

Neutrinos and anti-neutrinos interact very rarely with matter and are neutral. This simplifies the neutrino dynamics a little, but the equations of motion obeyed by them are still complicated, due to the inclusion of non-linear terms in dense environments. Below we very briefly discuss the various potentials that arise to be included into the Hamiltonian.

### 2.2.1 Vacuum

This term in the Hamiltonian arises simply because of the fact that the flavor eigenstates are not exactly equal to the mass eigenstates. As mentioned earlier, the flavor states and the mass states are related through the unitary matrix.

The Hamiltonian for the two neutrino system in the mass basis is diagonal and is given as,

$$H_{\text{mass}} = \frac{1}{2E} \begin{bmatrix} m_1^2 & 0 \\ 0 & m_2^2 \end{bmatrix} + p\mathbb{1} \quad (2.12)$$

where  $E$  is the energy of the neutrino, and  $p$  is the momentum. Since the momentum term is proportional to the identity matrix it cannot influence the flavor transformations, hence we can drop it. We can rewrite the matrix in a traceless form by writing the individual masses in terms of the mass difference, which is the physical observable,  $\Delta m^2 = (m_2^2 - m_1^2)$ . By performing unitary transformation using the matrix  $U$ , we can transform this to the flavor basis, which, for two flavors is the two dimensional rotation matrix as defined in Eq. (2.2).

$$H_{\text{flavor}} = UH_{\text{mass}}U^\dagger = \frac{U\mathbf{M}^2U^\dagger}{2E} \quad (2.13)$$

In doing so, the matrix picks up non-diagonal terms which causes the neutrinos to flavor transform. If we call  $\omega = \frac{\Delta m^2}{2E}$ , then when mapping this matrix onto a vector, we get the vacuum term Hamiltonian vector to be,

$$\vec{H}_v = \omega\vec{B}; \vec{B} = \begin{pmatrix} \sin(2\theta_V) \\ 0 \\ \mp \cos(2\theta_V) \end{pmatrix} \quad (2.14)$$

where  $\theta_V$  is the vacuum mixing angle for the two neutrino flavors we consider, which is set to  $\theta_V = 0.15$  throughout this thesis unless specified otherwise. This value is within the bounds set experimentally [6][17][18]. The sign of  $\omega$  is negative for anti-neutrino vacuum Hamiltonian and the cosine term is negative for normal mass hierarchy & positive for inverted hierarchy.

### 2.2.2 Matter interactions

Neutrinos undergo charged current (CC) interactions with their partner charged lepton present in the medium. But since the fraction of  $x$  flavor neutrinos and the leptons, in astrophysical sites, are overwhelmingly outnumbered by the fraction of electrons and electron (anti-)neutrinos present, we need to consider only the CC interaction between electron (anti-)neutrinos, electrons and positrons.

We can ignore the neutral current interactions of neutrinos on nucleons, as it is equally favorable for all flavors hence its Hamiltonian is proportional to the identity matrix and it does not affect flavor conversions. Thus the only set of Feynman diagrams to be considered is for the coherent neutrino-electron forward scattering charged current interactions, which is essentially refraction. These diagrams are given in Fig. 2.2.

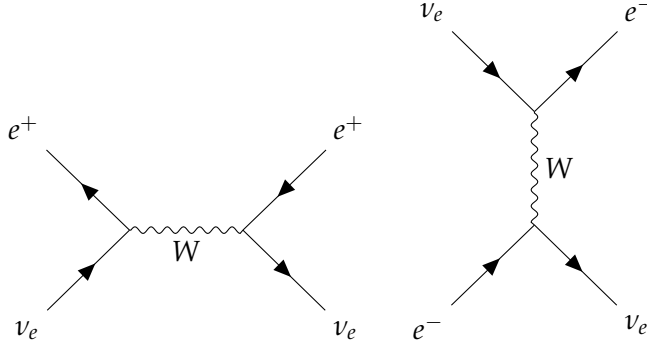


Figure 2.2: Charged current scattering of neutrino on electrons and positrons in the medium.

This interaction is dependent on the number of scatterers present in the medium and takes the form,  $\sqrt{2}G_F N_e(r)$ , where  $G_F$  is the Fermi constant and the term  $N_e(r)$  is the electron density in the medium. This can be a function of distance since the distribution of matter in the astrophysical system can vary with distance in whichever direction we choose to look. Since this interaction is flavor dependent and the media in most astrophysical sites are dominated by electrons, the Hamiltonian of this process is not proportional to identity matrix. It takes the form,

$$H_m = \begin{pmatrix} \sqrt{2}G_F N_e(r) & 0 \\ 0 & 0 \end{pmatrix}, \quad (2.15)$$

corresponding to the electron flavored (anti-)neutrino population number in the density matrix formalism. This matrix when converted into a vector accounts for,

$$\vec{H}_m = \begin{pmatrix} 0 \\ 0 \\ \lambda(r) \end{pmatrix}, \quad (2.16)$$

where  $\lambda(r) = \sqrt{2}G_F N_e(r)$ .

When this term cancels the vacuum term of the Hamiltonian, a resonant flavor transformation occurs which is called the MSW resonance. This resonant phenomenon has been widely studied in the literature [19][20][15][21].

### 2.2.3 Self Interactions

The self-interaction potential arises and becomes significant when the medium is densely populated by neutrinos and anti-neutrinos. In such a medium, neutrinos can undergo coherent forward scattering with other neutrinos and anti-neutrinos in the medium. Because of the nature of this interaction, this potential is dependent on the momentum unit vectors, which signifies the direction of propagation. The Feynman diagrams of the interactions responsible for this potential are given in Fig. 2.3.

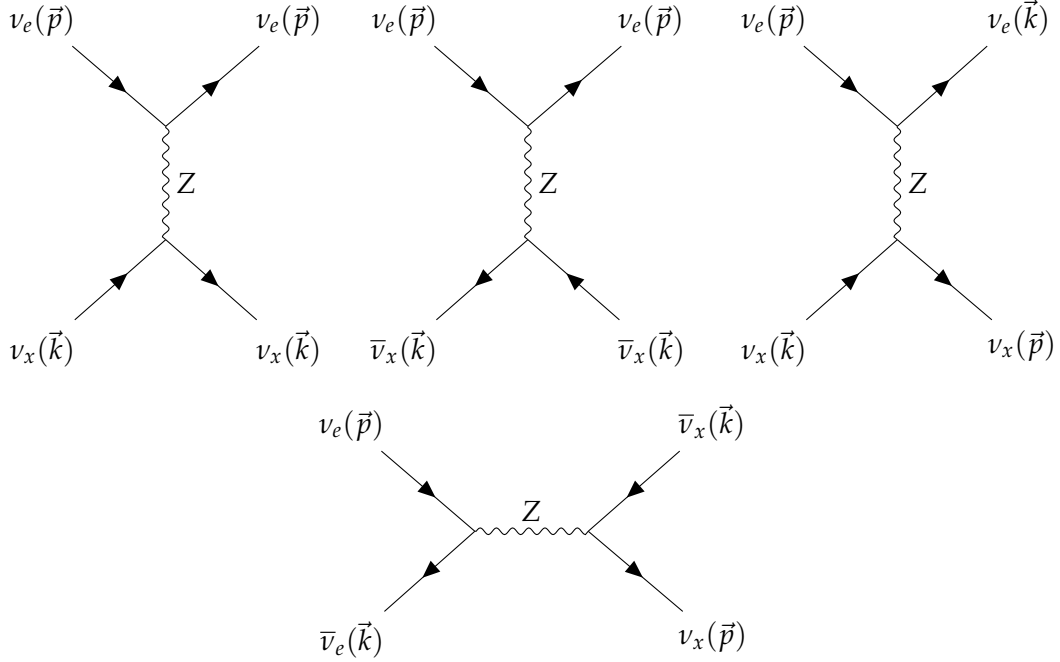


Figure 2.3: Feynman diagrams for coherent forward scattering of neutrinos on other neutrinos and anti-neutrinos in the medium. Flavor changing contribution to the Hamiltonian is from the momentum-exchanging interactions.

The potential corresponding to this type of scattering interaction just from their kinematics obtain a direction dependent term of the form  $(1 - \hat{p} \cdot \hat{p}')$  [13][22]. This is because this forward scattering is a type of current-current interaction between the neutrino and the background neutrino with dependence on the dot product of their 4-momenta. Hence if the two neutrino beams are travelling parallel then this term cannot contribute. It must be pointed out that such a momentum dependent term also appears for the neutrino-electron coherent forward scattering discussed above for matter potentials, but since the electrons interact strongly with other particles in the medium and respond to the electromagnetic profile of the astrophysical system, they isotropize themselves thereby making the  $(1 - \hat{p} \cdot \hat{p}')$  unimportant. This is not the case with neutrinos, therefore this term is significant for the self-interaction potential. Physically, this can be understood to imply that the test neutrino beam and the background neutrino beam can interact and refract only if their trajectories intersect or makes them to come close enough. This type of scattering can occur between neutrinos and anti-neutrinos in the background medium as well as shown in the diagrams above. As a consequence, this potential also develops dependency on the anti-neutrino population numbers and the anti-neutrino density matrix.

So this term of the Hamiltonian has the form,

$$H_{\nu\nu}(r) = \int_{\nu'} \sqrt{2}G_F N_{\nu,\bar{\nu}}(r)(1 - \vec{v} \cdot \vec{v}')(\rho_{\nu'} - \bar{\rho}_{\nu'})d\nu', \quad (2.17)$$

where  $N_{\nu,\bar{\nu}}(r)$  is a term proportional to the number density of neutrinos and anti-neutrinos in the

system, and the integration is over the momentum of the background neutrino as we consider contributions on the test neutrino, from all the scatters present in the medium.

For the general geometries of the astrophysical systems we consider, we can assume the dot product of the momentum vectors to be constituted by just the product of the cosines of the direction of the test neutrino beam and the direction of the background neutrino beam, if we assume an azimuthal symmetry along the  $z$ -axis [23][24][25]. The neutrinos for both the test and the background beams can be emitted along multiple directions and energies, leading to interactions with the test beam along multiple directions. Accordingly, we have to integrate along the possible values of energies and angles at each point in space(time) as we evolve the system. So the density matrix is now a function of energy, angle and the radial distance point along which we solve the equations,  $\rho(E, \theta, r)$ . The self-interaction term accounts for the contributions from all possible directions and energies by integrating over the angles and energies.

The polarization vectors of neutrinos and anti-neutrinos must be normalized to unity irrespective of their dependencies. The normalization factor can be different for the neutrino vector and the anti-neutrino vector and can also possess energy dependence. In literature, the normalizations are done with respect to the flux function of neutrinos and anti-neutrinos for a particular system. The self interaction term for multi-energy scenario then becomes,

$$H_{\nu\nu}(r) = \sqrt{2}G_F N_{\nu,\bar{\nu}}(r) \int (1 - \cos \theta \cos \theta') (j\rho(E, \theta') - \bar{j}\bar{\rho}(E, \theta')) d \cos \theta' dE, \quad (2.18)$$

which in the polarization vector formalism is given by,

$$\vec{H}_{\nu\nu}(r) = \sqrt{2}G_F N_{\nu,\bar{\nu}}(r) \int (1 - \cos \theta \cos \theta') (j\vec{P}(E, \theta') - \bar{j}\vec{\bar{P}}(E, \theta')) d \cos \theta' dE, \quad (2.19)$$

where  $j$  and  $\bar{j}$  are normalization terms proportional to the flux of the neutrinos and anti-neutrinos. These factors are typically functions of energy. Thus, we see that this term couples the anti-neutrino polarization vector with the neutrino polarization vector, and makes the problem non-linear. But for the majority of the thesis, we will work with single energy approximations and so the energy dependence in the self interaction terms would be relaxed and the factors  $j$  and  $\bar{j}$  can be replaced by some constants proportional to the number density of (anti-)neutrinos for the particular energy along the direction we are solving for.

The inclusion of the self-interaction term gives rise to many interesting phenomenology associated with the collective oscillations as we shall see in the following sections.

### 2.3 Equations of Motion

With the terms of the Hamiltonian discussed, we can now write down the full equations of motion to be solved. As mentioned above, we predominantly work with single energy approximation since the phenomenon of Matter-Neutrino Resonance is independent of energy.

While approaching this problem numerically, it is common to also use single-angle approximation, where we assume that neutrinos and anti-neutrinos are emitted only at a single angle. This approximation is often done with the assumption that the geometry is spherically symmetric, so that a simulation along one radial direction would be enough to explain the flavor evolution from the whole neutrino emitting body. This is called as the ‘neutrino-bulb model’ [16][23], which would be an approximation for a SN environment. But in the case of BNS mergers, the geometries are more complicated as we will see in chap. 5.

The full equations of motion for the single angle scenario, with mono-energetic neutrinos, are given by,

$$\frac{d\vec{P}}{dr} = [+ \omega \vec{B} + \lambda(r) \hat{z} + \mu(r)(\alpha \vec{P} - \beta \vec{\bar{P}})] \times \vec{P}; \quad (2.20)$$

$$\frac{d\vec{\bar{P}}}{dr} = [- \omega \vec{B} + \lambda(r) \hat{z} + \mu(r)(\alpha \vec{P} - \beta \vec{\bar{P}})] \times \vec{\bar{P}}, \quad (2.21)$$

where  $\mu(r) = \sqrt{2}G_F N_{\nu, \bar{\nu}}(r)$  and  $\lambda(r) = \sqrt{2}G_F N_e(r)$ . The factors  $\alpha$  and  $\beta$  are kept to regulate the fraction of neutrinos and anti-neutrinos in the system, they are the replacements to the energy dependent normalizations  $j$  and  $\bar{j}$ .

As we can see, the self-interaction term of the equations of motion is significantly simplified, but it still couples the equations of motion for neutrinos and anti-neutrinos. This term is significant only when the medium is neutrino rich and dense. This is the simplest form of neutrino flavor evolution that can be considered, which includes the vacuum, matter and the neutrino forward scattering contributions. It essentially makes up a coupled system of 6 ordinary differential equations, that have to be solved with respect to the distance the neutrino/anti-neutrino beams travel. If there is a range of values for the energies of  $\nu$  and  $\bar{\nu}$ , then we split that range into  $N_E$  bins and we integrate over the energies in the self interaction term of the equation of motion. This will increase the number of coupled ODEs to solve to  $6 \times N_E$ .

Without making the single angle assumption, we get a fixed range of emission angles with  $\theta \in [0, \pi]$ . We then split this range into  $N_\theta$  number of bins. For such a scenario, the equations of motion becomes,

$$\frac{d\vec{P}_i}{dt} = [+ \omega \vec{B} + \lambda(r) \hat{z} + \mu(r) \int_\sigma (1 - \cos \theta_i \cos \theta_\sigma)(\alpha \vec{P}_\sigma - \beta \vec{\bar{P}}_\sigma) d \cos \theta_\sigma] \times \vec{P}_i \quad (2.22)$$

$$\frac{d\vec{\bar{P}}_i}{dt} = [- \omega \vec{B} + \lambda(r) \hat{z} + \mu(r) \int_\sigma (1 - \cos \theta_i \cos \theta_\sigma)(\alpha \vec{P}_\sigma - \beta \vec{\bar{P}}_\sigma) d \cos \theta_\sigma] \times \vec{\bar{P}}_i \quad (2.23)$$

where the index  $\sigma$  sums over all the angular bins (angle integration) and the index  $i$  denotes the corresponding angular bin of the polarization vector. The term  $d \cos \theta$  is just a multiplicative constant with value  $\left| \frac{(\cos \theta_{\max} - \cos \theta_{\min})}{N_\theta} \right|$ . Since we do not consider the emission surface, we do not include the  $(\cos \theta_i)^{-1}$  term in the RHS of the equations of motion.

The problem gets complicated when we remove the single angle assumption as seen from Eq. (2.22),(2.23). If we have an angular dependence on  $\vec{P}$  and  $\vec{\bar{P}}$ , then we will have one polarization vector for  $\nu$  and  $\bar{\nu}$ , corresponding to each angular bin, which is indexed as  $i$  in the above equations. The other index  $\sigma$  denotes the integration index of polarization vectors over all the angular bins. Because neutrinos are neutral, the only way for them to scatter off other neutrinos is when their respective paths intersect. This introduces a geometric dependence on the equations as explained in the previous section. The directionality of the beams are governed by the  $(1 - \cos \theta_i \cos \theta_\sigma)$  term. Thus, with one value of energy, the number of coupled equations to solve in the multi-angle scenario becomes  $6 \times N_\theta$ .

## 2.4 Collective Oscillations

In neutrino dense systems, the flavor evolution undergoes many interesting phenomena, which are broadly classified as collective oscillations [26][25][27][16]. This is because in such dense systems with very high (anti-)neutrino number densities, the self-interaction term of the Hamiltonian becomes significant and since it couples all the energy modes of neutrinos together, it forces the many different neutrino vectors to undergo coherent, synchronized flavor oscillations. This is called as the ‘synchronized mode’ of collective oscillations. This is different because usually the different energy modes flavor evolve independently in the absence of the self interaction term as the vacuum term is energy dependent.

The coherence is broken at some point and the polarization vectors completely swap their signs thereby producing significant flavor transformation. This is called the ‘bipolar evolution’. But throughout the process the system conserves the Electron-Lepton Number (ELN). The distance at which the synchronization breaks into bipolar evolution is determined by how large the self interaction term is compared to the vacuum term. The presence of matter, in the case of collective oscillations neither influences the flavor evolution nor suppresses it in the single angle limit. The dependency of this phenomena is only on the magnitude of  $\mu(r)$  and the vacuum term. The system ultimately results in a state where the fluxes of electron neutrinos and anti-neutrinos swap their values with the  $x$ -flavored counterparts at some discrete energy. This phenomenon is called as the ‘spectral split’ or ‘spectral swap’ [26][23][25][28][29][30]. The effects of collective oscillations on neutrino flavor evolution have been extensively studied with respect to Core-Collapse Supernovae in the literature as it can influence the dynamics of the system [31][27][32][33][34][35].

As an example scenario, we consider the system solved in [25], to build our solver code (sec. 7.2.1). Here the system has a potential distribution of the form in Fig. 2.4. It clearly shows the distances where the system enters the bipolar regime and it also marks the distance where spectral split happens.

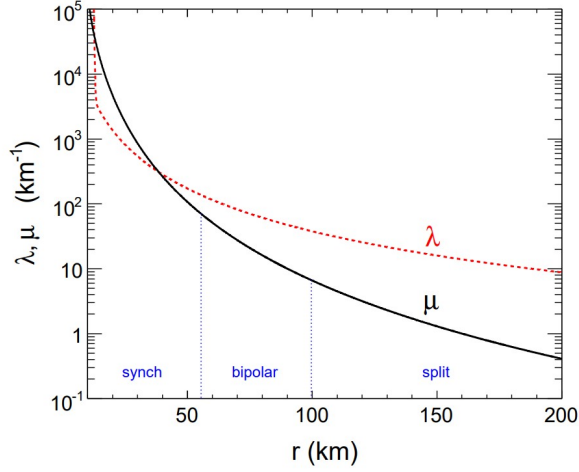


Figure 2.4: Potential profile for the system considered from [25].

The evolution of the  $z$  component of the polarization vectors is shown in the figure below,

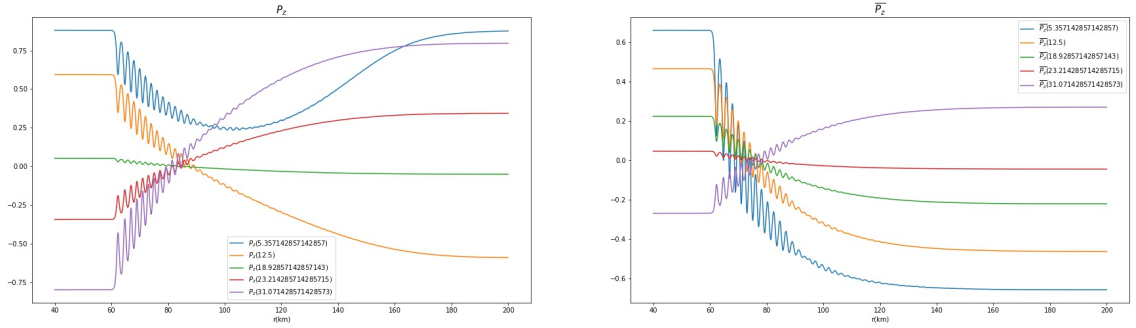


Figure 2.5: Evolution of  $z$ -component of neutrino (left) and anti-neutrino (right) polarization vectors of different energies. We can see that the blue curve in the left plot returns to its original value in the spectral split limit.

Until  $\approx 61$  km, the self interaction magnitude is high enough to sustain the vectors in a synchronized mode as seen from the figure above, where all the vectors of different energies are seen to be evolving uniformly. But once it crosses 61 km,  $\mu(r)$  enters the limits where it forces the system to undergo oscillations and sign swapping which results in flavor transformation. This is equivalent to the polarization vector nutating and flipping its orientation in the flavor space. But after  $\approx 100$  km, the oscillations fade out and the system enters the spectral split limit. This is because the bipolar regime cannot cause complete flavor transformation of all neutrinos and anti-neutrinos since the system has to conserve the electron lepton number (ELN). If the  $ELN > 0$ , then the spectral split happens for neutrinos only above a critical energy value below which the neutrinos remain in their initial flavor. But anti-neutrinos can completely flavor transform. The value of this critical energy, above which the neutrinos flavor transform, can be computed from the ELN conservation condition. For the sys-

tem considered, this value is somewhere around 7 MeV. This can be seen to be happening in Fig. 2.5 where for neutrinos the blue curve ( $\approx 5$  MeV) is seen to return to its original value while all the other curves flip their signs completely. If we plot the  $z$ -component of the energy integrated polarization vectors for neutrinos and anti-neutrinos and their difference in Fig. 2.6, we can see that the system conserves the ELN. We can also see that the anti-neutrinos completely change their orientation to the equal and opposite signed value but the same does not happen with the neutrinos.

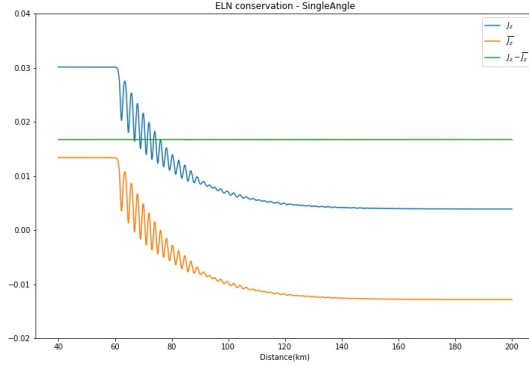


Figure 2.6: The value of  $z$ -component of the energy and angle integrated polarization vectors of neutrinos (blue) and anti-neutrinos (orange) with their difference (green) is presented. We can see that the difference is conserved throughout the distance interval.

Anti-neutrino polarization vector can always reverse its direction completely because its polarization vector is smaller than the neutrino polarization vector (when  $ELN > 0$ ) which can undergo this only to an extent. The same happens in the multi-angle scenario but the oscillations are smeared out due to interference between the various angular modes. Collective oscillations are interesting, also because they can be compared to classical oscillating systems like coupled pendulums [25][36], and the synchronized oscillations can be compared with the oscillations of spin for a system of electrons in an external magnetic field [37].

Now that we have covered the basic phenomenology of collective oscillations we can now move onto a situation where the sign of the self-interaction term is negative and opposite to that of the matter term in the next section.



## Chapter 3

# Matter-Neutrino Resonance

Matter-Neutrino resonance is one of the consequences of collective oscillations covered in the previous chapter. At distances very close to a supernova or a merger, the density of neutrinos would be very high and as previously stated, the self interaction term cannot be neglected. Neutrinos diffuse and decouple very quickly from the medium, thus the self potential decreases very quickly when compared to the matter potential. At such high densities if there are more neutrinos than anti-neutrinos in the medium, usual collective oscillations and the associated phenomena could occur. All of these only depends on how big the self potential is when compared to the vacuum term.

But when there is an abundance of anti-neutrinos over neutrinos, the self potential term is of the opposite sign to the matter term, which results in a cancellation between the matter potential and self-interaction potential when they cross each other. This cancellation creates a resonance which is called as the Matter-Neutrino Resonance (MNR). A brief but comprehensive overview of MNR is given in the following sections.

### 3.1 Matter-Neutrino Resonance in Astrophysical scenarios

Matter-Neutrino Resonance has the potential to play a very important role in the nucleosynthesis [38][39] of heavy elements in astrophysical systems like Binary Neutron Star mergers [40]. Since this phenomenon has the capacity to completely flavor transform neutrinos, certain important processes of nuclear capture responsible for the nucleosynthesis cannot happen. It is unique, because it creates an asymmetry in the flavor evolution by flavor transforming neutrinos almost completely in the single angle case [18], and partially in the multiangle case [24][41]. This process can keep happening over a large distance and happens for both mass hierarchies of neutrinos. From the previous studies, we know that certain conditions must be satisfied for the MNR to occur in astrophysical systems [18]. The conditions are listed as follows,

1. The number flux of anti-neutrinos must be greater than the flux of neutrinos. This condition is trivially understood because only then will the self-interaction term of the Hamiltonian acquire

a negative sign to cancel the matter term.

2. There should be a crossing between the matter potential and the self interaction potential and before the point of crossing we should have  $\mu(r) > \lambda(r)$ . This condition is worth understanding, which is described in the following subsection.
3. The vacuum mixing angle  $\theta_V$ , should be of suitable order for a significant MNR to occur, since for smaller vacuum mixing angles, the system will not be adiabatic enough to allow resonance to happen. In other words, it is important because by setting  $\theta_V$  we are defining how perturbed the system is when it starts. The system becomes resonant only above a certain value of vacuum mixing angle. We should also keep in mind that we cannot arbitrarily decide the value of  $\theta_V$ . It should be in accordance with the range allowed by the experimental bounds set for it.
4. The fluxes of the other flavors of neutrinos should be lesser than the flux of electron flavored (anti)neutrinos to make sure that the self interaction terms of the Hamiltonian has a significant magnitude. This is because the EOMs we evolve are for the electron flavor, if they are dominated by the other flavors then the polarization vectors  $\vec{P}$  and  $\vec{\bar{P}}$  will not be big enough to induce MNR

### 3.1.1 Theory behind Matter-Neutrino Resonance

As mentioned in the previous sections, when the Hamiltonian matrix is decomposed into a three component vector, the diagonal elements of the matrix are mapped onto the z-component of the vector, while the real and imaginary parts of the off diagonal terms become the x and y components of the vector respectively. When we write out the full Hamiltonian vector, it takes the form,

$$\vec{H} = \begin{pmatrix} \omega \sin 2\theta_V + V_{\nu\nu}^x \\ V_{\nu\nu}^y \\ \mp\omega \cos 2\theta_V + \lambda(r) + V_{\nu\nu}^z \end{pmatrix}; \text{ where } \vec{V}_{\nu\nu} = \mu(r) \int d \cos \theta (\alpha \vec{P} - \beta \vec{\bar{P}}) \quad (3.1)$$

The condition for Matter-Neutrino Resonance occurs when  $\lambda(r) + V_{\nu\nu}^z \approx 0$ . When this happens, the z-component of the Hamiltonian becomes minimum which means the off-diagonal components of the Hamiltonian matrix are much bigger than the on-diagonal terms thereby enabling flavor transformations to happen. This resonant transformation occurs very close to the source when compared to the MSW resonance, which happens at a large distance from the origin as seen from the image below where we solve the flavor equations of motion for a model potential profile.

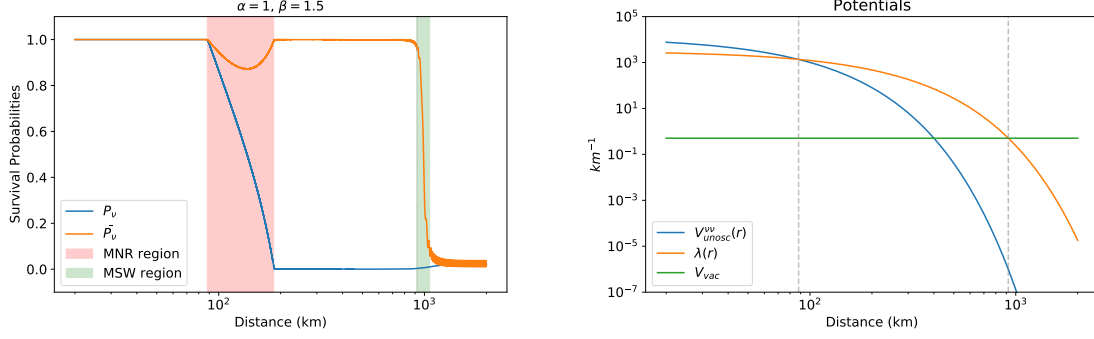


Figure 3.1: Comparison of resonance distance between MNR and MSW. In the left plot we see the survival probabilities of neutrinos (blue) and anti-neutrinos (orange) with the MNR region and MSW region highlighted in pink and green color bands respectively. We can see that MNR occurs very close to the source of neutrinos while MSW resonance happens only around  $10^3$  km. In the right plot the three potential profiles for the case the equations were solved are presented.

Although there is much left to be understood with respect to the full multi-angle Matter-Neutrino resonance, in [18], an analytical description to describe single angle MNR was attempted. An understanding of this phenomenon by drawing similarities to the well understood MSW resonance were also attempted [42]. The z-components of the flavor isospin vector [26] around the resonance region was described in [18], to be,

$$s_z \approx \frac{(\beta^2 - 1)\mu(r)^2 - \lambda(r)^2}{4\lambda(r)\mu(r)}; \bar{s}_z \approx \frac{-(\beta^2 - 1)\mu(r)^2 + \lambda(r)^2}{4\beta\lambda(r)\mu(r)} \quad (3.2)$$

where  $\beta$  is the ratio between anti-neutrinos and neutrinos, which describes the anti-neutrino excess. If we then assume  $R = \lambda(r)/\mu(r)$ , then from these expressions the survival probability for electron neutrinos and anti-neutrinos can be obtained to be,

$$P_{ee} \equiv P(\nu_e \rightarrow \nu_e) = \frac{1}{2} \left( 1 + \frac{\beta^2 - R^2 - 1}{2R} \right) \quad (3.3)$$

$$\bar{P}_{ee} \equiv P(\bar{\nu}_e \rightarrow \bar{\nu}_e) = \frac{1}{2} \left( 1 + \frac{\beta^2 + R^2 - 1}{2\beta R} \right) \quad (3.4)$$

Since this description does not take the effects of multi-angle trajectories into account, we cannot expect this to successfully describe the evolution of survival probability, for multi-angle simulations. But this does correctly describe the evolution for the single angle case as checked in the plot below.

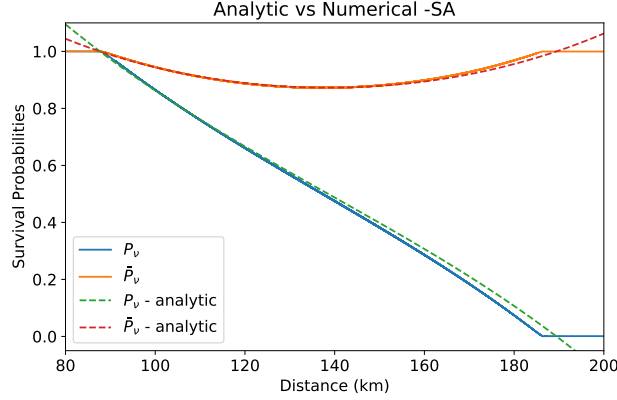


Figure 3.2: Comparison between the numerical (solid lines) and analytical solutions (dashed lines) for the evolution of survival probability for a single angle scenario. The analytic values coincides with the numerical result only within the resonance region.

We can also see that the analytical solution fits only for the resonance region while it diverges from the numerical result outside the region. The duration for which the resonance lasts is dependent on how steep the crossing between the potentials are. This duration is described to be [18],

$$\delta t_1 \approx \tau \ln \left( \frac{\beta + 1}{\beta - 1} \right), \quad (3.5)$$

where  $\tau$  is called the scale height between the potentials, with the form,

$$\tau = \left| \frac{d}{dr} \ln \left( \frac{\lambda(r)}{\mu(r)} \right) \right|^{-1}, \quad (3.6)$$

which has the slope of the potentials. For the plots of the model presented above,  $\tau \sim 63.2$  resulting in  $\delta t_1 \sim 102$  km, which coincides with the duration of MNR undergone in Fig. 3.2. The duration of the resonance is also characterized by its dependence on the vacuum mixing angle  $\theta_V$  through another timescale  $\delta t_2$  given by,

$$\delta t_2 \approx \frac{\beta}{\omega \sin 2\theta_V \langle V_{\nu\nu}^y \rangle} \quad (3.7)$$

where  $\langle V_{\nu\nu}^y \rangle$  is an average of  $y$ -component of the self-interaction potential. During the resonance,  $\delta t_1 = \delta t_2$  condition is satisfied, from which we can infer the dependence of MNR on the vacuum mixing angle, the anti-neutrino excess and the potential profiles.

The basic understanding of the flavor transformations happening during MNR is explained as follows. The resonance begins with  $\lambda(r) \simeq V_{\nu\nu}^z$ , where  $V_{\nu\nu}^z = \mu(r)(\alpha P_z - \beta \bar{P}_z)$  for notational convenience. At this point, the flavor evolution for both  $\vec{P}$  and  $\vec{\bar{P}}$  begins. But for the system to sustain the resonance, the self-interaction term should keep cancelling the matter term by staying negative. This can happen in two ways,

1.  $\beta\bar{P}_z$  term in  $V_{\nu\nu}^z$  stays large thereby maintaining the overall term negative.
2.  $\alpha P_z$  term in  $V_{\nu\nu}^z$  becomes negative by flavor transforming.

The system realizes both of these conditions to maintain the resonance for as long as possible. This ultimately results in a large flavor transformation for neutrinos and very low flavor transformation for anti-neutrinos. The system breaks out of resonance in the single-angle case only when all available neutrinos are flavor transformed, which mostly happens when  $\mu(r) \ll \lambda(r)$ .

From Eq. (3.7), we can infer that the vacuum mixing angle should be greater than a certain value to allow for the resonance. The requirement for second condition from the listing in 3.1 to be satisfied is explained as follows. In Eq. (3.6), we can see that MNR depends on the gradient of  $\lambda(r)$  and  $\mu(r)$ , but we do not necessarily see why  $\mu(r) > \lambda(r)$  is required before the crossing. The basic condition for MNR to occur is  $\lambda(r) + \mu(r)D_z \simeq 0$ , where  $D_z = (\alpha P_z - \beta\bar{P}_z)$

The crossing enables maximal flavor mixing condition to be possible as we saw above. If before crossing  $\mu(r) > \lambda(r)$  and  $\mu(r)$  gradually decreases with distance, then after crossing, the multiplicative factor can change its value to compensate for the decrease in  $\mu(r)$  by flavor transforming neutrinos and anti-neutrinos in the way described above. This sustains the resonance and continues cancellations to keep happening. But on the other hand, if  $\lambda(r) > \mu(r)$  before crossing and the value of  $\mu(r)$  keeps increasing with distance then even though the sum of potentials crosses zero, the system is not compelled to change the multiplicative factor,  $D_z$  and hence no flavor transformation happens and as a result the system does not undergo resonance. This can also be understood in terms of the adiabaticity parameter as defined in [43] where the above mentioned scenario is equivalent to the system being highly non-adiabatic thereby not resulting in any resonant phenomena.

This means that only for certain profiles of potentials with crossings and conditions satisfying those mentioned and discussed above can support this type of resonant flavor transformation.

### 3.1.2 Standard and Symmetric MNR

In the literature, there have been two kinds of Matter-Neutrino Resonance spotted so far. The type of MNR we study throughout this thesis is called as the 'Standard MNR', where the neutrinos alone flavor transform to a much greater extent when compared to anti-neutrinos. The second kind of MNR is undergone by the system which results in a complete flavor transformation for both neutrinos and anti-neutrinos equally [39],[44]. An example where standard, and symmetric neutrinos were spotted is given below, where we can see that in the symmetric MNR region, the survival probabilities drop together for neutrinos and anti-neutrinos, but in the standard MNR region, only the anti-neutrino survival probability comes back while neutrino probability stays low,

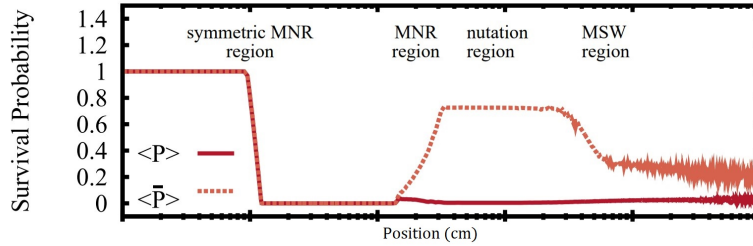


Figure 3.3: Simulation results from [44] showing symmetric and standard MNR for neutrinos and anti-neutrinos. We can see that the symmetric MNR results in a drop of survival probability for both neutrinos and anti-neutrinos.

From previous studies, it has been noted that a necessary condition for symmetric MNR to occur is that the sign of the self-interaction potential  $V_{\nu\nu}$  should turn from negative to positive [43]. This means that the system, initially dominated by anti-neutrinos should eventually enter a neutrino dominated regime. This transition is called symmetric, because this MNR occurs close to the region where the ratio of anti-neutrinos to neutrinos,  $\beta$  is around 1. But this type of MNR doesn't occur in the scenarios studied in this thesis.

## 3.2 Description of the Models studied

In this thesis, we mainly try to study two properties of MNR, the angle dependence of MNR and the influence of neutrino advection to MNR. These two checks to MNR are important as they contribute to the understanding of the validity of this phenomenon. With these conditions in our mind, we first choose a simple toy model, with constant matter potential  $\lambda$  and an exponentially decreasing  $\mu(r)$  as seen in Fig. 3.4.

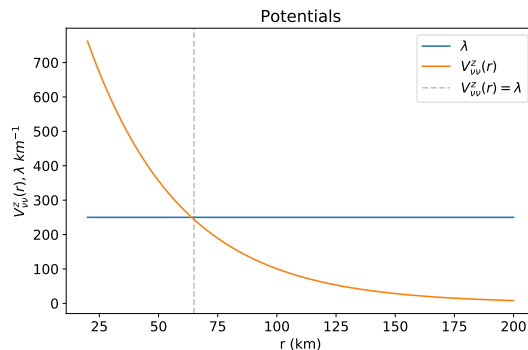


Figure 3.4: Constant matter potential and exponentially decreasing neutrino self potential with crossing around 65 km corresponding to the values in Eq. (3.8).

We model our potentials in such a way that they equivalently resemble the astrophysical environment of a Binary Neutron Star merger remnant. Thus we want both  $\lambda$  and  $\mu$  to decrease and intersect at a

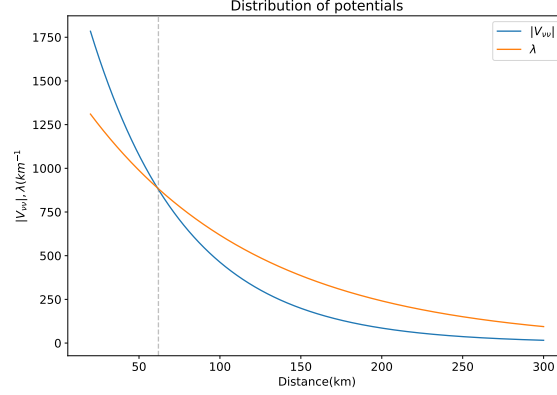


Figure 3.5: Exponentially decreasing matter and self interaction potentials with crossing around 62 km corresponding to the values in Eq. (3.9)

short distance, preferably around 50-70 km. We have chosen the matter and self-interaction potentials to be,

$$\begin{aligned}\lambda &= 250 \text{ km}^{-1} \\ \mu &= 2.53 \times 10^3 \times e^{-\frac{0.38}{15}r} \text{ km}^{-1}\end{aligned}\tag{3.8}$$

where  $\mu(r)$  starts out a high value and exponentially decreases with distance  $r$  (km).

For such a distribution of the potentials, we set  $\alpha = 1$  and  $\beta = 1.5$ , where these constants just signify the flux of neutrinos and anti-neutrinos at that particular energy. We work with  $\theta_V = 0.15$  throughout this thesis.

The second model we consider is the case where both the matter and the self interaction potentials decrease exponentially with distance as seen in Fig. 3.5. In functional form, we have chosen,

$$\begin{aligned}\lambda(r) &= 1.58 \times 10^3 \times e^{-(0.235/25)r} \text{ km}^{-1} \\ \mu(r) &= 5 \times 10^3 \times e^{-(0.253/15)r} \text{ km}^{-1}\end{aligned}\tag{3.9}$$

In the upcoming sections, we shall investigate the flavor evolution, for single angle and multi-angle scenarios and study the angle dependence of the Matter-Neutrino Resonance. We will also use the models described above to study the effects of advection to the resonance, before we move on to apply the concepts and study the robustness of the resonance using the simulation dataset of a Binary Neutron Star merger.



## Chapter 4

# Study of Angle Dependence of MNR

Angle dependence of MNR has been previously studied for neutrino bulb model, for particular angular emission ranges, and have also been investigated along trajectory dependent cases in neutron star merger scenarios before [41][24][45]. It was seen from previous studies that the inclusion of multi-angle emission and trajectories suppressed the effects of the Matter-Neutrino resonance.

Here we study the effects of different angular distributions for neutrinos and anti-neutrinos, on the results of the resonant phenomena without considering the emission surface. The cases presented in this section are,

- Angle Independent results
- Angle Dependence only on  $\vec{P}$
- Angle Dependence only on  $\vec{\bar{P}}$
- Non-uniform Angle Dependence on both  $\vec{P}$  &  $\vec{\bar{P}}$

We find that the effects of MNR are most suppressed when there is angular dependence on neutrinos. We also find that when multiangle flavor equations of motion are solved with MNR conditions satisfied, there is a drastic difference in the evolution of the survival probability between normal and inverted mass hierarchies which has not yet been reported in the literature. The results obtained in this section are included to be published in a paper which is under process.

We first look at the angle independent flavor evolution results. Then we move on to various cases in which we include angle dependence on the initial values of the polarization vectors for neutrinos and anti-neutrinos, using the Eq. (2.22) and (2.23). We look at the angular range  $\theta_0 \in [0, \pi]$ . We bin the interval into 25  $N_\theta$  bins and results are converging well for this choice.

## 4.1 Angle Independent results

### 4.1.1 Single Angle Scenario

The survival probabilities for neutrinos and anti-neutrinos for the constant  $\lambda$  and for the case where both potentials decrease with distance, with the parameters  $\alpha$  and  $\beta$  set to be 1 and 1.5 respectively are presented. The results are in Fig. 4.1,

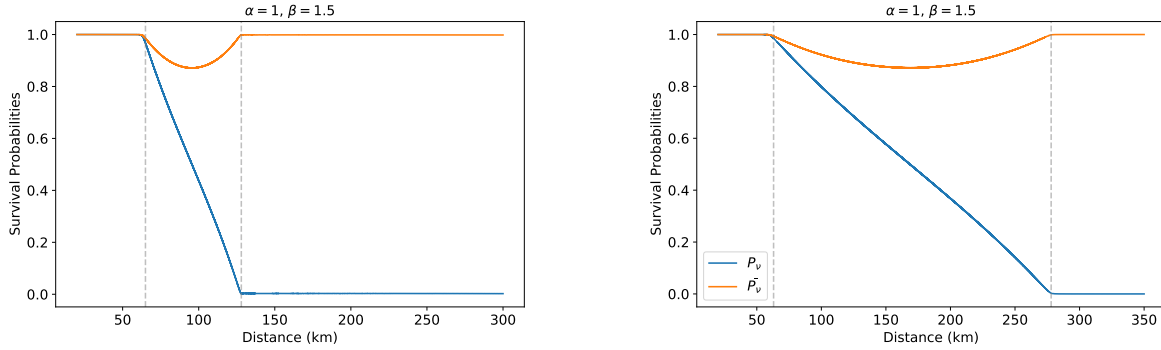


Figure 4.1: Survival probabilities of electron flavored neutrinos and anti-neutrinos for constant matter potential from Fig. 3.4 (left) and for the case where both  $\lambda$  and self interaction potential decrease exponentially with distance, from Fig. 3.5 (right)

The results presented above can be understood as follows. Since we set  $\beta > \alpha$ , abiding to the first condition to produce MNR in the listing in 3.1, we will be starting with a negative self interaction term in the Hamiltonian. The sum of the matter potential and the self-interaction potential slowly increases as  $\mu(r)$  decreases. It then gradually hits the point where self-interaction is equal and opposite sign of  $\lambda$ . At this point the sum is,

$$\lambda(r) + \mu(r)(\alpha P_z - \beta \bar{P}_z) = 0 \quad (4.1)$$

which is the Matter-Neutrino Resonance condition. This condition enables flavor transformation to happen, which is by definition asymmetric for neutrinos and anti-neutrinos in the case of MNR as described in the previous sections.

This is very evident by looking at the evolution of the sum in Eq. (4.1), for the cases presented above, in Fig. 4.2. First we look at the case with constant matter potential, and we see that the flavor evolution begins at exactly the point where the sum of the matter and self interaction potentials hit zero, and it gets stuck in resonance for around 60 km as seen in Fig. 4.2

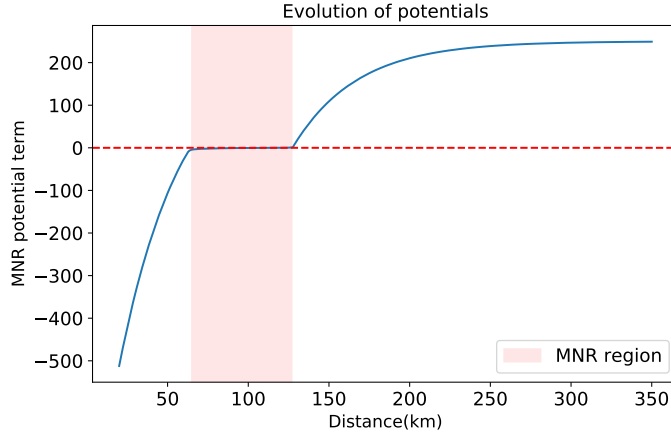


Figure 4.2: Evolution of potential sum (blue line) for the case with constant  $\lambda$ . We can see that the sum gets stuck to 0 in the pink region signifying the occurrence of MNR

The system breaks out of resonance after the survival probability of all the neutrinos drops to zero, thus resulting in a complete flavor transformation as theoretically expected.

If we now look at the case where both the potential terms are dropping exponentially in Fig. 3.5. We immediately observe that the distance where resonance is sustained is very large. This is expected because here both  $\lambda(r)$  &  $\mu(r)$  are decreasing in a very similar fashion. Thus the difference that the self potential term has to compensate for is increasing at a much slower rate when compared to the case where  $\lambda$  was a constant. Hence the system can keep sustaining the resonance for a longer time while flavor transforming  $\nu$  &  $\bar{\nu}$  at a slower rate. This is exactly realized in Fig. 4.3, where the overall result matches Fig. 4.1, but this happens at a much slower rate and for a longer distance.

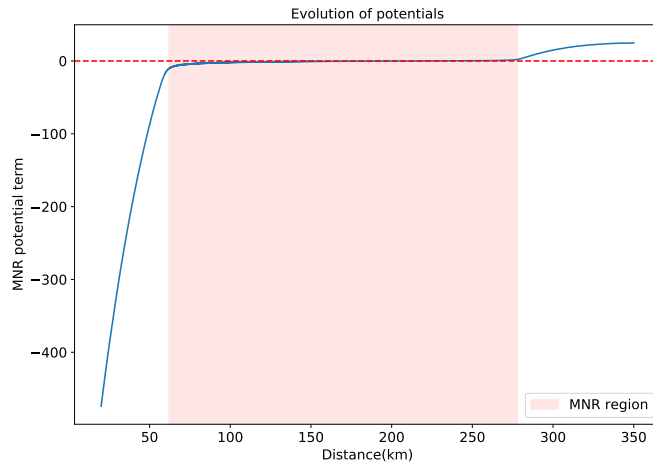


Figure 4.3: Evolution of the sum of the potentials (blue line) for the case where both  $\lambda(r)$  &  $\mu(r)$  drop exponentially with distance

We can also calculate the duration for the resonance to be sustained using Eq. (3.5) for both the cases discussed above, since we have not yet included angular dependencies on the vectors. For the constant  $\lambda$  profile, the value of  $\tau \simeq 40$  and it corresponded to  $\delta t \simeq 63.5$  km, which matches the duration of resonance in Fig. 4.2. Similarly for the case with both potentials exponentially decreasing, we get  $\tau \simeq 134$ , which results in  $\delta t \simeq 216$  km, which is seen to happen in Fig. 4.3.

Any potential distribution satisfying the conditions to produce MNR, will produce similar results in the single angle case. Complications and interesting effects arise in the multiangle case which is covered in the following sections.

### 4.1.2 Multi-angle Scenario

The survival probability for neutrinos and anti-neutrinos in the multi-angle limit but without any angle dependence looks like Fig. 4.4

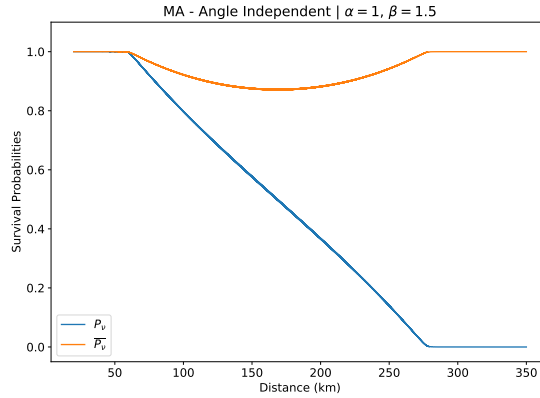


Figure 4.4: Survival probabilities of neutrinos (blue) and anti-neutrinos (orange) in the multi-angle limit without any angular dependence. We can see that it resembles the single angle result in Fig. 4.1

Since there is no angle dependence on the initial vectors, we expect the result to agree exactly with the single angle result, though there are more than one angular bins. This is because there is no distinction between them as all the bins would evolve together as a single angular bin. We see that happening in Fig. 4.5. We can also see that the results match the single angle results for the case where both the potentials are decreasing, which was presented in the previous section.

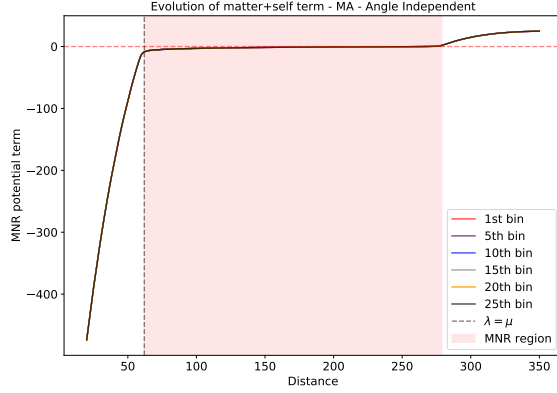


Figure 4.5: Survival probability for multiangle scenario, without any angular dependence on the initial vectors. We see that all the angular bins evolve together like the single angle case. It is reminded that we have 25 equally spaced angular bins in the range  $[0, \pi]$ .

Next we move on to include angular dependence on the vectors in the following sections.

## 4.2 Angle dependence only on $\vec{P}$

We include a forward peaked angular distribution into the initial value of  $\vec{P}$ , while  $\vec{\bar{P}}$  remains independent of angular contributions. The form of the angular distribution we choose is  $1 + x \cos \theta$  where  $\theta$  here refers to the emission angle and  $x$  is simply a constant of the range  $x \in [0.1, 1]$ . We want to study how the survival probability and the overall evolution of the the sum of the potentials terms differ, when we slowly increase the fraction of angular contribution to the initial values of the polarization vectors. We normalize the vectors such that the polarization vectors add up to 1 when integrated over the cosine of the emission angle, i.e  $\int \vec{P} \times d(\cos \theta) = 1$ , and  $\vec{\bar{P}}$  is also normalized in the same manner.

Thus the polarization vectors are initialized as,

$$\begin{aligned}\vec{P}_i &= [0, 0, 1 + x \cos \theta_i] \\ \vec{\bar{P}}_i &= [0, 0, 1]\end{aligned}\tag{4.2}$$

We increase  $x$  in steps of 0.1 to see if there are any changes in the way the angular bins evolve. We present the results for this setup applied to the potential profiles described in Fig. 3.5 below.

The survival probabilities for select values of  $x$  are plotted in Fig. 4.6. The corresponding plots that shows the evolution of the sum of the potentials term, for just three representative angles of tangential, radial and anti-tangential angular bins for  $x = [0.1, 0.2, 0.4, 0.5, 0.7, 0.9]$  in Eq. (4.2) is shown in Fig. 4.7. This should help us understand the overall behavior as all the other bins are bound between these three.

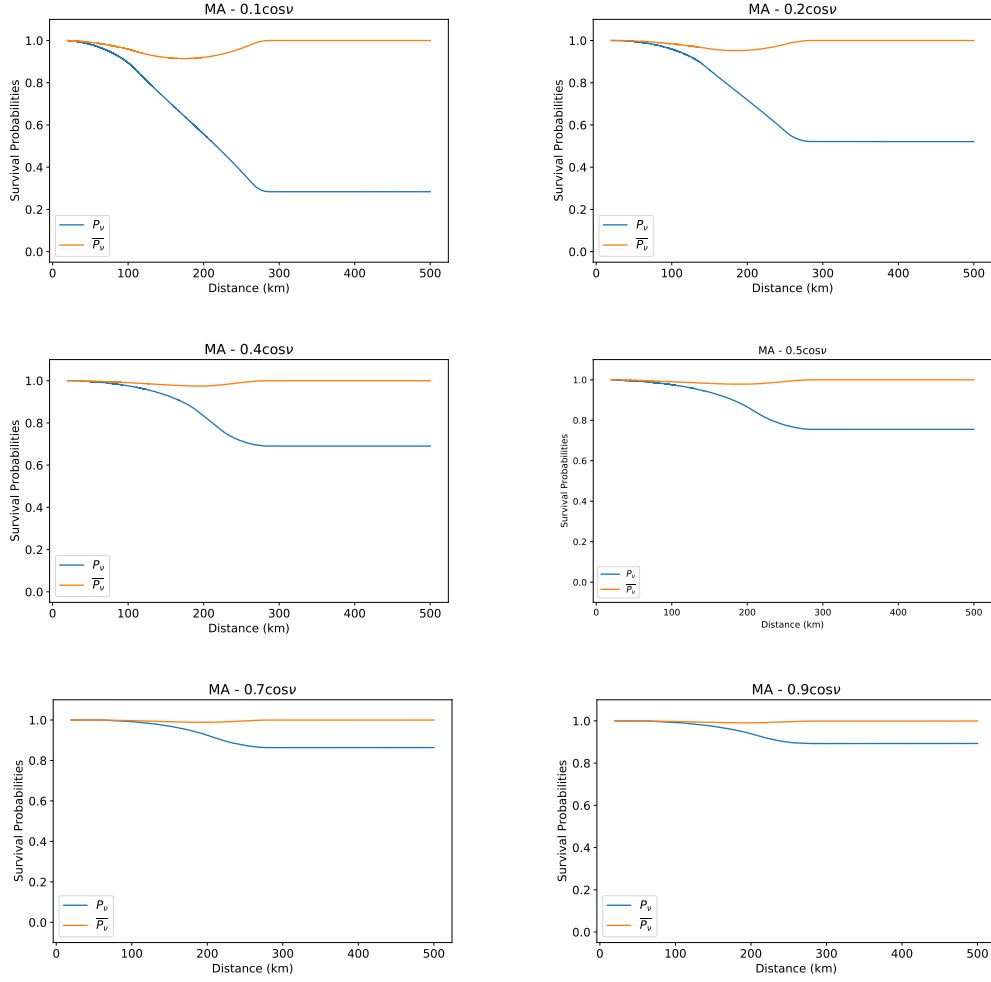


Figure 4.6: Survival probabilities with increasing angle dependence only on  $\vec{P}$ , for the cases  $x = [0.1, 0.2, 0.4, 0.5, 0.7, 0.9]$ . We can see that as the angular contribution on neutrinos increases, the flavor transformation due to MNR decreases.

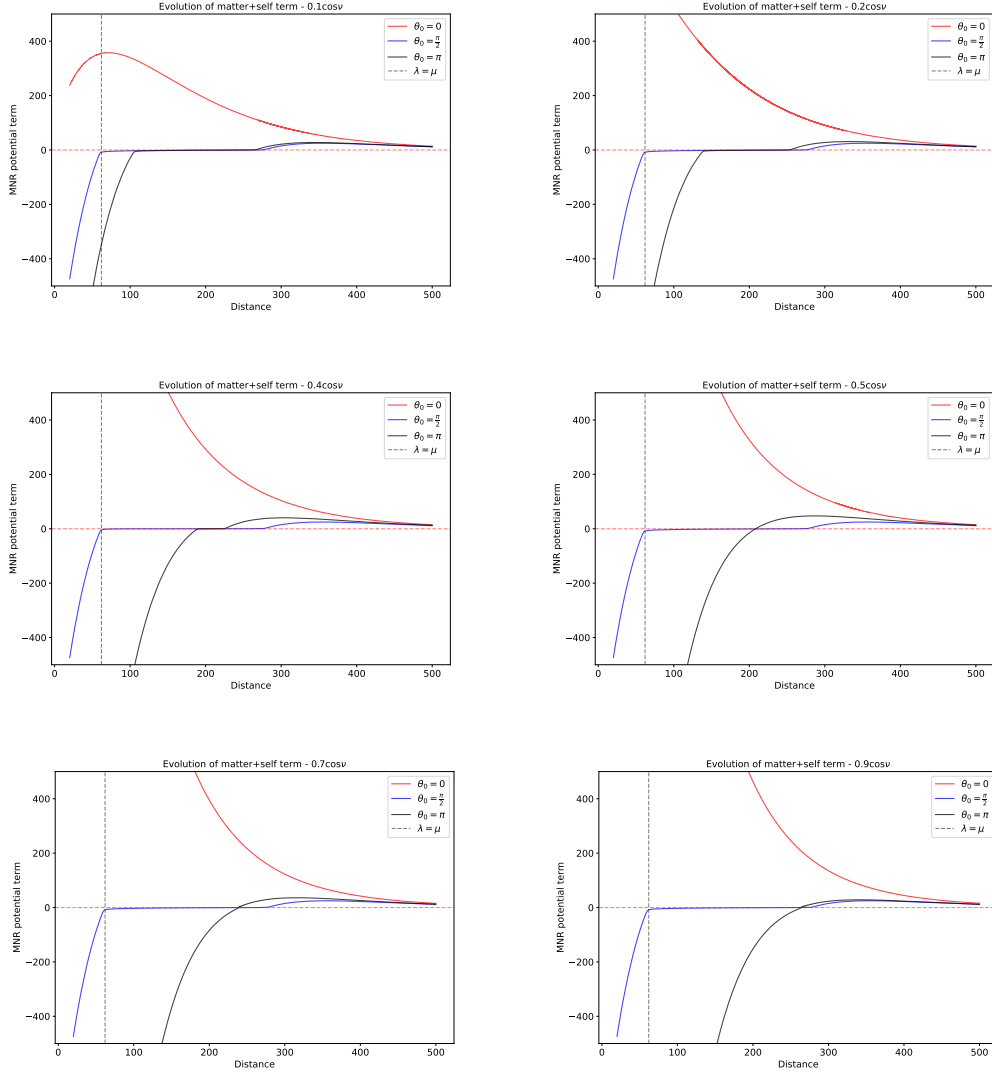


Figure 4.7: Evolution of the sum of the potentials, with angle dependence only on  $\vec{P}$  for tangential (red), radial (blue) and anti-tangential (black) angular bins with  $x = [0.1, 0.2, 0.4, 0.5, 0.7, 0.9]$  in Eq. (4.2).

To let the system reach its asymptotic steady state, we increase the simulation range from 350 km to 500 km as seen in Fig. 4.6 and 4.7. The following observations can be made by looking at the plots presented,

- We can immediately observe that the plots for survival probability looks very different, in terms of behavior compared to Fig. 4.4. We see that with increasing value of  $x$ , the effect of MNR decreases, i.e, if the neutrinos are more forward peaked then, the change in survival probability due to MNR is suppressed.
- In the evolution of the potential sum, Fig. 4.7, we observe that the order of the bins hitting the resonance is in such a way that the MNR boundary is in the front, thus the bins emitted at

$\theta_0 = 0$  hits it first while the bins emitted at  $\theta_0 = \pi$  hits it last.

- We observe that the radially emitted bin always undergoes MNR as seen in Fig. 4.7 and the tangentially emitted bin, never undergoes MNR. The bin emitted anti-parallel to the tangential bin, seems to undergo resonance for small values of  $x$ , but the distance for which it resonates slowly decreases, upto the limit where it just passes through the zero point. This lack of sufficient bins undergoing resonance would explain the rather quick decrease of MNR characteristics in Fig. 4.6.

### 4.3 Angle Dependence only on $\vec{P}$

In this section we include angle dependence only on  $\vec{P}$  while keeping  $\vec{P}$  independent. Thus we initialize the polarization vectors as,

$$\begin{aligned}\vec{P}_i &= [0, 0, 1] \\ \vec{P}_i &= [0, 0, 1 + x \cos \theta_i]\end{aligned}\tag{4.3}$$

We present the results for four values of  $x = 0.1, 0.4, 0.6, 0.9$ . The survival probabilities are shown in Fig. 4.8, while the corresponding the sum of the potentials evolution is shown in Fig. 4.9, followed by the discussion of results.

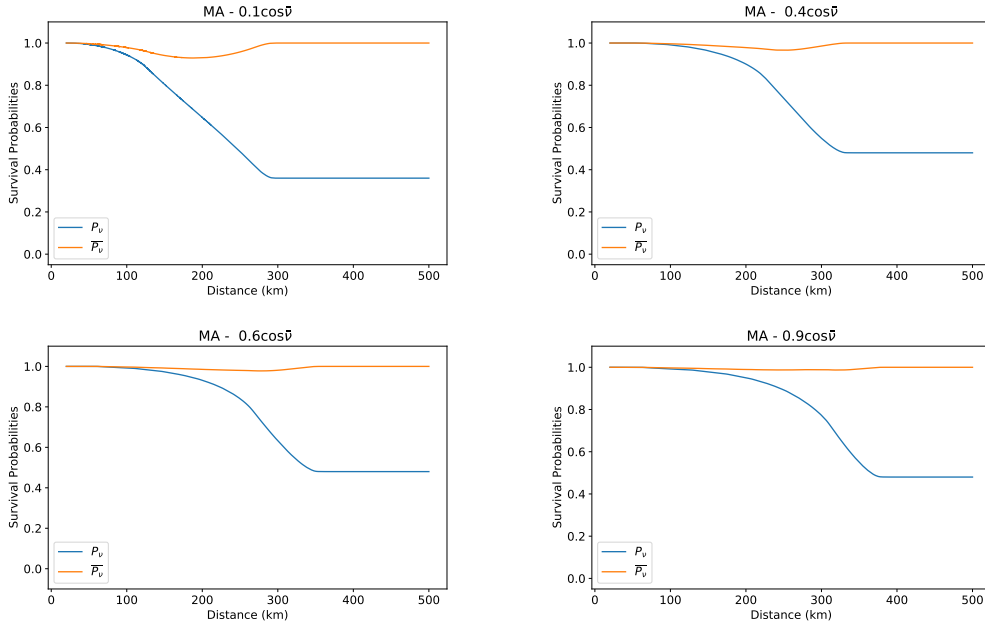


Figure 4.8: Survival probabilities with Angular dependence only on  $\vec{P}$  for cases  $x = 0.1, 0.4, 0.6$  and  $0.9$

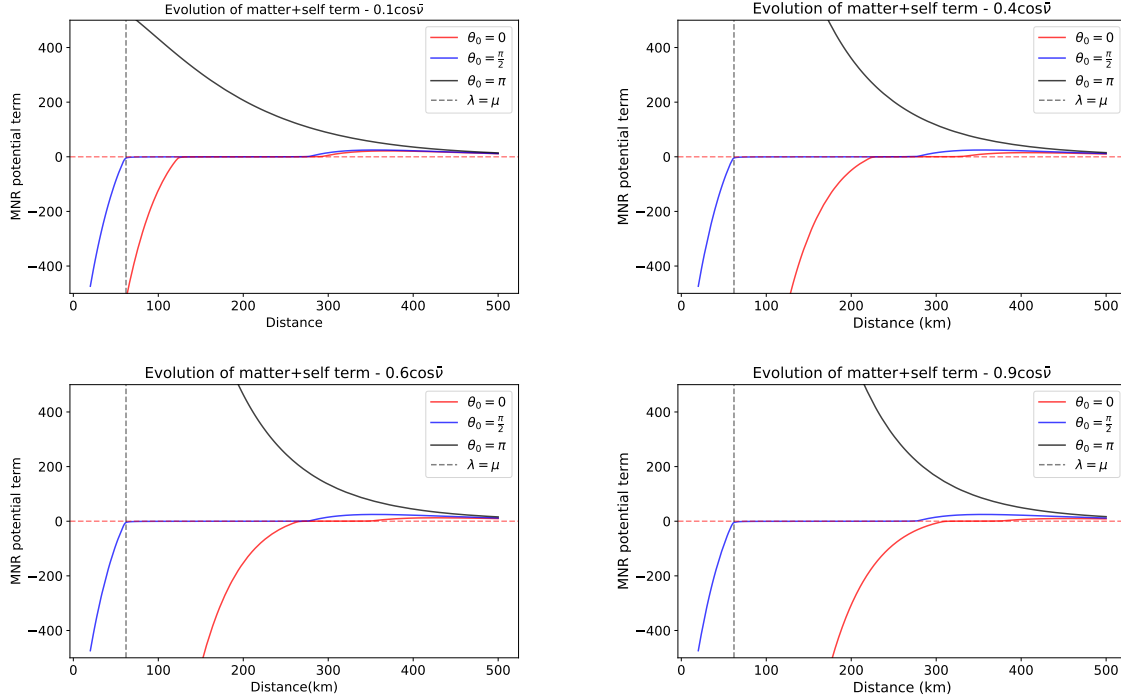


Figure 4.9: Evolution of the sum of potentials, with angle dependence only on  $\vec{P}$  for tangential, radial and anti-tangential angular bins with  $x = 0.1, 0.4, 0.6$  and  $0.9$

The following observations are made from the plots presented above,

- In Fig. 4.8, we see that there is a some significant MNR for all the cases as opposed to how it was when neutrino vectors had angular dependence, Fig. 4.6. This is substantiated by the Fig. 4.9 as well.
- With increasing angular contribution, we see that the point where the process begins keeps shifting to the right, and ultimately it starts at a much larger distance, and happens quicker than the case with less angular dependence.
- We can also see that the survival probability slowly approaches 0.5 with gradual increase in the value of  $x$ , it almost reaches 0.5 for  $x = 0.9$ .
- It is also interesting to see the resonance taking place for different angular bins at drastically different distances. Here, although the actual self interaction potential goes to zero around 250 km (since  $\mu(r)$  goes to zero around 250 km), the resonance seems to be happening well beyond that distance.
- In the plots for evolution of the sum of the potentials, we can see that the order of the bins hitting MNR boundary has reversed when compared to how it was in Fig. 4.7 as we can see that the bin emitted anti-tangentially  $\theta_0 = \pi$  hits the MNR boundary first as opposed to the bin emitted at  $\theta_0 = 0$ .

- We can also observe the way the resonance happens in all the cases and infer the reason why  $x = 0.1$  case looks more like an actual MNR result when compared to  $x = 0.9$ . This is because of the fact that at any point there are a significant number of bins undergoing MNR in the former case, while in the latter, there is a lag in between them. The distance at which the red curve hits the MNR boundary keeps shifting to the right with increasing values of  $x$ . For instance, both the tangential and radial bins are undergoing MNR in the  $x = 0.1$  case, while in for  $x = 0.9$ , there is a gap of around 10 km, between where the radial bin breaks off and the tangential bin resonates. Ultimately the last bin, also breaks off at around 380 km, which is where the flavor transformation stops happening in Fig. 4.8.

#### 4.4 Non-uniform angle dependence on both $\vec{P}$ & $\vec{\bar{P}}$

In this section we present the results for the case where we include angular dependence in ascending order of  $x$  for  $\vec{P}$  and in descending order for  $\vec{\bar{P}}$ . Thus we initialize the polarization vectors in the following way,

- $\vec{P}_i = [0, 0, x \cos \theta_i]$
- $\vec{\bar{P}}_i = [0, 0, (1 - x) \cos \theta_i]$

The survival probabilities for this case is presented in Fig. 4.10, while the evolution of the the sum of the potentials is shown in Fig. 4.11, followed by a discussion of results. We also present the zoomed in version of the evolution of potentials for select values of  $x$  and  $1 - x$  with some more additional bins in Fig. 4.12.

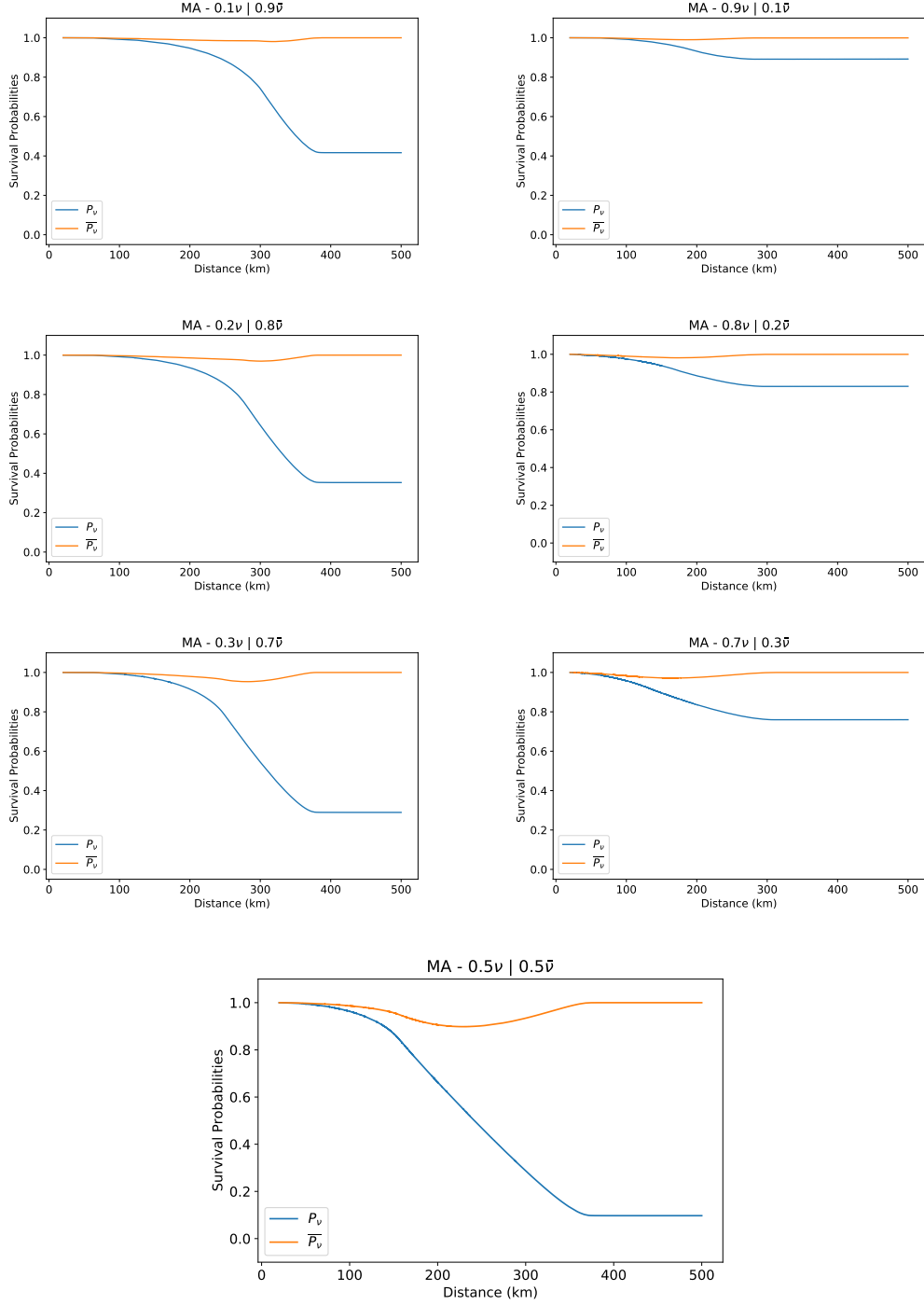


Figure 4.10: Survival probabilities for non-uniform angle dependence. The plots are arranged in a way where  $x$  and  $(1 - x)$  plots are in a single row. It starts from the left, goes till  $x = (1 - x)$  with equal angular contribution of 0.5 on both neutrinos and anti-neutrinos, then goes up on the right from it. The exact values of the angular dependence for neutrinos and anti-neutrinos are given in the plot titles as  $x\nu|(1 - x)\bar{\nu}$ . We can see that the system  $\nu$  evolves from the case dominated by angle dependence on neutrinos to the case dominated by angle dependence on anti-neutrinos.

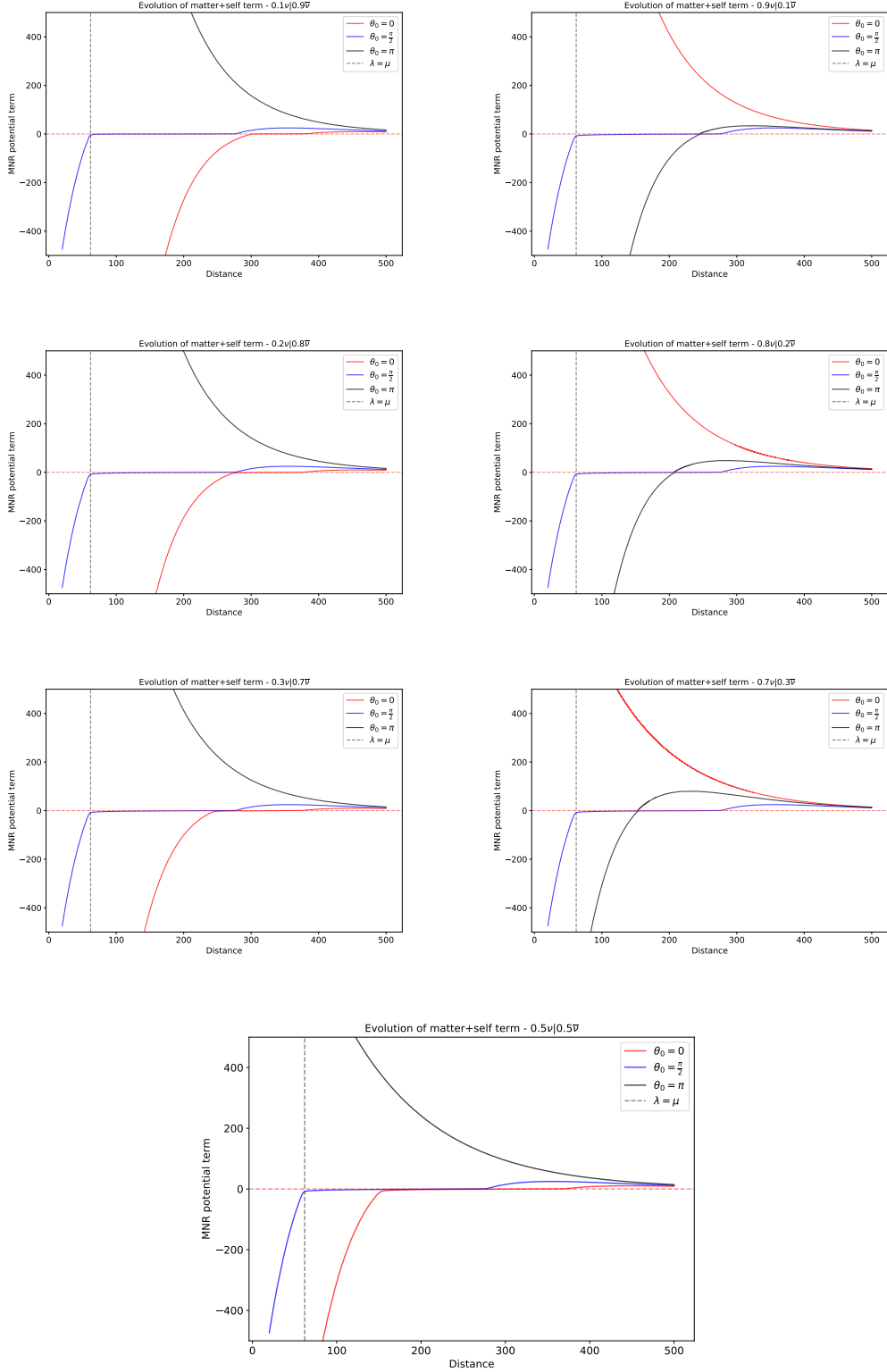


Figure 4.11: The evolution of the sum of the potentials for non-uniform angle dependence. The plots are arranged in a way where  $x$  and  $(1 - x)$  plots are in a single row. It starts from the left, goes down till  $x = (1 - x)$  at  $0.5, 0.5$ , then goes up on the right from it. The exact values of the angular dependence for neutrinos and anti-neutrinos are given in the plot titles as  $x \nu | (1 - x) \bar{\nu}$

The following observations can be made from the plots presented above,

- The Fig. 4.10 shows that there is very clear Matter-neutrino resonance happening for most of the combinations of  $x$  and  $1 - x$  except when the angle dependence is significantly large for neutrinos when compared to the anti-neutrinos. Then it starts to show the familiar decrease, which was observed in the survival probabilities in Fig. 4.6. So it can be thought of as a characteristic trend when the angle dependence on neutrinos dominates.
- We can also observe in Fig. 4.10 that there is a persistent MNR, for all the cases where the angle dependence of anti-neutrinos dominates. Looking at it sequentially, we can observe that the system starts behaving in a way similar to the model presented in Fig. 4.8, then slowly turns into behaving like the model presented in Fig. 4.6. This makes sense because the values of  $x$  and  $1 - x$  is very similar to the values studied separately in those cases.
- If we now look at Fig. 4.11, we see that all angular bins decouple from resonance before  $\approx 370$  km and there are no bins in the MNR boundary above it, for all the seven scenarios. This is correlated by where the flavor evolution stops in Fig. 4.10, which is very close to 370 km in the cases where it is distinctly seen.
- There is a swapping of the order of bins hitting MNR which is clearly seen in Fig. 4.11, where the system transitions from more angle dependence on neutrinos to more angle dependence on anti-neutrinos, by observing the black and red curves. We have plotted the curves in such a way that the swapping of red and black curves is visible, in the left and right plots of a row.
- It is also seen that although the red and black curves swap places, the bin corresponding to the black curve does not participate in the resonance anywhere. It just passes through it.
- In Fig. 4.12, some interesting cases of the behavior of angular bins are presented to observe the way the tangential and the anti-tangential bins swap places.

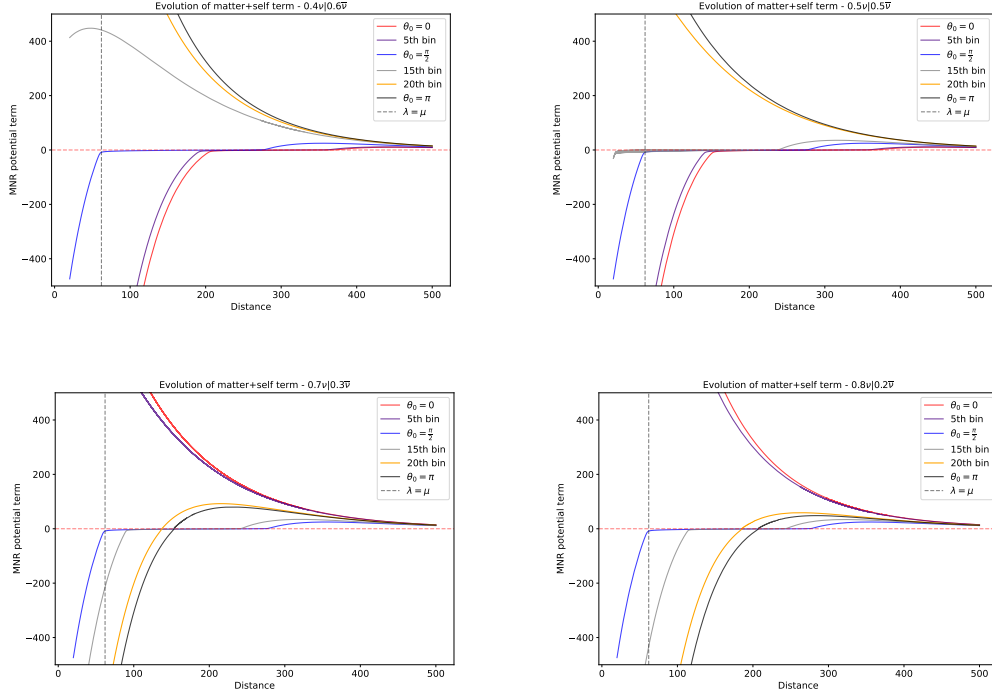


Figure 4.12: The evolution of the sum of potentials zoomed in, with a bit more bins for some select values of  $x$  and  $1 - x$

From the results presented, we can observe that in all the cases discussed so far, the Matter-Neutrino Resonance ultimately, does not affect the survival probability of anti-neutrinos. Thus interestingly, although the extent of the suppression of MNR effects brought by inclusion of angular dependence on the polarization vectors can be seen for neutrinos, the anti-neutrinos are still preserved in the original electron flavor, for all combinations of angle distributions on the initial values.

## 4.5 Comparing Normal and Inverted Mass Hierarchies

As stated in the previous chapters, neutrinos have small but non-zero masses with no one-to-one correspondence with their flavor states. Due to the minuteness of the neutrino mass, we cannot measure the individual mass states directly. Instead, we rely on the neutrino flavor oscillations to calculate the mass-squared differences. We have measured two values of the mass-squared difference [6], from solar neutrino observations and atmospheric neutrino observations but we have no means to determine the hierarchy of the three masses since we have not been able to measure the values of the individual mass states as depicted in Fig. 4.13. The hierarchy could be normal ( $m_3 > m_2 > m_1$ ) or inverted ( $m_2 > m_1 > m_3$ ). This is the neutrino mass hierarchy problem [46].

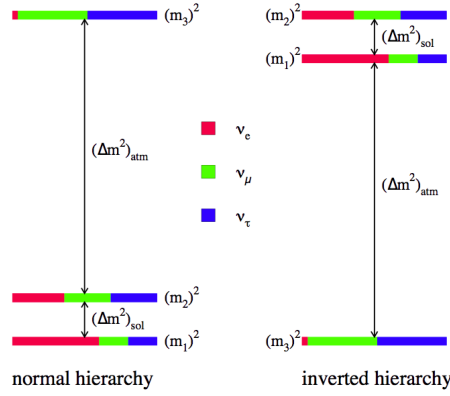


Figure 4.13: Since we have not been able to measure the individual neutrino masses, we cannot determine if the mass hierarchy is normal or inverted. This is known as the neutrino mass hierarchy problem. The mass ordering for normal and inverted hierarchy is presented in the figure. (image from Wikipedia)

Although MNR is a common resonance undergone by the (anti-)neutrinos of both mass hierarchies, there are some differences in the end result between them. In this section we study this occurrence. In [42], the flavor evolution for both hierarchies was studied in the single angle limit and there is no major difference in the survival probabilities, which matches what we find when we solve the single angle flavor equations of motion. But when we include multiangle effects with angular distributions on the polarization vectors, the inverted hierarchy shows angle dependent instabilities. The following plots were made by solving the multiangle equations of motion with  $\alpha = 1$  and  $\beta = 1.5$  for normal and inverted hierarchy. Angular dependence of the form  $1 + x \cos \theta$  is assumed, where  $x \in 0.1, 0.9$ . For angular dependence only on the neutrino polarization vector, the results look like,

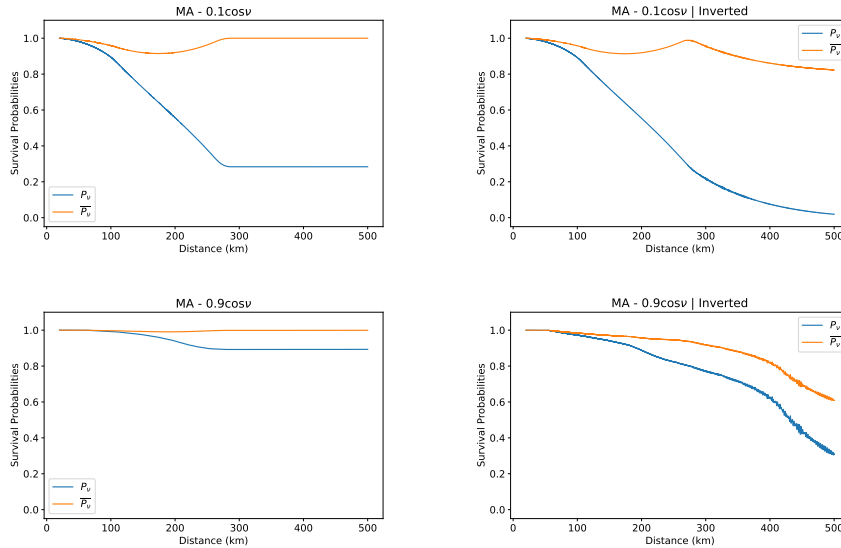


Figure 4.14: Survival probabilities with angle dependence only on  $\vec{P}$  in normal (left) and inverted (right) mass hierarchies for the minimum and maximum angular contribution i.e.  $x = 0.1$  &  $0.9$ .

For angular dependence only on anti-neutrinos, the results are,

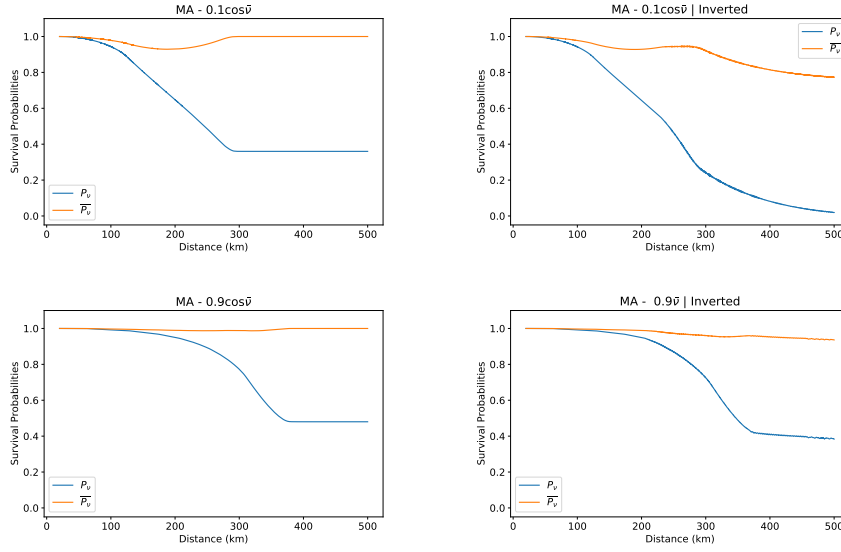


Figure 4.15: Survival probabilities with angle dependence only on  $\vec{P}$  in normal (left) and inverted (right) mass hierarchies for the minimum and maximum angular contribution i.e.  $x = 0.1$  &  $0.9$ .

As we can see, although the behavior inside the MNR region is very similar for both hierarchies, there is a distinct downward trend observed in the survival probability for the inverted hierarchy which results in a drastic difference at the end of the interval. And the effects are much more significant for the cases with angular dependence on neutrino polarization vector. To understand this better, we choose to look at the angular distribution of the polarization vectors for neutrinos and anti-neutrinos at the point where the difference kicks in between normal and inverted hierarchies, which is  $\simeq 287$  km for the case with angular dependence on neutrinos and  $\simeq 370$  km for angular dependence on anti-neutrinos.

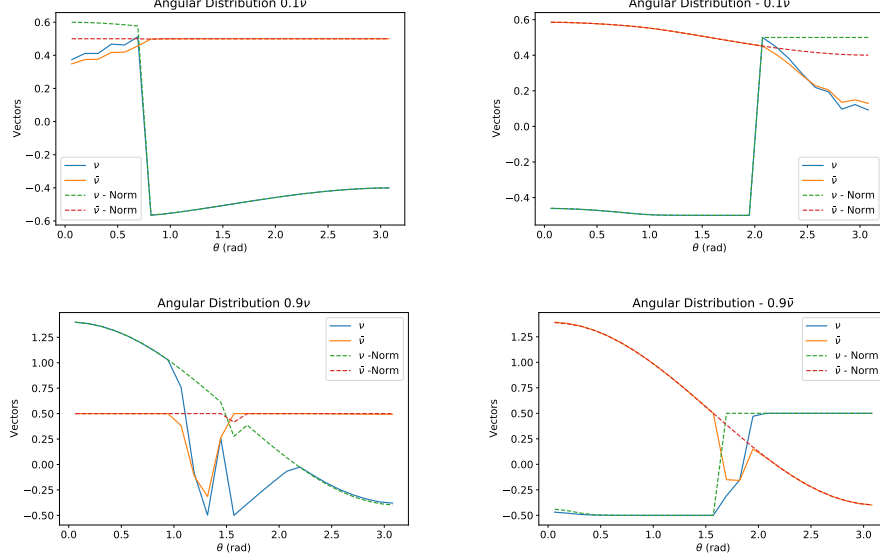


Figure 4.16: Angular Distributions of the polarization vectors at the point where the difference in flavor evolution between normal and inverted mass hierarchies kick in for the four cases discussed. The solid lines in the plots present the angular distribution for the inverted hierarchy while the dashed lines present the normal hierarchy. The cases for which the plots correspond to is given in the titles as  $x\nu$  for angular dependence on neutrinos and  $x\bar{\nu}$  for angular dependence on anti-neutrinos.

We observe that only the polarization vectors corresponding to some angles are undergoing MNR while the others are not disturbed. This is dependent on the type of angular distribution chosen for  $\vec{P}$  and  $\vec{\bar{P}}$ . We can also observe a downward trend for polarization vectors in the inverted hierarchy after a particular value of  $\theta$ . This tells us that for inverted hierarchy, the polarization vectors after MNR, seem to follow some instability that has an angular distribution. This is in agreement to what was reported in [47], where the authors point out an alternate version of what we present. They report that only the normal hierarchy can experience angle dependent instability while the inverted cannot be subjected to instabilities dependent on  $\theta$  based on Eq. 24 in the paper. Here we notice the opposite, because the scenario we study has more anti-neutrinos than neutrinos in the system which includes a Matter-Neutrino Resonance while the system studied in that paper had more neutrino abundance, which flips the effects. This result, showing angle dependent instabilities for the case with more anti-neutrinos than neutrinos in the system has not been reported in the literature so far.

Till now, we have been assuming an equivalence between the radial distance  $r$  and the time evolved  $t$ , when we solve the equations of motion, because we have been solving the equations along only one direction and since we assume relativistic neutrinos, the equivalence is valid. But in a realistic astrophysical scenario, the flow of neutrinos will not be strictly restricted along one direction. Suppose there occurs a situation where some fraction of neutrinos are flowing simultaneously in different directions with respect to the direction we evolve the system, in order to take the effects induced by those beams into account, we need to modify the flavor equations of motion. We can do this by including the advection term at the expense of the  $r$ - $t$  equivalence. This is covered in detail in the next

section.

## 4.6 Advective effects

In this section we first discuss the inclusion of advection into the flavor equations of motion and then we present the results for various model cases studied.

### 4.6.1 Motivation

Advection is an important process that is responsible for the transportation of particles in an astrophysical system. We choose to look at the effects of advection on Matter-Neutrino Resonance for two reasons, the first being that by including advection, we study the phenomena with more relevance to the actual neutrino flavor transformations happening in real-time astrophysical scenarios, the second being that although multiple studies have been undertaken to understand the fast flavor evolution and pairwise conversion phenomenon including the advective term [48][49][50][51], MNR has not been studied in detail with spatial advection. When the spatial advection is factored into the equations of motion, we can no longer apply  $r = t$  condition. The density matrices, hence the polarization vectors, become explicit functions of space and time, while  $r$  and  $t$  are independent of each other. Thus the equations of motion have to be modified. The advection operator has the form  $\vec{v} \cdot \vec{\nabla}_r$  where  $\vec{v}$  is the velocity of the particle we consider and  $\vec{\nabla}_r$  is the spatial gradient. The modified equations of motion for multiangle flavor evolution with the advection operator is given as,

$$\begin{aligned} \left( \frac{\partial}{\partial t} + (\hat{v} \cdot \hat{r}) \frac{\partial}{\partial r} \right) \vec{P}_i &= [+ \omega \vec{B} + \lambda(r) \hat{z} + \mu(r) \int_{\sigma} (1 - \cos \theta_i \cos \theta_{\sigma}) (\alpha \vec{P}_{\sigma} - \beta \vec{P}_{\sigma}^{\rightarrow}) d \cos \theta_{\sigma}] \times \vec{P}_i, \\ \left( \frac{\partial}{\partial t} + (\hat{v} \cdot \hat{r}) \frac{\partial}{\partial r} \right) \vec{P}_i^{\rightarrow} &= [- \omega \vec{B} + \lambda(r) \hat{z} + \mu(r) \int_{\sigma} (1 - \cos \theta_i \cos \theta_{\sigma}) (\alpha \vec{P}_{\sigma} - \beta \vec{P}_{\sigma}^{\rightarrow}) d \cos \theta_{\sigma}] \times \vec{P}_i^{\rightarrow}. \end{aligned} \quad (4.4)$$

For the case we consider we focus only on the flavor evolution along the radial direction, hence the ‘vectorness’ of the velocity and gradient can be dropped. The value we choose for velocity can also be simply put to be 1 since we consider only relativistic neutrinos and we work in natural units.

### 4.6.2 Advection for two beams

We select a trajectory with the potential profile shown in the Fig. 3.5 and we want to look only at two beams, moving forward and backward along that trajectory. Advection along multiple angles could influence the flavor evolution significantly but as a first step with minimal complications involved, we focus only on two angles along a trajectory.

We do this by choosing the emission angle  $\theta$  to be equal to 0 for the forward beam and  $\pi$  for the backward beam so that the cosine of these angles would equal 1 and  $-1$ . Corresponding to the (anti)neutrino flow in forward direction,  $\hat{v} \cdot \hat{r} = +1$  and backward direction,  $\hat{v} \cdot \hat{r} = -1$ . Now for neutrinos going forwards, the initial value is not going to depend on angles since it must have  $\cos \theta = +1$  for the z-component, and similarly for flow backwards,  $\cos \theta = -1$  and  $d \cos \theta$  in Eq. (4.4) becomes

unity. We also choose different values of  $\beta$  for the forward and backward beams to study the effects of advection explicitly. This would be reasonable since the anti-neutrino excess would not be exactly constant in a real astrophysical scenario, consequently the backward beam and forward beam would experience slightly different potentials. For the case with  $\beta_f = 1.5$  and  $\beta_b = 1.45$ , if we plot the matter and self interaction potentials, we can see that there are now two crossings instead of one, because the unoscillated self potential depends on the values of  $\beta$ .

There are now two different values of anti-neutrino excess, therefore the self potential of the forward beam will not intersect the matter potential at the same point where the backward beam intersects, as seen in the Fig. 4.17.

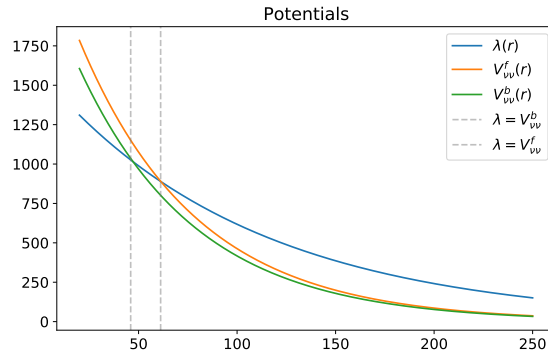


Figure 4.17: Same potential profile as Fig. 3.5, but for different values of  $\beta$ , we see two crossings corresponding to each beam.

For such a setup, when we solve the equations of motion with zero advection, we can immediately spot the two points of crossing where there is a change in the survival probability as seen in the Fig. 4.18. It resembles a MNR type conversion since the neutrinos are affected more when compared to the anti-neutrinos.

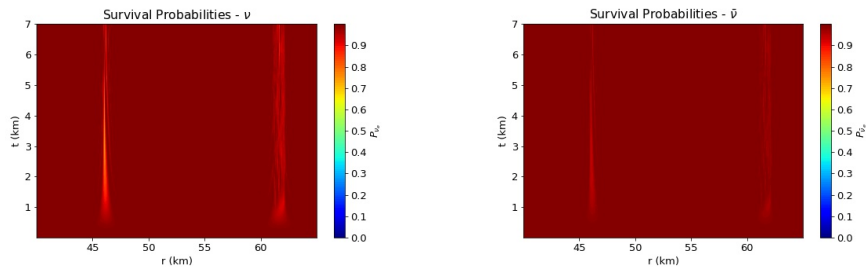


Figure 4.18: The survival probabilities for neutrinos (left) and anti-neutrinos (right) without the advective contribution are presented. The plots clearly show the two points of MNR crossings where the survival probability has decreased by a small amount but without any advection, this drop stays within the two points for the entire time interval.

We can also look at the state of the polarization vectors at the end of the simulation, and we can clearly

spot the two crossings. For an explanation of how the advection code is designed refer section. 7.2.4 of the Appendix.

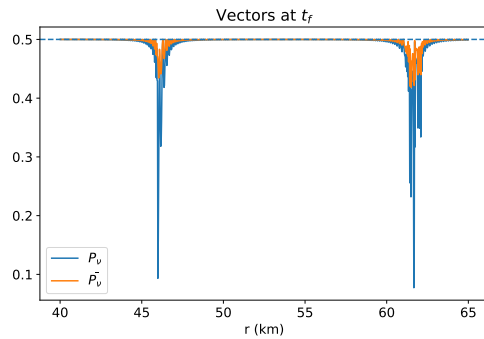


Figure 4.19: The polarization vectors for neutrinos and anti-neutrinos without advection at the end of the simulation time. This again shows the dips at the two points of crossings.

If we then turn on the advective contribution, we can then see that the advection, propagates the disturbance to a wider range of distances with increasing time, as seen in the Fig. 4.20

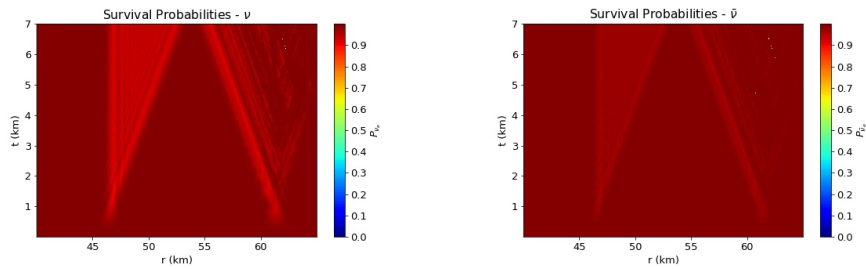


Figure 4.20: The survival probabilities of neutrinos (left) and anti-neutrinos (right) with advection. Advection makes the MNR affect more distance range with time.

To look at how much flavor transformation has occurred, we can also look at the r-bin averaged survival probability as a function of time in Fig. 4.21. We can see that although there is a trace of MNR, its effects are severely suppressed with the inclusion of advection.

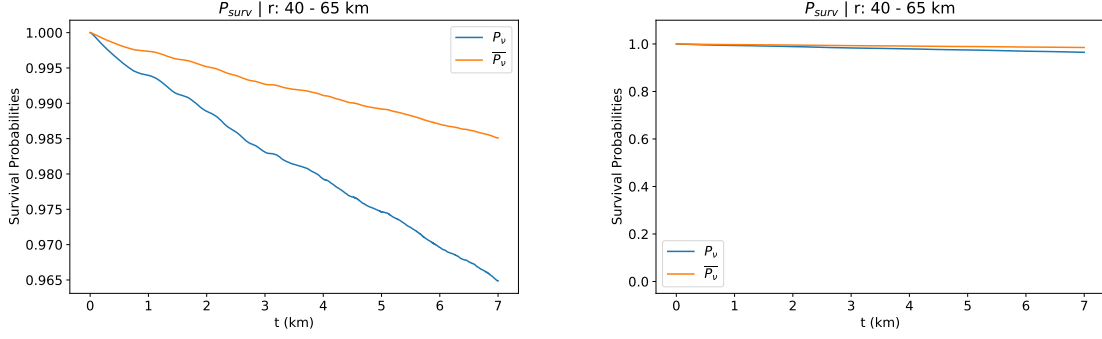


Figure 4.21: r-bin averaged survival probability (right) as a function of time, with an enlarged version (left), for the potentials described in Fig. 4.17.

We can also look at various combinations of values of  $\beta_f$  and  $\beta_b$ . In all the cases studied it was noted that the advection moves the disturbance in the direction with a lesser anti-neutrino excess as seen from the figures below where we plot the angle integrated polarization vectors for neutrinos and anti-neutrinos for the initial state and the final time snapshot.

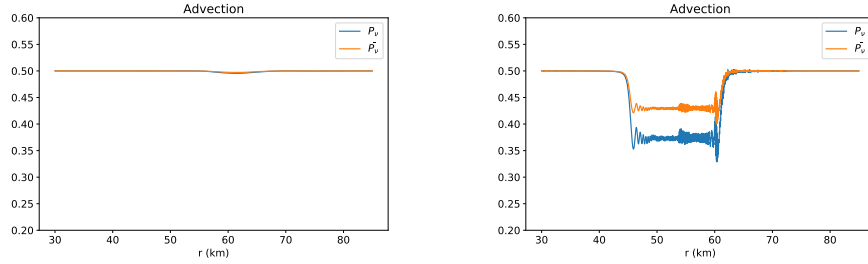


Figure 4.22: The polarization vector configuration in the initial state (left) and the final state (right) are presented. For  $\beta_f = 1.5$  and  $\beta_b = 1.25$ , we see that advection moves the disturbance backwards.

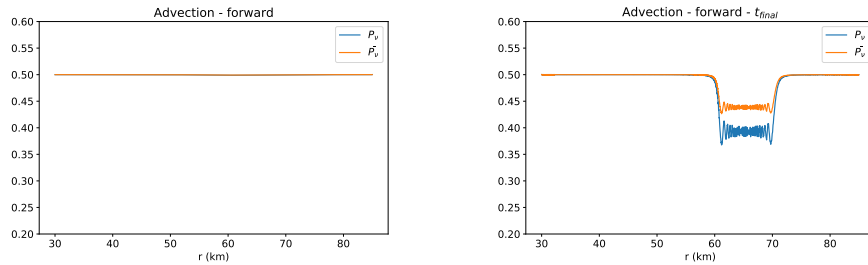


Figure 4.23: The polarization vector configuration in the initial state (left) and the final state (right) are presented. For  $\beta_f = 1.25$  and  $\beta_b = 1.5$ , we see that advection moves the disturbance forwards.

Now we move on to look at the potential profile with a constant matter potential described in Fig. 3.4. We can set the values of  $\beta$  for forward and backward beams to be similar but functions of the distance, as seen in Fig. 4.24, so that they have their MNR crossings close to each other. We solve the

equations, in a very similar way as before with first solving it without the advective contribution to spot the crossing points and then including the advection. It results in a very slight change in survival probability but it produces a result that fits the trend we expect as shown in the Fig. 4.25

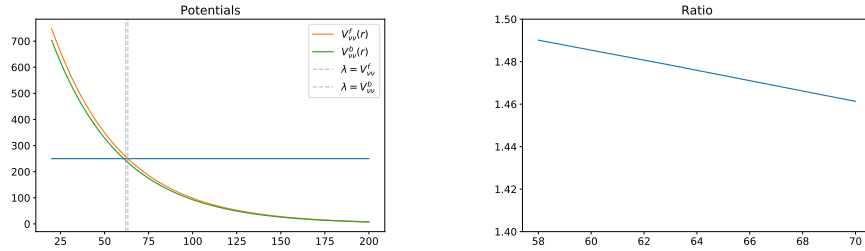


Figure 4.24: Potentials described in Fig. 3.4 but with two beams with crossings close to each other (left) and the ratio of anti-neutrino number density to neutrino number density for the region close to the crossings (right).

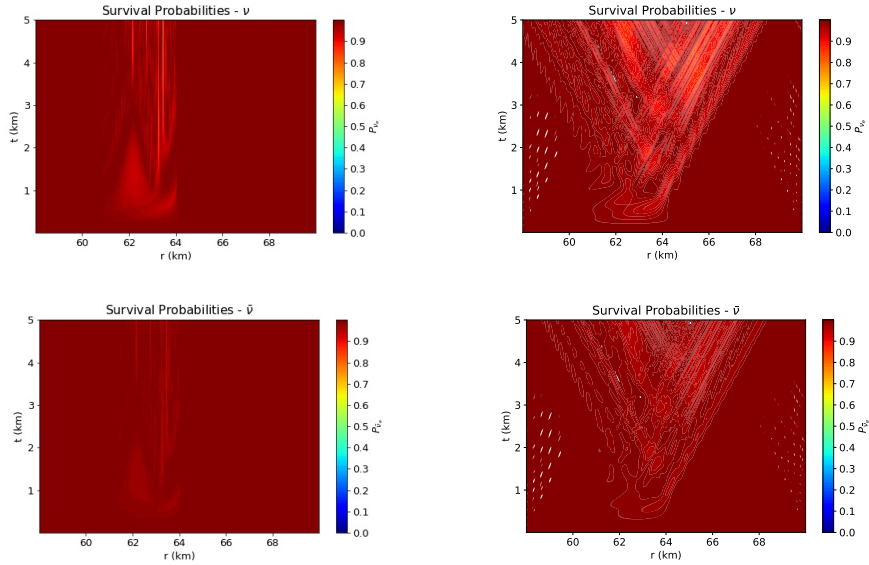


Figure 4.25: Heatmaps presenting the change in the survival probability for neutrinos and anti-neutrinos with (right column) and without (left column) advection as a function of distance  $r$  and time  $t$  for the potential profile in Fig. 4.26

Even we if we choose a different kind of potentials and ratios, with a larger MNR region and crossings being indistinguishably close, we see very similar results.

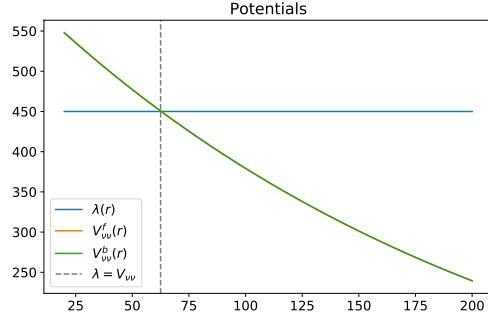


Figure 4.26: Potentials described in Fig. 3.4 but with two beams with crossings close to each other and the ratio of anti-neutrino number density to neutrino number density for the region close to the crossings.

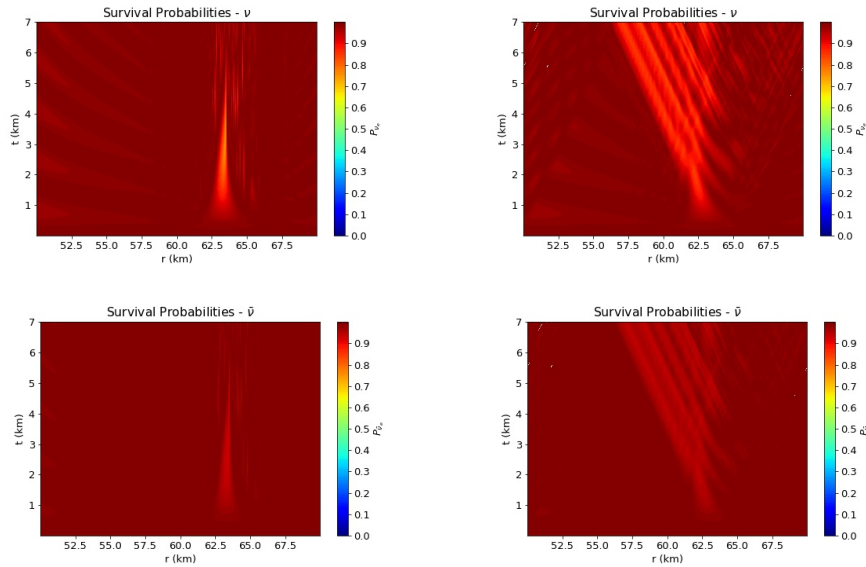


Figure 4.27: Heatmaps presenting the change in the survival probability for neutrinos and anti-neutrinos with (right column) and without (left column) advection as a function of distance  $r$  and time  $t$ .

From looking at Fig. 4.26, we can see that if the profiles of the self potentials and  $\lambda(r)$  were swapped, so that the self potential remains constant while the matter potential exponentially decreases from a larger value, there would be no MNR if we solve the equations with increasing distance, i.e from left to right of the plot. But if we solve the equations in the other way, i.e from right to left, the conditions required for MNR to occur would be satisfied thus producing an MNR. We have checked individually without advection if an MNR occurs when solved in the reverse direction.

So for such a setup, we solve the equations including the advective term with two beams moving in opposite directions to see if we get any interesting results. But as shown in the figures, we do not see any signs of MNR occurring. One possible explanation for the lack of MNR would be because the

dependency of the Hamiltonian for the forward beam, is entirely on the backward beam evolution and vice-versa, due to the  $(1 - \cos \theta \cos \theta')$  in the equations of motion. Thus the dependency matrix for the case took the form,

$$\begin{pmatrix} & \text{Forward} & \text{Backward} \\ \text{Forward} : & 0 & 2 \\ \text{Backward} : & 2 & 0 \end{pmatrix}$$

The evolution gave MNR in the previous case when evolved without advection because there was only one beam and the Hamiltonian depended only on itself.

To test if changing the dependency resulted in a different output, we changed values of  $\theta$  for both beams thereby effectively changing the beam direction in which case the dependency matrix looked like,

$$\begin{pmatrix} & \text{Forward} & \text{Backward} \\ \text{Forward} : & 0.708 & 1.433 \\ \text{Backward} : & 1.428 & 0.36 \end{pmatrix}$$

As it can be seen, the dependency is still highly swapped for the forward and backward beams but there is also a slightly significant contribution from the corresponding beam evolution as well.

When solved for such a setup, again there was no sign of MNR occurring anywhere, as seen in the figures below.

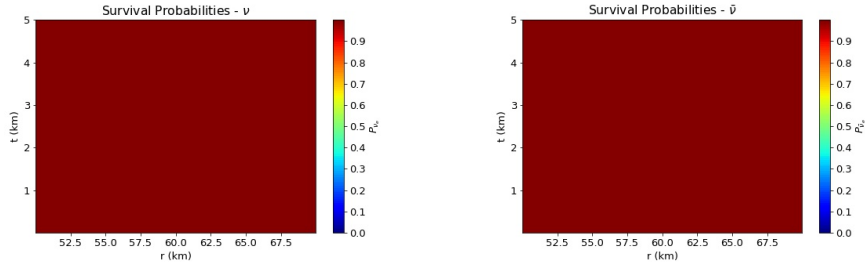


Figure 4.28: No signs of MNR even after changing the dependencies as seen from the survival probabilities for neutrinos (left) and anti-neutrinos (right).

This could mean that the flavor equations of motion become incompatible with the MNR conditions irrespective of the dependencies for the beams if  $\lambda(r) > V_{\nu\nu}(r)$ . This result is significant because such a potential occurs in the Binary Neutron Star Merger scenario studied in the following section.

## 4.7 Summary

In this chapter, we have studied the angle dependence of Matter-Neutrino Resonance by assuming a forward peak angular distribution which we applied to the neutrino and anti-neutrino polarization vector and we observed that the effects of MNR are indeed suppressed when multiangle effects are included, which is in accordance with what is reported in the literature. In particular we observed that the suppression of MNR was most significant for the case with maximum angular contribution to the neutrino polarization vector. We also observed the difference in the flavor evolution between normal and inverted mass hierarchies in the context of MNR, which occurs only when multiangle effects are included. In addition, we also checked the effects of advection on MNR, for the first time, by assuming a two-beam system along a particular trajectory with the potentials profiles defined in chapter 3. It was observed that inclusion of advection makes the effects of MNR almost negligible which makes us question the occurrence of MNR in realistic settings.



## Chapter 5

# Binary Neutron Star Merger Data

All compact binary mergers are interesting in their own respects but we focus on NS-NS merger. NS-NS mergers are highly complicated in their geometries and are quite unique in their emission properties [12],[10].

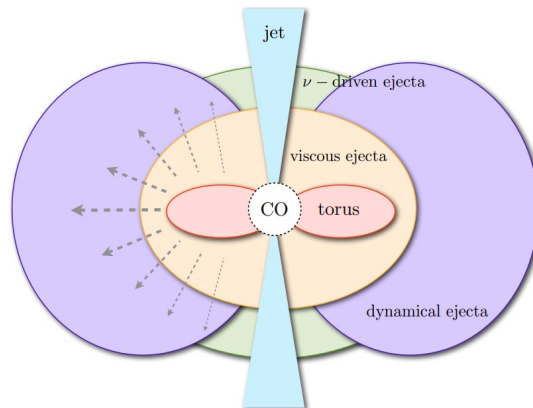


Figure 5.1: Emission schematic for a Compact Binary Merger taken from [40]

Compared to the supernova case discussed in the earlier sections, this is a totally unique astrophysical scenario because of the abundance of neutrons in the region surrounding the remnant. This makes Binary mergers a valid location for the production of elements heavier than Iron as it requires a neutron rich medium. The process by which the heavy element production happens is theorized to be r-type nucleosynthesis which is viable to occur in the equatorial disk regions of the remnant. This process of nucleosynthesis involves rapid capture of neutrons in the medium (hence the name r-type) and converting it into protons. This 'protonization' completely depends on the neutrino abundance in the medium since the weak process corresponding to it cannot happen without neutrinos of the correct flavor.

Binary neutron star mergers are also an important site to study the phenomenology of neutrino fla-

vor evolution with non-negligible contributions from the self-interaction of neutrinos due to the ample neutrino and anti-neutrino number densities. It also offers a unique scenario where due to the abundance of neutrons and protonization taking place, the emission is dominated by anti-neutrinos, which has a smaller decoupling radius when compared to neutrinos. This is important because it immediately makes the self interaction potential negative thereby creating many possibilities of Matter-Neutrino Resonance to occur and as we have seen in the previous sections, MNR has the capacity to completely flavor transform neutrinos which could significantly impact the r-type nucleosynthesis of heavy elements [52],[53]. Thus it becomes significant to understand the flavor evolution of neutrinos through the various potentials in the media. The emission timescales and geometries are also interesting as seen in Fig. 5.1 where the dynamical ejecta is followed by  $\nu$ -driven ejecta and finally the viscous ejecta is emitted from the accretion disk. The geometry of the system is toroidal as opposed to almost spherical geometries for Core-Collapse Supernovae.

In this thesis we study the possibilities of the occurrence of MNR along with the effects it creates in the vicinity of the neutrino and anti-neutrino decoupling region. We use the data sets from the results for a hydrodynamical simulation of a binary Neutron Star merger remnant for three different time snapshots of 10-ms, 20-ms and 50-ms. The simulation data used in this thesis corresponds to one of the models (M3A8m3a5) presented in [52], which as described in the paper to be the simulation result of one  $1.1 M_{\odot}$  NS and  $2.3 M_{\odot}$  NS, producing a  $3 M_{\odot}$  Black-Hole remnant with dimensionless spin parameter 0.8 and accretion torus mass  $0.3 M_{\odot}$ . The data set contained the values for 12 different parameters along 172 angular points and 428 radial distance points. (data shape -  $428 \times 172 \times 12$ ). Out of which the first six and the last six angular bins were redundant so the data was reshaped accordingly, the final shape was  $428 \times 160 \times 12$ . After reshaping, the angular bin distribution was from  $\theta = [0, \pi]$ . The radial distance spanned from 8 km to 28000 km. The distances focused in this thesis is only till around 300 km which encloses the neutrino decoupling regions.

The 12 different parameters are listed below,

- Radial Distance (cm)
- Polar Angle (rad)
- Mass Density ( $\text{g}/\text{cm}^3$ )
- Neutrino number density ( $1/\text{cm}^3$ )
- Anti-Neutrino number density ( $1/\text{cm}^3$ )
- Neutrino Number flux along radial direction ( $1/\text{cm}^2/\text{s}$ )
- Neutrino Number flux along angular direction ( $1/\text{cm}^2/\text{s}$ )
- Anti-Neutrino Number flux along radial direction ( $1/\text{cm}^2/\text{s}$ )
- Anti-Neutrino Number flux along angular direction ( $1/\text{cm}^2/\text{s}$ )
- Temperature (MeV)

- Electron chemical potential (MeV)
- Electron fraction

respectively.

## 5.1 Calculation of Potentials

We can calculate the matter and the self interaction potential using the following quantities from the dataset directly as explained below.

- Mass density  $\rho(r)$
- Neutrino number density  $N_\nu(r)$
- Anti-neutrino number density  $N_{\bar{\nu}}(r)$
- Electron Fraction  $Y_e(r)$

While keeping the dimensions of units in mind, the formulae we use to calculate the potentials is described in the following section.

### Matter Potential $\lambda(r)$ :

The dataset contains the mass density and the electron fraction so we can take the following information to calculate the matter potential,

- $\sqrt{2}G_F = 6.422 \times 10^{-43} \text{ km}^2$ ,
- Mass Density  $\rho(r) = F(r) \times 10^{26} \frac{\text{g}}{\text{cm}^3}$ ,
- Electron Fraction  $Y_e(r) = \left( \frac{n_e}{n_p + n_n} \right)$ ,

where  $F(r)$  is some function for the value of mass density at each radial point,  $G_F$  is the Fermi constant,  $n_e$ ,  $n_p$ , and  $n_n$  are the number of electrons, protons and neutrons in the medium. But since neutrinos interact specifically only with electrons we need to convert the mass density into baryon number density so that the product  $n_B Y_e$  gives the number of electrons required for the matter potential.

To convert the mass density into baryon number density we simply divide the mass density  $\rho(r)$  by the mass of a nucleon. We choose the mass of the proton as our divisor. Choosing to use the mass of the neutron does not change the result since the mass of a neutron is almost equal to the mass of a proton. Thus,

$$n_B(r) = \frac{\rho(r)}{m_p} \quad (5.1)$$

Hence the matter potential in our case becomes,

$$\lambda(r) = \sqrt{2}G_F n_B(r) Y_e(r) \quad (5.2)$$

**Self Interaction Potential  $\mu(r)$ :**

To calculate the self interaction potential, we just use the same Fermi constant as above and we use the neutrino and anti-neutrino number densities directly from the data as they are in the desired units of  $1/\text{Length}^3$ . With the neutrino and anti-neutrino number densities  $N_\nu(r)$  and  $N_{\bar{\nu}}(r)$  from the dataset, we can directly calculate the self interaction potential to be,

$$\mu(r) = \sqrt{2}G_F(N_\nu(r) - N_{\bar{\nu}}(r)). \quad (5.3)$$

But since this difference can be negative, we usually work with the absolute value of this quantity.

## 5.2 Spatial distribution of potentials

Now that we know how the parameters appear we can use the formulae to calculate the relevant potentials. First, we look radially outwards from the centre of the merger remnant, hence we plot the potentials in the polar coordinates,  $R, \theta$ . For the three data sets of 10-ms, 20-ms and 50-ms snapshots, the matter potential  $\lambda$ , the modulus of neutrino self potential  $\mu$  and sum of the two looks like,

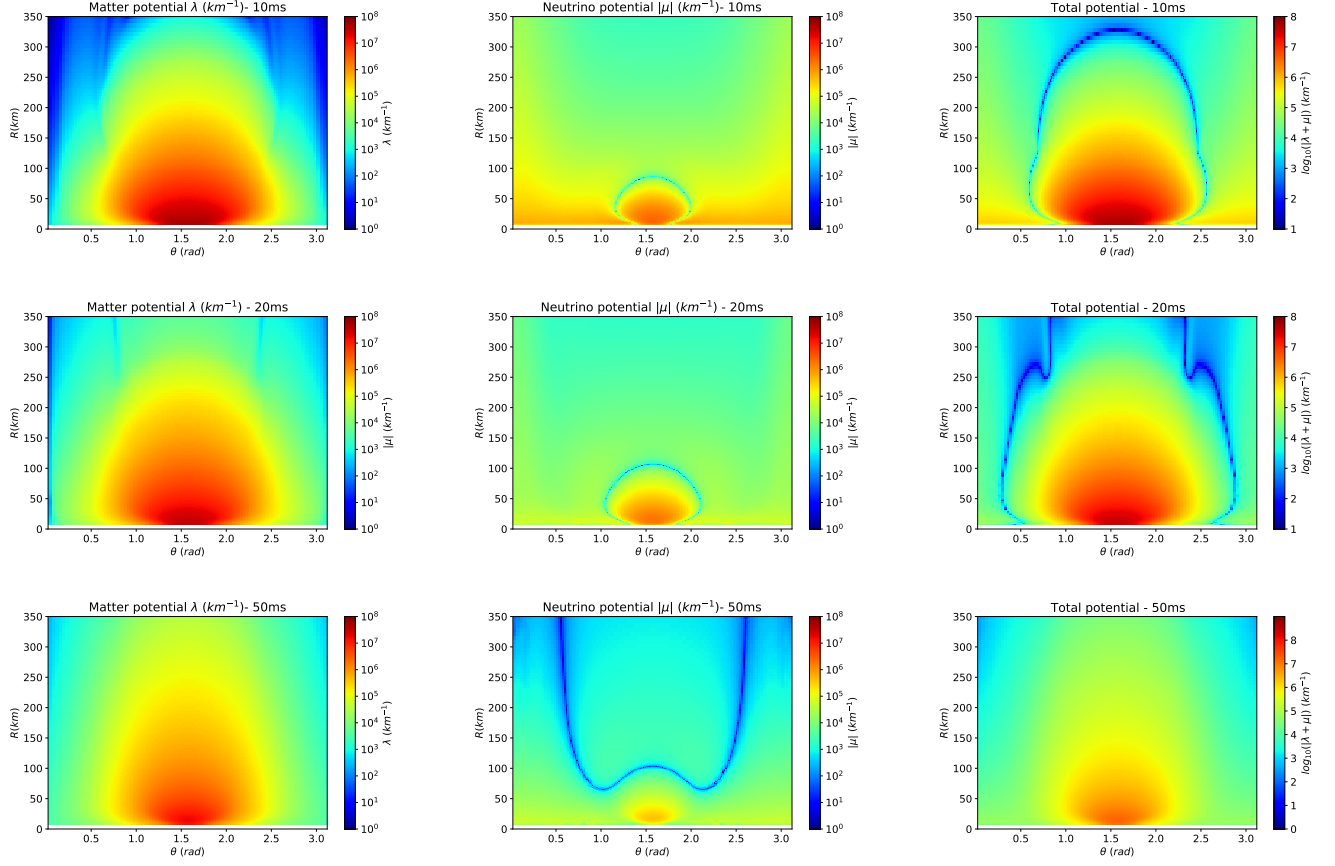


Figure 5.2: The potentials  $|\mu(r)|$  (middle column) and  $\lambda(r)$ (left column) along with the total potential  $|\mu(r) + \lambda(r)|$  (last column) for the three snapshots, where  $\lambda(r), \mu(r)$  have been explained in the previous sections. The blue and cyan surfaces in the middle column shows the boundary separating regions which are neutrino-dominated from the regions which are anti-neutrino dominated. The blue spots on the cyan boundary in the last column signifies the points where there is a cancellation between  $\mu(r)$  and  $\lambda(r)$ .

It can be seen from the contours of the matter potential that with increasing time, more matter is getting dispersed outwards. For the 10-ms snapshot, most of the matter is concentrated close to the merger remnant and also is highly dense in the equatorial region. But for 20-ms and 50-ms, the whole contour is glowing which confirms that the matter has been dispersed to greater distances.

The blue(cyan) contours in the second column signifies the boundary separating the regions which are neutrino-dominated from the regions dominated by anti-neutrinos. We can see that this boundary is compactly bound around the equatorial region at the early time snapshots before it expands in both the radial and the angular directions as it can be inferred from the 50-ms snapshot.

The distinct cyan surfaces with blue spots in the last column of the figures above signify the points where there is a cancellation happening between the neutrino self potential and the matter potential. These are the points where MNR could occur. It can be seen that there are no MNR points for the 50

ms snapshot as the matter and self potentials do not cancel in the radial distance range we are looking at. But there are potential cancellation points in both 10ms and 20 ms snapshots. The cancellation surface expands along the  $\theta$  axis and the  $R$  axis from 10-ms to 20-ms. For 50-ms, it is nowhere to be seen.

This cancellation is not sufficient to produce Matter-Neutrino Resonance as  $|\mu(r)|$  is not the whole self interaction term. The cancellation should happen between  $\lambda(r)$  and  $|\mu(r)(1 - \beta(r))|$ , where  $\beta(r)$  is the ratio of anti-neutrino number density to the neutrino number density. This basically signifies the anti-neutrino excess. MNR occurs only if  $\beta(r) > 1$  because only then the self term is negative.

If we now call  $V_{eff} = |\mu(r)(1 - \beta(r))|$ , then the contours for the sum of  $\lambda(r) + V_{eff}(r)$  for the three snapshots are given below.

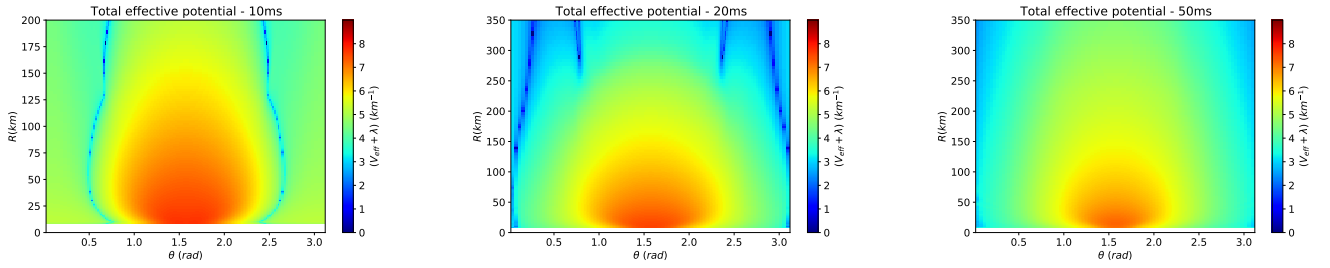


Figure 5.3: The log of effective potential  $|\mu(r)(1 - \beta(r)) + \lambda(r)|$  for the three time snapshots.

As seen from the above figures, the locations of MNR are heavily constrained. The boundary where the effective potential vanishes keeps expanding along the  $\theta$  axis with each time snapshot. For the 20-ms, the vanishing boundary has moved very close to the poles compared to the near-equatorial positioning in 10-ms snapshot and for 50-ms it is not present anywhere in the radial distance range we are looking at.

Even then not all the points in 10ms data, where the effective potential goes to zero, can contribute to MNR because the plot only shows the points where the potentials cancel, but it does not show if the cancellation satisfies the second condition from the listing in 3.1 to produce MNR. Almost all the blue dots above 50 km has  $\lambda(r) > |\mu(r)(1 - \beta(r))|$  just before the point of cancellation and so the change in potential is very non-adiabatic to produce MNR as discussed in the previous sections.

By considering the above plots for the three snapshots, it makes more sense to focus on the 10ms snapshot as the cancellation points are at relatively close distance along a particular radial trajectory. It is also seen that along the angles which pass through the cancellation surface when looked at radially, there are always two cancellation points.

This gives us the freedom to choose how to approach these cancellation points as the potentials are trajectory dependent. We choose to look at a few representative trajectories from the dataset that crosses the cancellation points, to see if MNR happens in any of them. The results are presented for solving the flavor equations of motion along the following trajectories,

- Radial trajectories.
- Vertical trajectories.
- Horizontal trajectories.
- Reversed vertical trajectories.

Finally we move on to include the advection term into the equations of motion and study the effects explored in the final section of chapter 4 as we get a promising scenario where advection could influence the flavor evolution.

### 5.3 Radial Trajectories

We choose to look at the radial trajectories for the angles  $\theta = 0.5, 0.52$  &  $0.56$  with respect to the  $y$ -axis presented in the plots above. For these radial trajectories, the effective potentials  $V_{eff}(r)$  and  $\lambda(r)$  are plotted below.

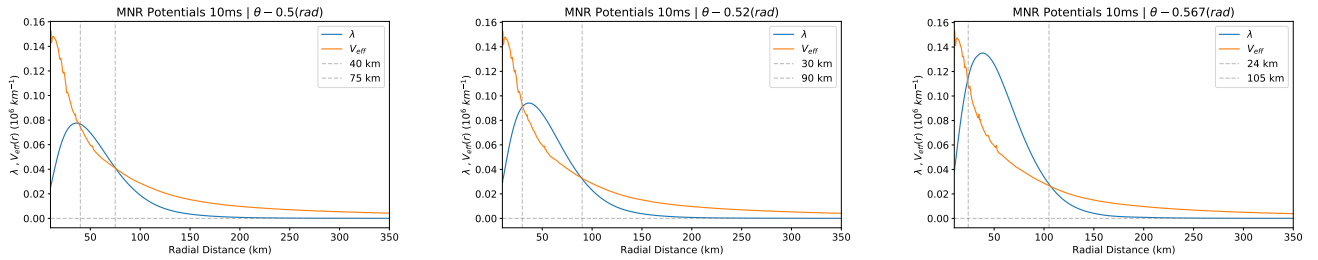


Figure 5.4:  $V_{eff}(r)$  &  $\lambda(r)$  for 0.5, 0.52, & 0.56 radian trajectories.

We can see a direct correlation between the blue spots in the contour and the crossings in the above plots signifying cancellations. The profiles of the potentials we obtain are interesting because the first point of crossing satisfies MNR condition  $V_{eff}(r) > \lambda(r)$ , but the second point of crossing does not. It can also be seen that after crossing the first point the matter potential reaches a peak and falls down steeply after the maximum. As a result, we see that although at the second crossing,  $\lambda(r) > V_{eff}(r)$ , it steeply goes to zero. For these trajectories, when we calculate the survival probability by solving the equations of motion for the polarization vectors without including any angle dependence, we get the results presented in Fig. 5.5.

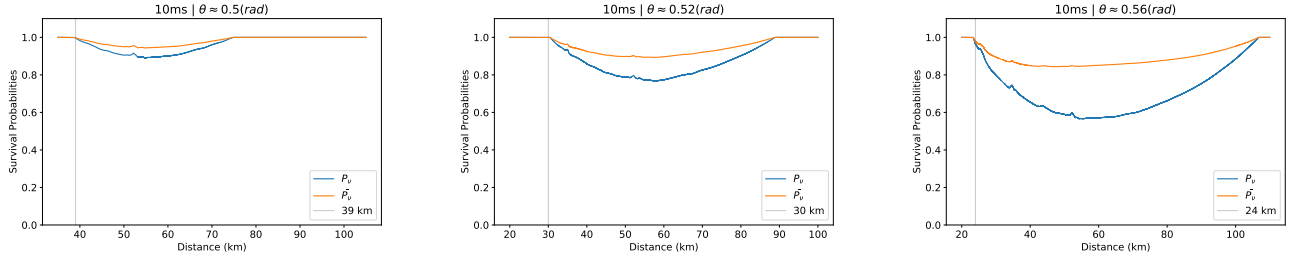


Figure 5.5: The survival probabilities for the 0.5, 0.52, & 0.56 radian trajectories from the 10ms data set. We can see that the resonance does not produce any significant flavor transformations.

**Discussion:** From the above plots we can identify the following points,

- We identify a new type of MNR happening. There is a dip in the survival probabilities for both neutrinos and anti-neutrinos almost exactly at the first crossing point in the potentials for all the three cases and it shows typical MNR like drop.
- The duration of MNR seems to be bounded between the two crossing points as there is no change in the survival probabilities after the second crossing is passed.
- The ‘gap’ between the survival probabilities for neutrinos and anti-neutrinos is proportional to the difference between  $\lambda$  &  $V_{eff}$  in the potentials plot.
- This is not a standard MNR as the system brings the survival probabilities of both neutrinos and anti-neutrinos to the original value, while being bounded between the crossing points, nor is it the symmetric MNR. This is a new type of MNR which does not produce any flavor transformation even though it went through the resonance.

To understand this better, we look at the evolution of the sum of the potentials which is given below,

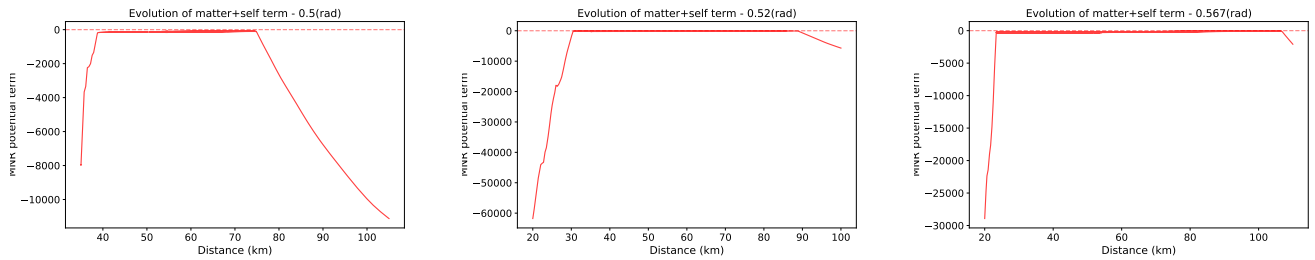


Figure 5.6: The evolution of sum of potentials for the three selected trajectories.

- From the above plots we can confirm that the system is indeed undergoing MNR since the sum of potentials is getting stuck at zero by cancelling each other.
- It can be seen that opposed to the other plots of the evolution of the potential sum, where, after starting out negative the sum passes over to the positive axis, here, the sum starts negative, and after getting stuck in resonance it dips into the negative axis again.

- The reason for dipping into the negative axis after resonance can be understood by looking at Fig. 5.4. In that plot after the second crossing point, we see that  $\lambda(r)$  drops to zero faster than the effective self potential term. The matter term is responsible for the positive contribution to the sum of potentials. Because here it goes down to zero quickly after the second crossing, the positive contribution goes to zero thus the sum is dominated by the negative self potential, hence the sum dips into the negative axis.
- Now to explain the shape of the survival probabilities, we have to realize that the flavor transformation occurs because the system tries its best to stay negative to cancel the matter potential. It does this by converting neutrinos thereby changing its sign while keeping anti-neutrinos in its original flavor, hence increasing its magnitude while staying negative to sustain the cancellation. But here since  $\lambda(r)$  is going down faster when compared to  $V_{eff}$  the system has to flavor transform only for the short duration where  $\lambda(r) \approx V_{eff}$  to maintain cancellation. After  $\lambda$  becomes less than  $V_{eff}$ , the difference is reversed and the system has to make the self interaction term more positive to keep cancelling and so it brings the neutrinos and anti-neutrinos to their original flavor. It might also be dependent on the slope of the two potentials, if  $\Delta\lambda < \Delta V_{eff}$ , then positive flavor transformation is favored, if it is the other way then negative flavor transformation is favored which undoes the conversion done at the start of the resonance.

Thus, the system undergoes MNR, but ultimately there is no significant change in the survival probability as the system undoes whatever change it made during the initial stages of the resonance. The analytical understanding of why the transformations are bound within the two crossings are yet to be explored.

### 5.3.1 Angle Dependence on radial trajectories

If we now introduce angle dependence into the initial conditions of the polarization vector, we see that it actually suppresses the flavor transformation drastically. We choose a forward streaming angular distribution of the form  $1 + x \cos \theta$  with  $x = 0.5$ . Applying this condition to the 0.52 radian trajectory, shows a clear suppression of the flavor transformation as seen below,

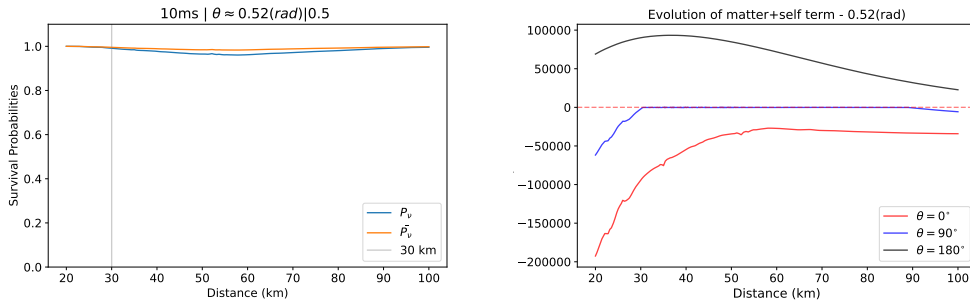


Figure 5.7: The survival probability (left) and evolution of sum of potentials (right) for 0.52 radian trajectory with angle dependence.

It can be seen that dip is very small and that only the radially emitted bin undergoes resonance while almost all other bins do not contribute to MNR. This means that radial trajectories does not support Matter-Neutrino resonance to occur.

## 5.4 Generic trajectories

We transform the parameters into cartesian co-ordinates  $(x, y)$  to look for more sites for MNR. We choose to focus only on the 10-ms dataset as it gives the most promising scenarios for MNR to occur. The transformed versions of the potentials are given below.

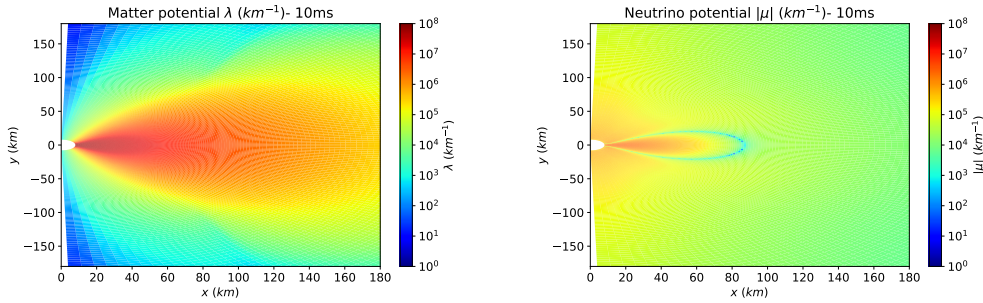


Figure 5.8: The matter (left) and the neutrino potential (right) for the 10ms data-set in cartesian co-ordinates.

The total potential contour map with cancellation points highlighted is given as follows,

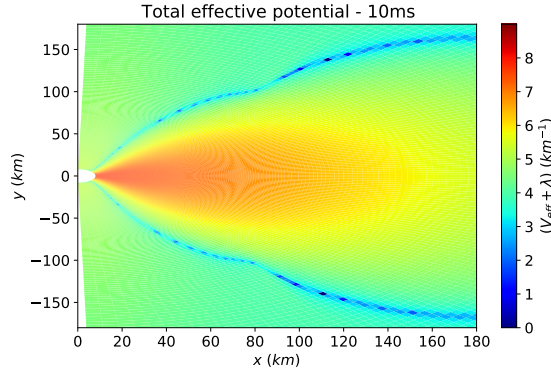


Figure 5.9: Contour map for the sum of potentials with cancellation points for 10-ms data-set in cartesian co-ordinates.

From the plots presented in Fig. 5.8, we can clearly see the torus in the equatorial region surrounding the merger remnant as depicted in Fig. 5.1. The region where the cancellation between the matter and self-interaction potentials could occur forms a boundary above and below the torus equatorial disk. The points where the sum of the potential vanishes can be spotted from the blue spots in Fig. 5.9.

### 5.4.1 Vertical Trajectories

We choose to look at the cancellation points vertically from the equator and track the potentials through the trajectories that hit the cancellation points marked in Fig. 5.10 to see if MNR can occur.

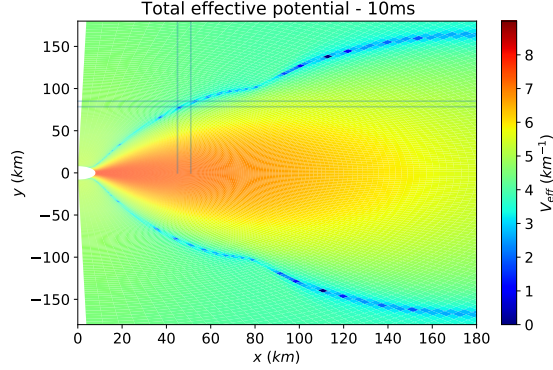


Figure 5.10: Total potential contour marked with the trajectories focused on.

But it is seen that though such trajectories have a crossing, it cannot produce MNR since the matter potential is greater than the self potential as seen in Fig. 5.11. This is reasonable as it matches the contours for the matter potential and the neutrino potential in Fig. 5.8. For these trajectories, the matter potential is way bigger when compared to the neutrino potential.

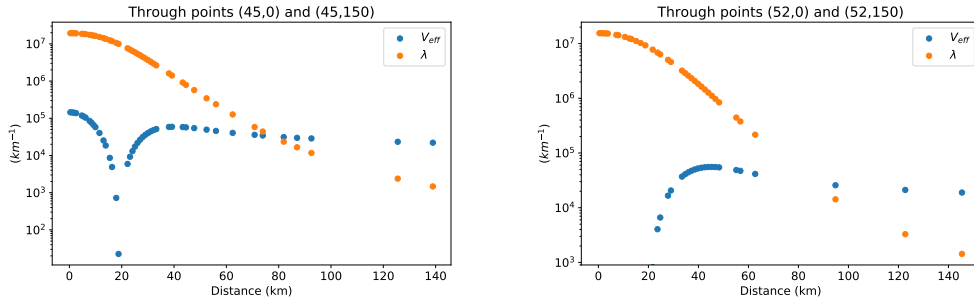


Figure 5.11: The evolution of matter and effective self interaction potential along vertical trajectories from the points (45,0) (left) & (52,0) (right). It can be seen that  $\lambda(r) > V_{eff}(r)$  along these trajectories.

Thus looking at radial trajectories and vertical trajectories for the 10 ms data-set shows no promising scenarios for standard MNR to occur. Although MNR happens for radial directions, because of the way the potentials change for those directions, the system does not produce any significant change in the neutrino and anti-neutrino flavor after the crossing points are passed.

## 5.4.2 Horizontal trajectories

By looking at the contours for the distribution of the matter potential and the self interaction potential, we then look at horizontal trajectories that hit the cancellation points, because for horizontal trajectories, the matter potential starts out to be much less than how it was for vertical trajectories. This would mean that there is a good chance that the MNR conditions are fulfilled.

So the shape of the potentials along the lines connecting the points (05, 65) and (155, 65), along with lines connecting (05, 77) to (155, 77) & (05, 83) to (155, 83) were explored. It can be seen that the self interaction potential is greater than the matter potential before the crossing happens as expected, but it can also be seen that the matter potential jumps to high values very quickly while the self potential stays relatively constant. Unlike the potential profile for the radial trajectories, there are no double crossings and the matter potential stays much larger than the self potential for a large distance. This is also in accordance with the contours made for the potentials.

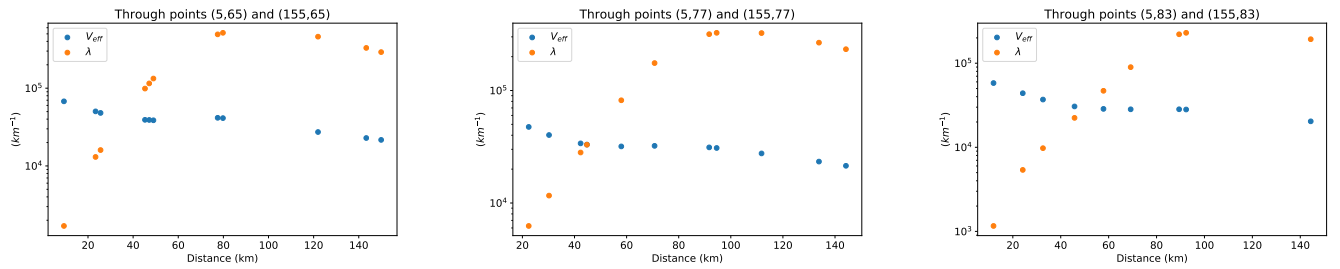


Figure 5.12: The evolution of matter and effective self interaction potential along horizontal trajectories from the points (05, 65), (05, 77) & (05, 83). It can be seen that the MNR conditions are fulfilled with  $V_{eff} > \lambda$ .

We simulate the flavor equations of motion for  $y = 65$  km trajectory with the vacuum mixing angle  $\theta_V \leq 0.2$  and we see that the system does not undergo MNR. It is because the jump of magnitude for  $\lambda(r)$  is very quick. Therefore, though the system passes through the cancellation point of  $\lambda(r) + V_{eff} = 0$  very quickly and does not have enough time to start flavor transforming. This is seen to be the case for the plot of potentials where it passes by zero in Fig. 5.13.

MNR is also dependent on the vacuum mixing angle as explained in the previous sections, Eq. (3.7). Given the sharp jump in the matter potential, for a successful MNR to occur, the value of  $\theta_V$  must be greater than the usual value used in all the previous simulations. When the vacuum mixing angle is slightly increased to  $\theta_V = 0.35$ , the initial perturbation of the polarization vector system is sufficient to make it undergo resonance as seen from the second row of plots in Fig. 5.13. But this cannot be considered as a realistic result since this value of mixing angle is slightly higher than the upper bound found experimentally [6]. So it is seen that there is a threshold where a slightly greater perturbation is enough to make the system undergo the resonance.

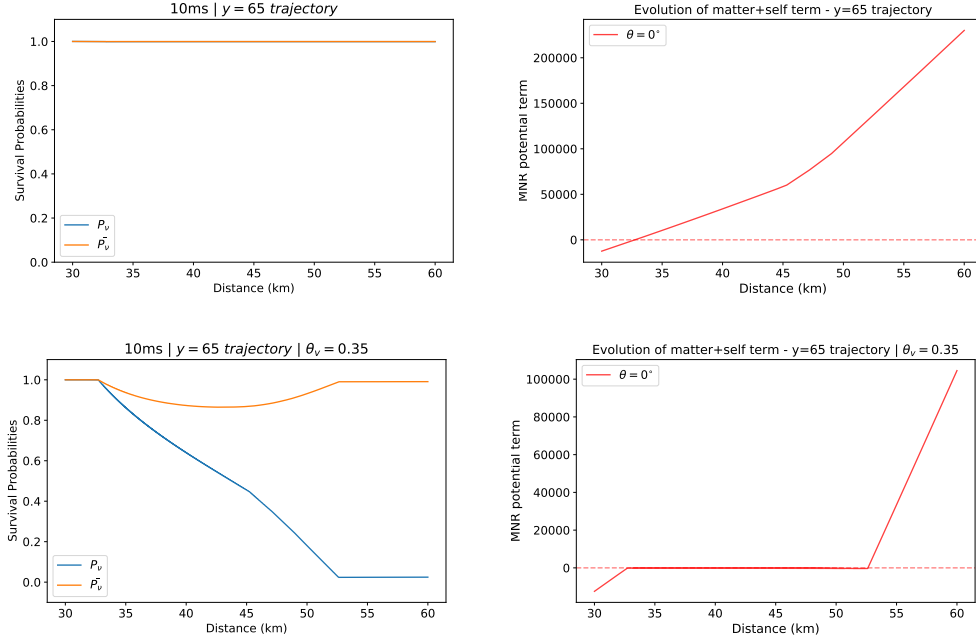


Figure 5.13: Survival Probability and the sum of potentials for the  $y = 65\text{km}$  trajectory. Though the potentials fulfill the MNR conditions, for  $\theta_V = 0.2$  (first row) there is no resonance. But  $\theta_V = 0.35$  produces resonance (second row).

### 5.4.3 Reversed vertical trajectories

As a next step, we consider the same potentials found in Fig. 5.11, but this time we check if a neutrino beam travelling in the opposite direction from right to left undergoes MNR, since the potential profiles and the system would satisfy the MNR conditions from the listing in 3.1, seeing that when viewed from right to left,  $V_{eff} > \lambda$ .

Specifically, we consider the vertical trajectory from (45,0) to (45,150). When the flavor equations of motion are solved for the potentials in the fore-mentioned trajectory, for a short distance around the point of crossing, it is noted that it does produce standard MNR as expected.

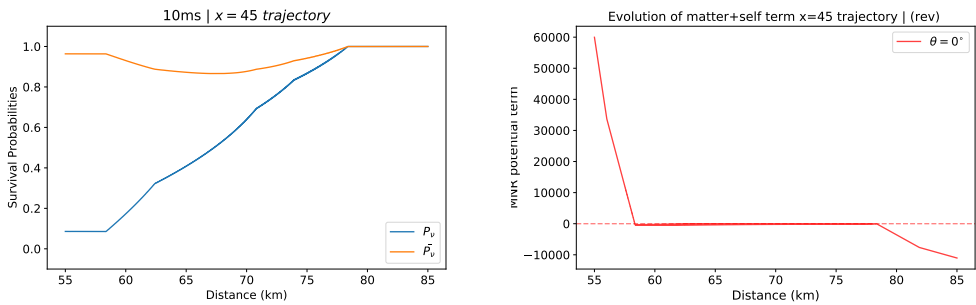


Figure 5.14: This plot shows the survival probability (left) and evolution of the potential sum (right) when the system is made to solve in the opposite direction.

It should also be noticed that this point of MNR crossing,  $\approx (45, 77)$  is way outside the neutrino emission surface for the remnant which means technically there should not be any neutrino beam travelling backwards which then would make the above result insignificant.

To get an idea of how forward peaked the distribution is, the ratio of neutrino flux in polar directions to the number density for neutrinos and anti-neutrinos are plotted as contours, which is given in a set of images below.

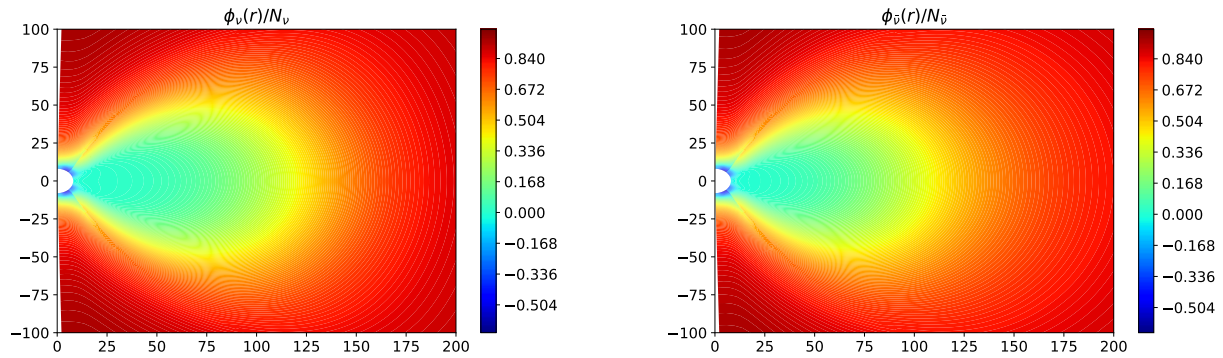


Figure 5.15: Contours for ratio of r-flux to number density individually for neutrinos (left) and anti-neutrinos (right) which clearly shows the trapping region and the decoupling region.

By looking at the above plot, Fig. 5.15 we can immediately identify the trapping region and hence the neutrino emission surface. We can also see that difference in the emission radius for neutrinos and anti-neutrinos, the anti-neutrinos have a smaller emission radius when compared to the neutrinos because they decouple quicker.

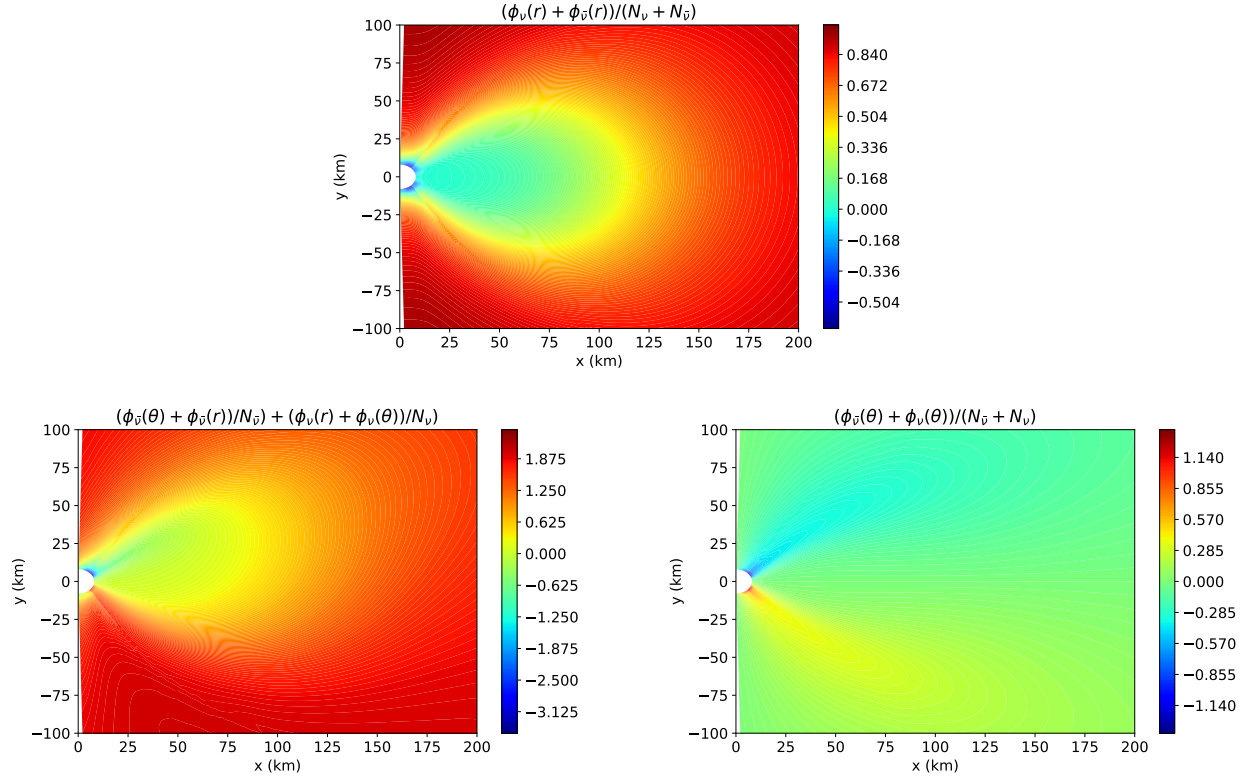


Figure 5.16: The ratio of total flux to the number density, individually in  $r$  direction (top),  $\theta$ -direction (bottom right) and the sum of both (bottom left), for both neutrinos and anti-neutrinos

By looking at the total fluxes for both neutrinos and anti-neutrinos in  $r, \theta$  directions in the above plot, Fig. 5.16, we can see that the value of the ratio of  $r$ -flux to number density at  $\approx (45, 77)$  is around 0.7, which means there could be a significant number of neutrinos travelling in the backward direction. So the reversed run for the vertical trajectory might be explaining something worthwhile. Although it has to be mentioned that the dataset used presents the values of the number flux and number density only along the radial direction, so the value of the ratio we get, might not be exactly applicable to the trajectory we focus on.

But if there is a good fraction of neutrinos moving backwards, then the flavor equations of motion or the initial conditions should be slightly modified to account for this fraction moving in the opposite direction. This is done by including the advective term as explained in chapter 4.

## 5.5 Inclusion of advective term

As explained above, there is a decent fraction of (anti)neutrinos which could be travelling in the backward, and the fact that the beam flowing forwards do not experience MNR but the beam flowing backwards does, presents an interesting scenario to study. To study this in a consistent way, an advective term is included into the EOMs and only two angular beams along this trajectory are considered, just forward flowing and backward flowing beams are included into the EOMs as it is

described in the advection study section in chapter 4. We focus on the particular trajectory that shows such behavior, and we apply the advection code for the potential profiles of that trajectory. The results are presented below.

As explained in the advection results of chapter 4, when the matter potential dominates the self-interaction potential at the point of crossing, the equations of motion becomes incompatible to favor flavor transformations. We get similar results when applied to the dataset as well.

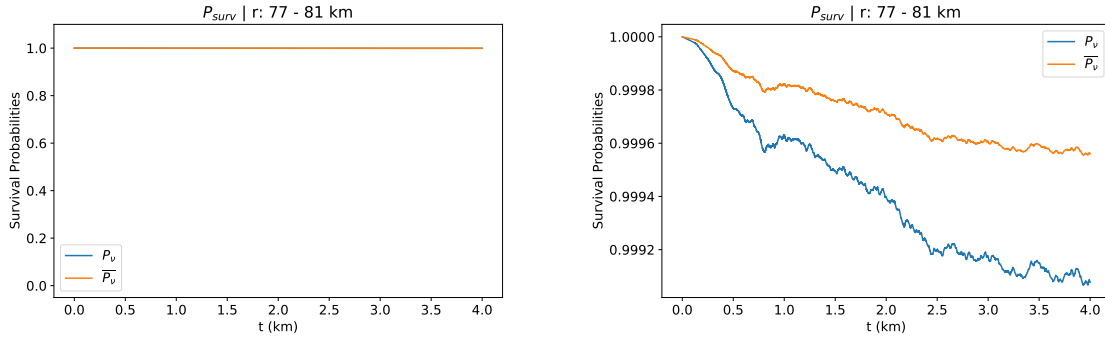


Figure 5.17: r-bin averaged survival probability (enlarged in the right side plot) as a function of time around the point of crossing in the left plot of Fig. 5.11

We can see that although there is a trace of MNR happening, the magnitude of its effects are of the order  $10^{-4}$  which is negligible and it can be seen that it does not affect the survival probability on the whole.

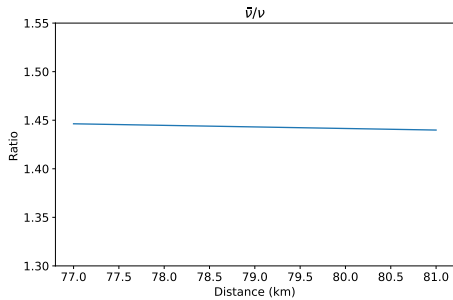


Figure 5.18: Ratio between  $\bar{\nu}$  and  $\nu$  near the point of resonance

Since the values of  $\beta$  for the forward and backward beams are similar, there is no preferred direction for the advection to move the disturbance, although it being small. Thus it can be seen to propagate the disturbance in both directions in Fig. 5.19.

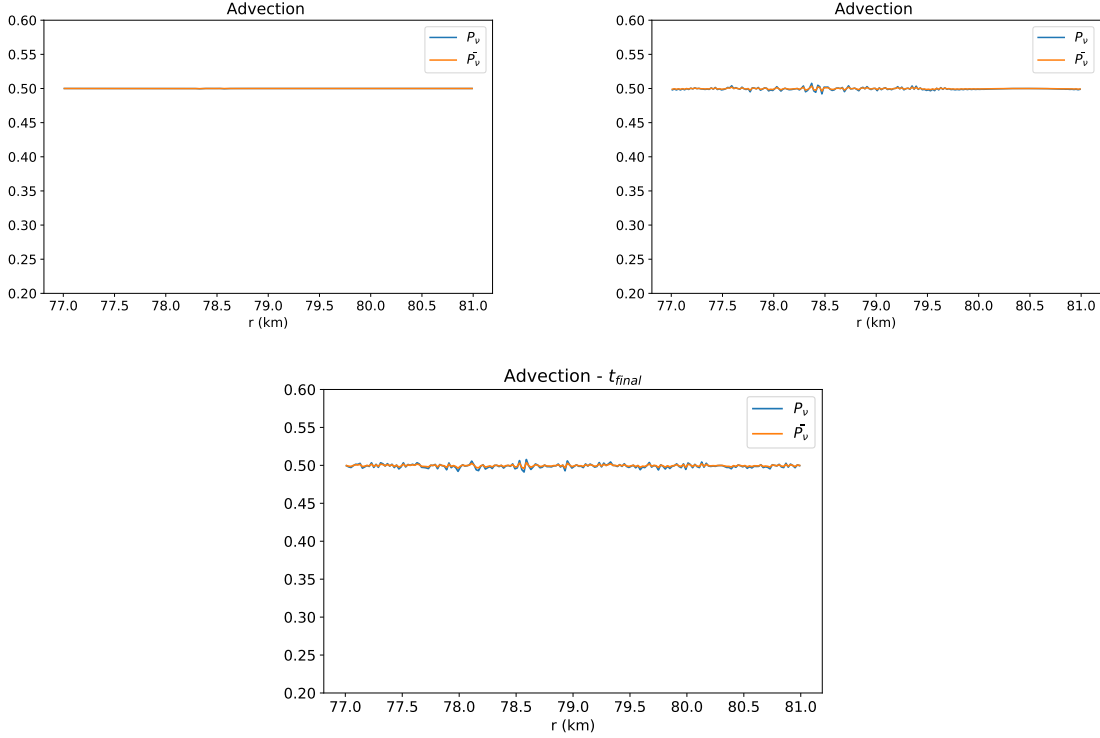


Figure 5.19: Polarization vectors of neutrinos and anti-neutrinos at three different time snapshots (top left - initial, top right - intermediate, bottom - final) for the advection code applied to the vertical trajectory.

We can see that as opposed to a significant dip in the polarization vectors around the crossing point seen in Fig. 4.23 and 4.22, all we see are small wiggles that propagate from the crossing point on both directions as expected, hence there is no change in the flavor of neutrinos and anti-neutrinos.

## 5.6 Summary

In this chapter, we studied the various potential profiles produced in a hydrodynamical simulation of a binary Neutron Star merger remnant and we chose a few representative trajectories to check if a scenario suitable to produce MNR was present. We observed that conditions for MNR were present only for the 10ms snapshot which was earliest time snapshot of the merger simulation. From the dataset corresponding to the 10-ms snapshot, we observed the potential profiles and concluded that MNR was a heavily constrained phenomenon, even in the case of a merger. By pointing out the MNR points, we chose three main types of trajectories and we found that none of these trajectories produced significant flavor transforming MNR. We identified a new type of MNR happening in the radial trajectories which ultimately did not produce any flavor transformations. We also included the advection for the case of vertical trajectories and we found no MNR, which complements the results obtained in the previous chapter. Thus after exploring the dataset along multiple trajectories, we can safely conclude that for this dataset there are no possibilities for MNR to occur.



## Chapter 6

# Discussion & Summary

In the literature, Matter-Neutrino Resonance has been studied mainly in the single angle limit, and the multiangle limit is considered only in a few papers. The multiangle effects are important to accurately describe the flavor evolution of neutrinos in the vicinity of the source. The advective effects that occurs in the dense media close to the source has not been accounted for in the studies undertaken so far with respect to MNR and the angular distributions used have also been simple. The implications for nucleosynthesis cannot be determined accurately without understanding MNR. This requires us to study this phenomenon in increasingly complicated situations.

In this thesis, we aimed to study the effects and prospects of Matter-Neutrino Resonance and its angle dependence properties with advective effects included, in Compact Binary merger systems using the datasets obtained from hydrodynamical simulation of a Binary merger remnant, which would be a good representation of the potentials to be expected in real astrophysical mergers.

After introducing the basic concepts of flavor transformation, in chapter 2 and collective oscillation phenomena briefly, we moved on to explain the theoretical basis for Matter-Neutrino Resonance by explicitly pointing out the conditions required for MNR to occur and other analytical results obtained in the literature, in chapter 3.

As a part of the thesis we independently developed a flavor simulation code including all three terms of the Hamiltonian (vacuum, matter and self) with the capability to simulate the polarization vectors with energy and angular dependence, as explained in the Appendix 7.2.1. We then applied that code to two model situations designed with similarity to a source of dense neutrino emission in mind, with and without angular dependence on the polarization vectors in chapter 4. We studied the effects of choosing a forward peaked angular distribution in steps, by slowly increasing the contribution of angle individually for neutrinos and anti-neutrinos, before moving on to including angle dependence on both. We found that there is a drastic suppression of Matter-Neutrino resonance when there was a forward peaked angle dependence on neutrinos and there was significant decrease in the effects of the resonance when there was an angular distribution only on anti-neutrinos, although not as much as it was with the neutrino case.

We saw that the system simply transitioned from a case where angle dependence was dominant on anti-neutrinos to a case where it was dominant on neutrinos, when we included the forward peaked distribution non-uniformly to neutrinos and anti-neutrinos. The suppression of MNR with the inclusion of multiangle effects is in accordance with what is reported so far in the literature. The results obtained in this thesis differ from the literature only with the fact that the anti-neutrinos are not affected in any case studied for a forward peaked angular distribution. We identified and discussed the difference in the flavor evolution of the polarization vectors between normal and inverted mass hierarchies in the multiangle limit, with an angular dependence on them. This difference between the survival probabilities of normal and inverted mass hierarchies in the context of MNR is a new result. We then attempted to study the effects of including the advective contribution to the equations of motion to understand the realistic implications of MNR and also with an ulterior motive to apply it to a particular scenario in the dataset. We found that the inclusion of advection very radically decreased the effects of MNR, but the system still showed MNR characteristics albeit being almost negligible in some cases. We also found that even with significant advective contribution, there was no change in the survival probabilities if the second condition in the listing 3.1 is not satisfied. The analytic reason for the equations becoming incompatible for flavor evolution has to be explored in future works.

We then looked into the merger simulation dataset for prospective MNR along multiple kinds of trajectories, which could cause implications to the nucleosynthesis theorized in the literature. We found that although there are possibilities for Matter-Neutrino Resonance to occur, it was only in the early stages of the merger. Though there were locations where the matter and the self-interaction potential cancelled, for the representative trajectories chosen, the potential profiles did not produce any significant Matter-Neutrino resonant flavor transformations. In the process, we identified a new type of MNR transformation, which, although does not produce any significant change in the flavor of neutrinos and anti-neutrinos, was a new result. We confirmed the results obtained in the advection studies done in chapter 4, that showed substantial decrease in resonant flavor transformation, by applying the advection code to a particular trajectory in the dataset. We have refrained from including angle dependence on the polarization vectors for most trajectories, simply because the potential profiles does not produce MNR even without including it.

Since these results have not been reported so far in the literature, a paper focusing on the results obtained from chapter 4 and 5 is under process.

From all the studies undertaken during the thesis, we have obtained enough results to arrive at the conclusion that Matter-Neutrino Resonance is a highly constrained and case-specific phenomenon, which can be produced only in very particular kinds of potential profiles and astrophysical scenarios. The datasets used in the thesis did not have any prospective situation to produce a significant flavor transformation due to Matter-Neutrino Resonance.

## Prospects and Outlook

As mentioned above, Matter-Neutrino Resonance is an extremely case-specific phenomenon, which means there could be possibility of this resonance occurring in some other Compact Binary Merger with different emission characteristic and potential profiles. But the realistic implications of the resonance might not be as significant as reported in the literature since the inclusion of advection made the effects of MNR almost negligible and inclusion of angle dependence also decreased its consequence. In a realistic scenario, the astrophysical system would have significant contributions due to matter and neutrino advection and based on the results obtained, it is highly doubtful that MNR would be produced in such a situation.

The cases studied in this thesis are only better approximations to the actual scenario, and are by no means conclusive. We mainly worked with two flavor and mono-energetic system, which are significant simplifications. Near the decoupling region, a purely forward peaked distribution is a good approximation in itself. But the forward peaked angular distribution we assumed to study the angle dependence, must be made more accurate. Including the collision terms to the equations of motion would help in determining the angular distributions of neutrinos and anti-neutrinos accurately as it is the main factor that influences the directional dependence of the neutrino and anti-neutrino emission. The collision terms are energy-dependent and we can no longer use the mono-energetic assumptions, this can complicate the problem significantly. The energy independent property of MNR must also be re-investigated when the collision terms are included as that property may be influenced.

There is scope for further investigations to be done with respect to Matter-Neutrino Resonance. Though this phenomenon is highly case-specific, we observed that advective effects made the consequence of MNR almost negligible. Thus the judgement of whether MNR is a realistic occurrence and whether it can influence the nucleosynthesis to the extent it is proposed in the literature must be left for future studies with more accurate choice of neutrino systems and more advanced simulation techniques.



# Chapter 7

## Appendix

### 7.1 Derivation of Bloch equation for Polarization vector

Starting from the von-Neumann equation,

$$i\frac{\partial\rho}{\partial t} = [H, \rho] \quad (7.1)$$

if we now insert the decompositions for  $\rho$  and  $H$ ,

$$\rho = \frac{\text{Tr}(\rho)}{2}(\mathbb{1} + \vec{P} \cdot \vec{\sigma}) ; H = \frac{1}{2}(\mathbb{1} + \vec{H} \cdot \vec{\sigma})$$

into the von-Neumann equation, after expanding the commutation we obtain,

$$i\frac{\text{Tr}(\rho)}{2}\frac{\partial}{\partial t}(\mathbb{1} + \vec{P} \cdot \vec{\sigma}) = \frac{\text{Tr}(\rho)}{2}\frac{1}{2}((\mathbb{1} + \vec{H} \cdot \vec{\sigma})(\mathbb{1} + \vec{P} \cdot \vec{\sigma}) - (\mathbb{1} + \vec{P} \cdot \vec{\sigma})(\mathbb{1} + \vec{H} \cdot \vec{\sigma}))$$

After some algebraic simplifications we arrive at,

$$i\frac{d\vec{P}}{dt} \cdot \vec{\sigma} = \frac{1}{2}[(\vec{H} \cdot \vec{\sigma})(\vec{P} \cdot \vec{\sigma}) - (\vec{P} \cdot \vec{\sigma})(\vec{H} \cdot \vec{\sigma})] \quad (7.2)$$

If we then make use of the identity,

$$(\vec{a} \cdot \vec{\sigma})(\vec{b} \cdot \vec{\sigma}) = (\vec{a} \cdot \vec{b})\mathbb{1} + i(\vec{a} \times \vec{b}) \cdot \vec{\sigma} \quad (7.3)$$

Then after simplification, eq.21 becomes,

$$i\frac{d\vec{P}}{dt} \cdot \vec{\sigma} = \frac{i}{2}[(\vec{H} \times \vec{P}) - (\vec{P} \times \vec{H})] \cdot \vec{\sigma}$$

which then reduces to the Bloch equation,

$$\frac{d\vec{P}}{dt} = \vec{H} \times \vec{P} \quad (7.4)$$

## 7.2 Method of designing solver code

Since the flavor equations of motion are too complicated they can only be solved numerically. For this thesis, the code is developed in **Python**, using the **RK45** method from **scipy.integrate** package. This method uses Dormand-Prince pair of formulae with adaptive stepping, using fourth-order method accuracy to control error and fifth order accurate formula for taking steps. The design of the code is described in the following sections.

### 7.2.1 Numerical scheme

In functional form, the multi-angle, multi-energy equations, simplified and rewritten in terms of just the emission angle, energy and the distance from the neutrinosphere, we have to solve would look like,

$$\frac{d\vec{P}_{ij}}{dr} = \frac{1}{\cos\theta_j} (+\omega\vec{B} + \lambda\hat{z} + \sum_{\beta=1}^{n_2} A_{\beta j} (\sum_{\alpha=1}^{n_1} (x_\alpha \vec{P}_{\alpha\beta} - y_\alpha \vec{\bar{P}}_{\alpha\beta})) d \cos\theta dE) \times \vec{P}_{ij} \quad (7.5)$$

$$\frac{d\vec{\bar{P}}_{ij}}{dr} = \frac{1}{\cos\theta_j} (-\omega\vec{B} + \lambda\hat{z} + \sum_{\beta=1}^{n_2} A_{\beta j} (\sum_{\alpha=1}^{n_1} (x_\alpha \vec{P}_{\alpha\beta} - y_\alpha \vec{\bar{P}}_{\alpha\beta})) d \cos\theta dE) \times \vec{\bar{P}}_{ij} \quad (7.6)$$

and  $n_1, n_2$  are the number of  $E$  bins and  $\theta$  bins, respectively. The explicit angular bin dependence is through the  $\frac{1}{\cos\theta_j}$  term.

For the  $n_1 = 2, n_2 = 2$  bin scenario, there would be 24 equations of motion to solve, since there would be  $P_{11}, P_{12}, P_{21}, P_{22}$  and similarly for anti-neutrinos,  $\bar{P}_{11}, \bar{P}_{12}, \bar{P}_{21}, \bar{P}_{22}$ , where  $P_{ij} = P(E_i, \theta_j)$  and each polarization vector has 3 components in them. Thus the flavor evolution problem becomes a huge set of coupled differential equations. ( $6 \times N_E \times N_\theta$ )

For such a scenario, the coupling self interaction term with the double integration, would have to be of the form,

$$A_{1j}((x_1 P_{11} - y_1 \bar{P}_{11}) + (x_2 P_{21} - y_2 \bar{P}_{21})) + A_{2j}((x_1 P_{12} - y_1 \bar{P}_{12}) + (x_2 P_{22} - y_2 \bar{P}_{22})) \quad (7.7)$$

where,

$$A_{\beta j} = \frac{L \cos\theta_\beta}{\sqrt{1 - L(1 - \cos^2\theta_\beta)}} (1 - \cos\theta_\beta \cos\theta_j) \quad (7.8)$$

and  $L = \frac{R^2}{r^2}$ . where we have already simplified the problem and have rewritten it in terms of just the emission angle, distance and energy and with,  $x = \phi_\nu(E)/\langle E_\nu \rangle$  and  $y = \phi_{\bar{\nu}}/\langle E_{\bar{\nu}} \rangle$ , where  $\phi(E)$  denotes the distribution function of neutrinos and anti-neutrinos and  $\langle E \rangle$  signifies the average energy.

So if there are two  $\theta$  bins with say  $\theta_1 = 0.25, \theta_2 = 0.75$ , then for the equation of motion of a polarization vector of the first angle bin,  $j = 0.25$  and  $\beta$  index is summed over the two angle bins, while  $j$  stays the same in both terms, as it is shown in Eq. (7.7). The integration happens in a similar way for the other polarization vectors of other angular bins, as well. Such a double integration happens at each time-step that the ODE solver takes. The geometric dilution of the neutrino density is taken care of by the  $r$ -dependence of the  $\cos \theta$  terms. Explicitly, the  $r$ -dependence is,

$$\cos \theta_{j,\beta} = \sqrt{1 - L(1 - \cos^2 \theta_{0=j,\beta})} \quad (7.9)$$

where,  $(j, \beta)$  denotes that the expression is same for all  $\cos \theta$ , whether it is the bin dependent variable or the integration variable. And finally  $dE = \frac{50-0}{n_1}$  and  $d \cos \theta = \frac{1}{n_2}$

## 7.2.2 Implementation of the integrals

First we can readily fix the initial values of the polarization vectors since we assume that the vectors, at the beginning are all fixed in the same direction for all the emission angles. Hence we create a tensor object  $P_0$  with three indices  $m, n, 6$ , where  $m$  is the index for the energy bins,  $n$  is the index for the angular bins and there are a total of six components inside this object, which includes three for neutrinos and three for anti-neutrinos.

So to simply state, the energy integration now picks up two  $\theta$  dependence. The integration now depends on the particular angle bin and the angle that is being integrated over, which are the  $j$  index and  $\beta$  index respectively in eq. (7.5) and (7.6).

We also create a new three index tensor object  $I$ , which will hold the distribution functions of the two flavors of neutrinos and anti-neutrinos which are hiding inside  $j$  and  $\bar{j}$  in Eq. (2.22) and (2.23). The  $I$  object ideally contains 3 copies of the distribution functions of neutrinos and 3 copies of the same for anti-neutrinos, which includes both the flavors in them. Hence we actually have two tensors with three indices, namely  $I_{mnk}$  and  $P_{mnk}$  where the  $k = 1, 2, ..6$ , out of which  $k = 1 - 3$  accounts for the neutrino components and  $k = 3 - 6$  is for anti-neutrino components of the polarization vector.

In the first step we contract the energy index for the two tensor objects, which for just 2 bins each, looks like,

$$I_{mnk} P_{nk}^m = \begin{bmatrix} I_{11k} P_{1k}^1 + I_{12k} P_{12k}^1 \\ I_{21k} P_{1k}^2 + I_{22k} P_{2k}^2 \end{bmatrix} \quad (7.10)$$

We can then split the  $k$  index into two parts, from 1-3 and 4-6, to subtract them, which would look like the terms  $(x_\alpha \vec{P}_{\alpha\beta} - y_\alpha \vec{\bar{P}}_{\alpha\beta})$  in equations (7.5) and (7.6), with  $x$  containing the copies of the energy distributions of neutrinos and  $y$  containing the same of anti-neutrinos. Thus the angle bin dependent energy integration now looks like,

$$E_{nk} = \sum_{k=1}^3 I_{mnk} P_{nk}^m - \sum_{k=4}^6 I_{mnk} P_{nk}^m \quad (7.11)$$

Then to create  $A_{\beta j}$  we create another tensor object with indices  $\beta, n$ , here both  $\beta$  and  $n$  have the dimensions of the angle bins. This is justified because  $A$  has dependence on the two  $\theta$ s, the integration variable and the angular bin itself. Then we contract the integration variable index of this tensor object with the  $n$  index of Eq. (7.10), and this will give us the correct result for the double integration we need, i.e, in the code we will be doing something like,

$$D = A_{\beta n} \left( \sum_{k=1}^3 I_{mk}^n P_k^{mn} - \sum_{k=4}^6 I_{mk}^n P_k^{mn} \right) \quad (7.12)$$

or

$$D = A_{jn} \left[ \begin{pmatrix} I_{m1}^n P_1^{mn} \\ I_{m2}^n P_2^{mn} \\ I_{m3}^n P_3^{mn} \end{pmatrix} - \begin{pmatrix} I_{m4}^n P_4^{mn} \\ I_{m5}^n P_5^{mn} \\ I_{m6}^n P_6^{mn} \end{pmatrix} \right] \quad (7.13)$$

where  $n$  is the integration variable index which is contracted with the corresponding  $A$ 's, and  $j$  is the angular bin index.

The  $k$  index is now explicitly expanded in (13) with  $(1, 2, 3)$  being the  $(x, y, z)$  components of  $\vec{P}$ , and  $(4, 5, 6)$  are the  $(x, y, z)$  components of  $\vec{\bar{P}}$ . This whole double integration would result in a simple 3 vector, because the "vectorness" comes only from  $P$ s and  $\bar{P}$ s and we are just subtracting the two. This then enters the Hamiltonian to act on the  $P_{ij}$ 's or  $\bar{P}_{ij}$ 's in Eq. (7.5) and (7.6). Thus we have developed a vectorized flavor evolution code with capacity to handle energy and angle dependence on the system.

### 7.2.3 General Multiangle-Single Energy case

The cases of MNR studied in this thesis concerns only mono-energetic systems with just angle dependence and excludes the emission surface. We also remove the spherical symmetry assumed in the previous section. This simplifies the problem a little. By removing the energy dependence of the system, the tensor  $I_{mnk}$  simply reduces to  $I_{nk}$ , where  $n$  corresponds to the number of angular bins like usual. The energy integration simply amounts to multiplying by 1 and so that can also be removed.

The form of the object  $A_{ij}$  also changes because we consider general geometry and so it reduces to  $(1 - \cos \theta_i \cos \theta_j)$ . Thus the modified set of equations are,

$$\frac{d\vec{P}_i}{dr} = (+\omega\vec{B} + \lambda\hat{z} + \sum_{j=1}^{n_2} (1 - \cos \theta_i \cos \theta_j) (\alpha\vec{P}_j - \beta\vec{\bar{P}}_j) d \cos \theta) \times \vec{P}_i, \quad (7.14)$$

$$\frac{d\vec{\bar{P}}_i}{dr} = (-\omega\vec{B} + \lambda\hat{z} + \sum_{j=1}^{n_2} (1 - \cos \theta_i \cos \theta_j) (\alpha\vec{P}_j - \beta\vec{\bar{P}}_j) d \cos \theta) \times \vec{\bar{P}}_i, \quad (7.15)$$

where  $\alpha$  and  $\beta$  are now simple scalar numbers. We always set  $\alpha = 1$  and we set  $\beta$  to be equal to the ratio of anti-neutrinos to neutrinos in the medium. Thus  $\beta$  simply signifies the anti-neutrino excess.

This quantity can also be made to be a function of  $r$ . The implementation of the angle integration remains the same and the code converges even for low number of angular bins.

#### 7.2.4 Advection Code

The new equations with the advective modification, for two beams corresponding to  $\theta = 0$  and  $\theta = \pi$ , in functional form are,

$$\left(\frac{\partial}{\partial t} + \frac{\partial}{\partial r}\right) \vec{P}_1(r, t) = [+ \omega \vec{B} + \lambda(r) \hat{z} + \mu(r) \sum_{\sigma} (1 - \cos \theta_{\sigma})(\alpha_{\sigma} \vec{P}_{\sigma} - \beta_{\sigma} \vec{\bar{P}}_{\sigma})] \times \vec{P}_1 \quad (7.16)$$

$$\left(\frac{\partial}{\partial t} - \frac{\partial}{\partial r}\right) \vec{P}_2(r, t) = [+ \omega \vec{B} + \lambda(r) \hat{z} + \mu(r) \sum_{\sigma} (1 + \cos \theta_{\sigma})(\alpha_{\sigma} \vec{P}_{\sigma} - \beta_{\sigma} \vec{\bar{P}}_{\sigma})] \times \vec{P}_2 \quad (7.17)$$

$$\left(\frac{\partial}{\partial t} + \frac{\partial}{\partial r}\right) \vec{\bar{P}}_1(r, t) = [- \omega \vec{B} + \lambda(r) \hat{z} + \mu(r) \sum_{\sigma} (1 - \cos \theta_{\sigma})(\alpha_{\sigma} \vec{P}_{\sigma} - \beta_{\sigma} \vec{\bar{P}}_{\sigma})] \times \vec{\bar{P}}_1 \quad (7.18)$$

$$\left(\frac{\partial}{\partial t} - \frac{\partial}{\partial r}\right) \vec{\bar{P}}_2(r, t) = [- \omega \vec{B} + \lambda(r) \hat{z} + \mu(r) \sum_{\sigma} (1 + \cos \theta_{\sigma})(\alpha_{\sigma} \vec{P}_{\sigma} - \beta_{\sigma} \vec{\bar{P}}_{\sigma})] \times \vec{\bar{P}}_2 \quad (7.19)$$

where the subscript 1 on the polarization vectors refer to the forward beam and 2 refer to the backward beam. Because these are partial differential equations and the polarization vectors have become explicit functions of  $r$  and  $t$ , we have to consider them as independent variables. To do this we adopt, finite difference method of the form,

$$f'(r) = \frac{f(r+h) - f(r-h)}{2h}$$

for evolution along r-dimension, thereby making  $N_r$  bins, and let solver take adaptive steps along the t-dimension. And so we need an initial condition for t-dimension and a whole set of initial conditions for each of the r-bins. Thus ultimately we need to solve,  $4 \times 3 \times N_r$  equations of motion. We apply periodic boundary condition with central difference method to the r-bins to avoid numerical instabilities.

The influence/feedback of the backward travelling neutrinos undergoing resonance would be accounted for because all the bins are coupled by the angle integration term of the self-potential. The implementation of the angle integration is exactly the same but the terms obtain an additional index corresponding to the r-bin.

# Bibliography

- [1] Matthew D. Schwartz. *Quantum Field Theory and the Standard Model*. Cambridge University Press, 2013. doi: 10.1017/9781139540940.
- [2] SNO Collaboration. Direct Evidence for Neutrino Flavor Transformation from Neutral-Current Interactions in the Sudbury Neutrino Observatory. *Physical Review Letters*, 89(1):011301, June 2002. doi: 10.1103/PhysRevLett.89.011301. URL <https://link.aps.org/doi/10.1103/PhysRevLett.89.011301>. Publisher: American Physical Society.
- [3] S. P. Mikheev and A. Yu Smirnov. Resonance enhancement of oscillations in matter and solar neutrino spectroscopy. In *Solar Neutrinos*. CRC Press, 1994. ISBN 978-0-429-50281-1. Num Pages: 5.
- [4] C Giunti, C. W Kim, and M Monteno. Atmospheric neutrino oscillations with three neutrinos and a mass hierarchy. *Nuclear Physics B*, 521(1):3–36, June 1998. ISSN 0550-3213. doi: 10.1016/S0550-3213(98)00105-9. URL <https://www.sciencedirect.com/science/article/pii/S0550321398001059>.
- [5] Phys. Rev. Lett. 81, 1562 (1998) - Evidence for Oscillation of Atmospheric Neutrinos, . URL <https://journals.aps.org/prl/abstract/10.1103/PhysRevLett.81.1562>.
- [6] Particle Data Group, . URL [https://pdg.lbl.gov/2022/listings/contents\\_listings.html](https://pdg.lbl.gov/2022/listings/contents_listings.html).
- [7] Francis Halzen and Kate Scholberg. *Neutrinos from Core-Collapse Supernovae and Their Detection*. January 2017. doi: 10.1007/978-3-319-21846-5\_8. URL <https://ui.adsabs.harvard.edu/abs/2017hsn..book.1655H>. Pages: 1655 Publication Title: Handbook of Supernovae ADS Bibcode: 2017hsn..book.1655H.
- [8] A. Marek and H.-Th Janka. DELAYED NEUTRINO-DRIVEN SUPERNOVA EXPLOSIONS AIDED BY THE STANDING ACCRETION-SHOCK INSTABILITY. *The Astrophysical Journal*, 694(1):664–696, March 2009. ISSN 0004-637X. doi: 10.1088/0004-637X/694/1/664. URL <https://doi.org/10.1088/0004-637x/694/1/664>. Publisher: American Astronomical Society.
- [9] A. Mirizzi, I. Tamborra, H.-Th. Janka, N. Saviano, K. Scholberg, R. Bollig, L. Hüdepohl, and S. Chakraborty. Supernova neutrinos: production, oscillations and detection. *La Rivista del Nuovo Cimento*, 39(1):1–112, January 2016. ISSN 1826-9850. doi: 10.1393/ncr/i2016-10120-8. URL <https://doi.org/10.1393/ncr/i2016-10120-8>.

- [10] M. Ruffert, H.-Th Janka, K. Takahashi, and G. Schaefer. Coalescing neutron stars – a step towards physical models. II. Neutrino emission, neutron tori, and gamma-ray bursts, June 1996. URL <http://arxiv.org/abs/astro-ph/9606181>. arXiv:astro-ph/9606181.
- [11] M. Ruffert and H.-Th Janka. Coalescing neutron stars -A step towards physical models - III. Improved numerics and different neutron star masses and spins. *Astronomy & Astrophysics*, 380(2):544–577, December 2001. ISSN 0004-6361, 1432-0746. doi: 10.1051/0004-6361:20011453. URL <https://www.aanda.org/articles/aa/abs/2001/47/aah2941/aah2941.html>. Number: 2 Publisher: EDP Sciences.
- [12] Francois Foucart, Evan OConnor, Luke Roberts, Matthew D. Duez, Roland Haas, Lawrence E. Kidder, Christian D. Ott, Harald P. Pfeiffer, Mark A. Scheel, and Bela Szilagyi. Post-merger evolution of a neutron star-black hole binary with neutrino transport. *Physical Review D*, 91(12):124021, June 2015. doi: 10.1103/PhysRevD.91.124021. URL <https://link.aps.org/doi/10.1103/PhysRevD.91.124021>. Publisher: American Physical Society.
- [13] G. Sigl and G. Raffelt. General kinetic description of relativistic mixed neutrinos. *Nuclear Physics B*, 406(1):423–451, September 1993. ISSN 0550-3213. doi: 10.1016/0550-3213(93)90175-O. URL <https://www.sciencedirect.com/science/article/pii/0550321393901750>.
- [14] Lihong V. Wang. Derivation from Bloch Equation to von Neumann Equation to SchrödingerPauli Equation. *Foundations of Physics*, 52(3):61, June 2022. ISSN 1572-9516. doi: 10.1007/s10701-022-00578-6. URL <https://doi.org/10.1007/s10701-022-00578-6>.
- [15] C. W. Kim, Jewan Kim, and W. K. Sze. Geometrical representation of neutrino oscillations in vacuum and matter. *Physical Review D*, 37(4):1072–1075, February 1988. doi: 10.1103/PhysRevD.37.1072. URL <https://link.aps.org/doi/10.1103/PhysRevD.37.1072>. Publisher: American Physical Society.
- [16] Huaiyu Duan, George M. Fuller, and Yong-Zhong Qian. Collective Neutrino Oscillations. *Annual Review of Nuclear and Particle Science*, 60(1):569–594, 2010. doi: 10.1146/annurev.nucl.012809.104524. URL <https://doi.org/10.1146/annurev.nucl.012809.104524>. \_eprint: <https://doi.org/10.1146/annurev.nucl.012809.104524>.
- [17] Daya Bay Collaboration. Spectral measurement of electron antineutrino oscillation amplitude and frequency at daya bay. *Phys. Rev. Lett.*, 112:061801, Feb 2014. doi: 10.1103/PhysRevLett.112.061801. URL <https://link.aps.org/doi/10.1103/PhysRevLett.112.061801>.
- [18] A. Malkus, A. Friedland, and G. C. McLaughlin. Matter-Neutrino Resonance Above Merging Compact Objects, April 2014. URL <http://arxiv.org/abs/1403.5797>. arXiv:1403.5797 [astro-ph, physics:hep-ph, physics:nucl-th].
- [19] S. P. Mikheyev and A. Yu. Smirnov. Resonant neutrino oscillations in matter. *Progress in Particle and Nuclear Physics*, 23:41–136, January 1989. ISSN 0146-6410. doi: 10.1016/0146-6410(89)90008-2. URL <https://www.sciencedirect.com/science/article/pii/0146641089900082>.

- [20] T. K. Kuo and James Pantaleone. Neutrino oscillations in matter. *Reviews of Modern Physics*, 61(4):937–979, October 1989. doi: 10.1103/RevModPhys.61.937. URL <https://link.aps.org/doi/10.1103/RevModPhys.61.937>. Publisher: American Physical Society.
- [21] A. Yu Smirnov. Neutrino Conversion and Neutrino Astrophysics, November 1998. URL <http://arxiv.org/abs/hep-ph/9811296>. arXiv:hep-ph/9811296.
- [22] P. Dedin Neto and E. Kemp. Neutrino(anti)neutrino forward scattering potential for massive neutrinos at low energies. *Modern Physics Letters A*, 37(08):2250048, March 2022. ISSN 0217-7323. doi: 10.1142/S0217732322500481. URL <https://www.worldscientific.com/doi/abs/10.1142/S0217732322500481>. Publisher: World Scientific Publishing Co.
- [23] Huaiyu Duan, George M. Fuller, J. Carlson, and Yong-Zhong Qian. Simulation of coherent non-linear neutrino flavor transformation in the supernova environment: Correlated neutrino trajectories. *Physical Review D*, 74(10):105014, November 2006. doi: 10.1103/PhysRevD.74.105014. URL <https://link.aps.org/doi/10.1103/PhysRevD.74.105014>. Publisher: American Physical Society.
- [24] Shashank Shalgar. Multi-angle calculation of the matter-neutrino resonance near an accretion disk. *Journal of Cosmology and Astroparticle Physics*, 2018(02):010–010, February 2018. ISSN 1475-7516. doi: 10.1088/1475-7516/2018/02/010. URL <https://doi.org/10.1088/1475-7516/2018/02/010>. Publisher: IOP Publishing.
- [25] Gianluigi Fogli, Eligio Lisi, Antonio Marrone, and Alessandro Mirizzi. Collective neutrino flavor transitions in supernovae and the role of trajectory averaging. *Journal of Cosmology and Astroparticle Physics*, 2007(12):010–010, December 2007. ISSN 1475-7516. doi: 10.1088/1475-7516/2007/12/010. URL <https://doi.org/10.1088/1475-7516/2007/12/010>. Publisher: IOP Publishing.
- [26] Huaiyu Duan, George M. Fuller, and Yong-Zhong Qian. Collective neutrino flavor transformation in supernovae. *Physical Review D*, 74(12):123004, December 2006. doi: 10.1103/PhysRevD.74.123004. URL <https://link.aps.org/doi/10.1103/PhysRevD.74.123004>. Publisher: American Physical Society.
- [27] Basudeb Dasgupta and Amol Dighe. Collective three-flavor oscillations of supernova neutrinos. *Physical Review D*, 77(11):113002, June 2008. doi: 10.1103/PhysRevD.77.113002. URL <https://link.aps.org/doi/10.1103/PhysRevD.77.113002>. Publisher: American Physical Society.
- [28] Basudeb Dasgupta, Amol Dighe, Alessandro Mirizzi, and Georg G. Raffelt. Spectral split in a prompt supernova neutrino burst: Analytic three-flavor treatment. *Physical Review D*, 77(11):113007, June 2008. doi: 10.1103/PhysRevD.77.113007. URL <https://link.aps.org/doi/10.1103/PhysRevD.77.113007>. Publisher: American Physical Society.
- [29] Huaiyu Duan, George M. Fuller, and Yong-Zhong Qian. Stepwise spectral swapping with three neutrino flavors. *Physical Review D*, 77(8):085016, April 2008. doi: 10.1103/PhysRevD.77.085016.

- URL <https://link.aps.org/doi/10.1103/PhysRevD.77.085016>. Publisher: American Physical Society.
- [30] Basudeb Dasgupta, Amol Dighe, Georg G. Raffelt, and Alexei Yu. Smirnov. Multiple Spectral Splits of Supernova Neutrinos. *Physical Review Letters*, 103(5):051105, July 2009. doi: 10.1103/PhysRevLett.103.051105. URL <https://link.aps.org/doi/10.1103/PhysRevLett.103.051105>. Publisher: American Physical Society.
- [31] A. E-Pretel, S. Pastor, R. Tomàs, G. G. Raffelt, and G. Sigl. Multi-angle effects in collective supernova neutrino oscillations. *Journal of Physics: Conference Series*, 120(5):052021, July 2008. ISSN 1742-6596. doi: 10.1088/1742-6596/120/5/052021. URL <https://doi.org/10.1088/1742-6596/120/5/052021>. Publisher: IOP Publishing.
- [32] Sovan Chakraborty, Sandhya Choubey, Basudeb Dasgupta, and Kamales Kar. The effect of collective flavor oscillations on the diffuse supernova neutrino background. *Journal of Cosmology and Astroparticle Physics*, 2008(09):013, September 2008. ISSN 1475-7516. doi: 10.1088/1475-7516/2008/09/013. URL <https://doi.org/10.1088/1475-7516/2008/09/013>. Publisher: IOP Publishing.
- [33] Gianluigi Fogli, Eligio Lisi, Antonio Marrone, and Alessandro Mirizzi. Neutrinos self interactions in Supernovae, May 2008. URL <http://arxiv.org/abs/0805.2530>. arXiv:0805.2530 [hep-ph].
- [34] Basudeb Dasgupta, Evan P. OConnor, and Christian D. Ott. Role of collective neutrino flavor oscillations in core-collapse supernova shock revival. *Physical Review D*, 85(6):065008, March 2012. doi: 10.1103/PhysRevD.85.065008. URL <https://link.aps.org/doi/10.1103/PhysRevD.85.065008>. Publisher: American Physical Society.
- [35] Yudai Suwa, Kei Kotake, Tomoya Takiwaki, Matthias Liebendörfer, and Katsuhiko Sato. IMPACTS OF COLLECTIVE NEUTRINO OSCILLATIONS ON CORE-COLLAPSE SUPERNOVA EXPLOSIONS. *The Astrophysical Journal*, 738(2):165, August 2011. ISSN 0004-637X. doi: 10.1088/0004-637X/738/2/165. URL <https://doi.org/10.1088/0004-637x/738/2/165>. Publisher: American Astronomical Society.
- [36] Meng-Ru Wu and Yong-Zhong Qian. Resonances driven by a neutrino gyroscope and collective neutrino oscillations in supernovae. *Physical Review D*, 84(4):045009, August 2011. doi: 10.1103/PhysRevD.84.045009. URL <https://link.aps.org/doi/10.1103/PhysRevD.84.045009>. Publisher: American Physical Society.
- [37] Sergio Pastor, Georg Raffelt, and Dmitry V. Semikoz. Physics of synchronized neutrino oscillations caused by self-interactions. *Physical Review D*, 65(5):053011, February 2002. doi: 10.1103/PhysRevD.65.053011. URL <https://link.aps.org/doi/10.1103/PhysRevD.65.053011>. Publisher: American Physical Society.

- [38] James Y. Tian, Amol V. Patwardhan, and George M. Fuller. Neutrino flavor evolution in neutron star mergers. *Physical Review D*, 96(4):043001, August 2017. doi: 10.1103/PhysRevD.96.043001. URL <https://link.aps.org/doi/10.1103/PhysRevD.96.043001>. Publisher: American Physical Society.
- [39] A. Malkus, J. P. Kneller, G. C. McLaughlin, and R. Surman. Neutrino oscillations above black hole accretion disks: Disks with electron-flavor emission. *Physical Review D*, 86(8):085015, October 2012. doi: 10.1103/PhysRevD.86.085015. URL <https://link.aps.org/doi/10.1103/PhysRevD.86.085015>. Publisher: American Physical Society.
- [40] Meng-Ru Wu, Irene Tamborra, Oliver Just, and Hans-Thomas Janka. Imprints of neutrino-pair flavor conversions on nucleosynthesis in ejecta from neutron-star merger remnants. *Physical Review D*, 96(12):123015, December 2017. doi: 10.1103/PhysRevD.96.123015. URL <https://link.aps.org/doi/10.1103/PhysRevD.96.123015>. Publisher: American Physical Society.
- [41] Alexey Vlasenko and G.C. McLaughlin. Matter-neutrino resonance in a multiangle neutrino bulb model. *Physical Review D*, 97(8):083011, April 2018. doi: 10.1103/PhysRevD.97.083011. URL <https://link.aps.org/doi/10.1103/PhysRevD.97.083011>. Publisher: American Physical Society.
- [42] Meng-Ru Wu, Huaiyu Duan, and Yong-Zhong Qian. Physics of neutrino flavor transformation through matterneutrino resonances. *Physics Letters B*, 752:89–94, January 2016. ISSN 0370-2693. doi: 10.1016/j.physletb.2015.11.027. URL <https://www.sciencedirect.com/science/article/pii/S0370269315008758>.
- [43] D. Väänänen and G.C. McLaughlin. Uncovering the matter-neutrino resonance. *Physical Review D*, 93(10):105044, May 2016. doi: 10.1103/PhysRevD.93.105044. URL <https://link.aps.org/doi/10.1103/PhysRevD.93.105044>. Publisher: American Physical Society.
- [44] A. Malkus, G.C. McLaughlin, and R. Surman. Symmetric and standard matter neutrino resonances above merging compact objects. *Physical Review D*, 93(4):045021, February 2016. doi: 10.1103/PhysRevD.93.045021. URL <https://link.aps.org/doi/10.1103/PhysRevD.93.045021>. Publisher: American Physical Society.
- [45] Y.L. Zhu, A. Perego, and G.C. McLaughlin. Matter-neutrino resonance transitions above a neutron star merger remnant. *Physical Review D*, 94(10):105006, November 2016. doi: 10.1103/PhysRevD.94.105006. URL <https://link.aps.org/doi/10.1103/PhysRevD.94.105006>. Publisher: American Physical Society.
- [46] X. Qian and P. Vogel. Neutrino mass hierarchy. *Progress in Particle and Nuclear Physics*, 83: 1–30, 2015. ISSN 0146-6410. doi: <https://doi.org/10.1016/j.pnnp.2015.05.002>. URL <https://www.sciencedirect.com/science/article/pii/S0146641015000307>.
- [47] Effect of collisions on neutrino flavor inhomogeneity in a dense neutrino gas - ScienceDirect, . URL <https://www.sciencedirect.com/science/article/pii/S0370269317307505>.

- [48] New Developments in Flavor Evolution of a Dense Neutrino Gas | Annual Review of Nuclear and Particle Science, . URL <https://www.annualreviews.org/doi/10.1146/annurev-nucl-102920-050505>.
- [49] Meng-Ru Wu, Manu George, Chun-Yu Lin, and Zewei Xiong. Collective fast neutrino flavor conversions in a 1D box: Initial conditions and long-term evolution. *Physical Review D*, 104(10): 103003, November 2021. doi: 10.1103/PhysRevD.104.103003. URL <https://link.aps.org/doi/10.1103/PhysRevD.104.103003>. Publisher: American Physical Society.
- [50] Shashank Shalgar, Ian Padilla-Gay, and Irene Tamborra. Neutrino propagation hinders fast pairwise flavor conversions. *Journal of Cosmology and Astroparticle Physics*, 2020(06):048–048, June 2020. ISSN 1475-7516. doi: 10.1088/1475-7516/2020/06/048. URL <https://doi.org/10.1088/1475-7516/2020/06/048>. Publisher: IOP Publishing.
- [51] Shashank Shalgar and Irene Tamborra. Neutrino Flavor Conversion, Advection, and Collisions: The Full Solution, July 2022. URL <http://arxiv.org/abs/2207.04058>. arXiv:2207.04058 [astro-ph, physics:hep-ph].
- [52] O. Just, A. Bauswein, R. Ardevol Pulpillo, S. Goriely, and H.-T. Janka. Comprehensive nucleosynthesis analysis for ejecta of compact binary mergers. *Monthly Notices of the Royal Astronomical Society*, 448(1):541–567, March 2015. ISSN 0035-8711. doi: 10.1093/mnras/stv009. URL <https://doi.org/10.1093/mnras/stv009>.
- [53] Signatures of hypermassive neutron star lifetimes on r-process nucleosynthesis in the disc ejecta from neutron star mergers | Monthly Notices of the Royal Astronomical Society | Oxford Academic, . URL <https://academic.oup.com/mnras/article/472/1/904/4079802>.